Volume 9
Number 22
21 November 2025
Pages 5953–6314

Sustainable Energy & Fuels

Interdisciplinary research for the development of sustainable energy technologies

rsc.li/sustainable-energy

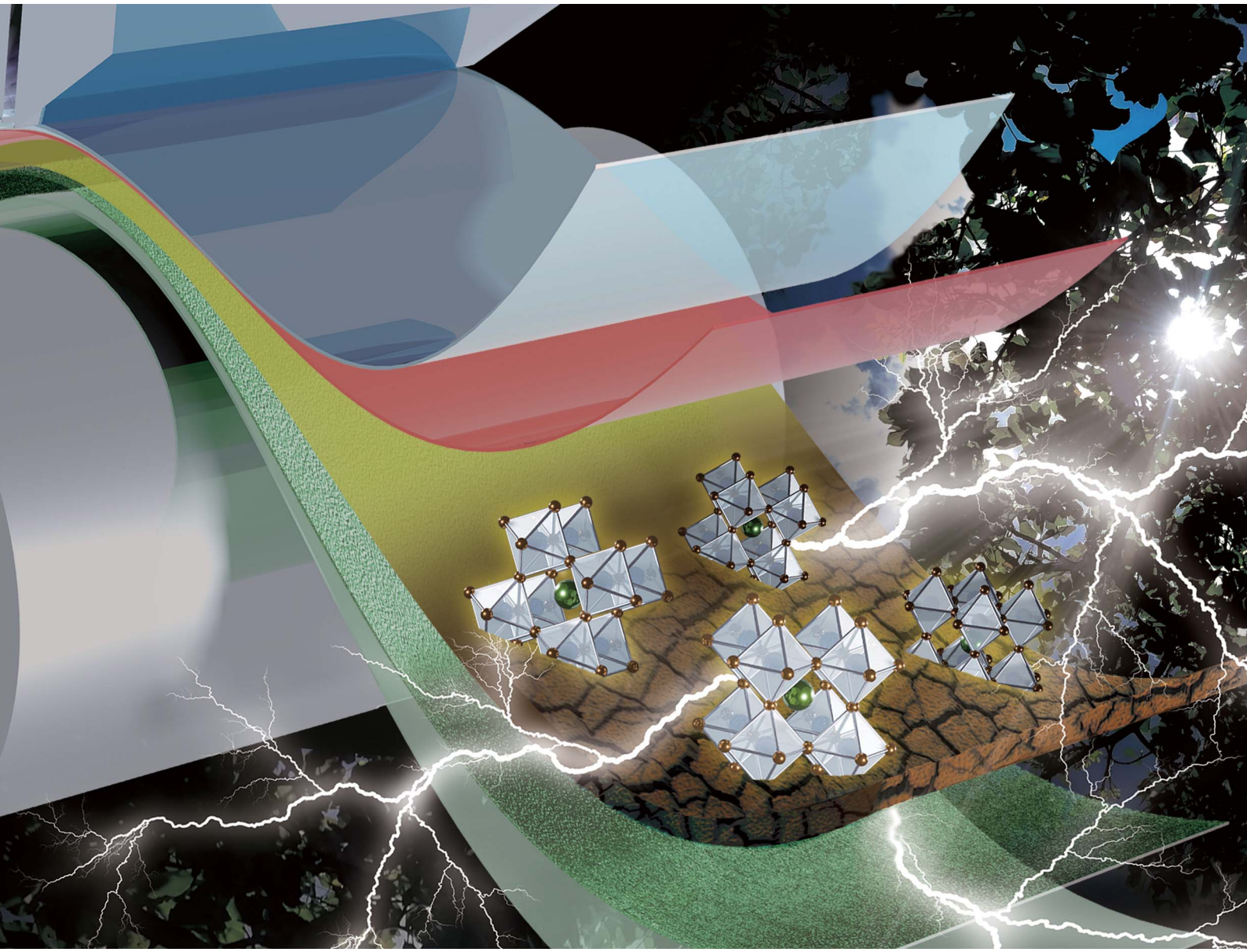

ISSN 2398-4902

ROYAL SOCIETY OF CHEMISTRY

REVIEW ARTICLE

Wei-Fang Su, Yu-Ching Huang *et al.*

Advances and strategies in scalable coating techniques for flexible perovskite solar cells

Sustainable Energy & Fuels

ROYAL SOCIETY OF CHEMISTRY

REVIEW

View Article Online
View Journal | View Issue

Cite this: *Sustainable Energy Fuels*, 2025, **9**, 5962

Advances and strategies in scalable coating techniques for flexible perovskite solar cells

Hou-Chin Cha,[ab] Shih-Han Huang,[b] Chia-Feng Li,[cd] Feng-Yu Tsai,[d] Wei-Fang Su *[cd] and Yu-Ching Huang *[bcef]

Perovskite solar cells (PSCs) have emerged as leading candidates for next-generation photovoltaics owing to their outstanding power conversion efficiencies (PCEs), low-cost materials, and compatibility with low-temperature, solution-based fabrication techniques. While certified PCEs of 27.0% have been reached on rigid substrates, transitioning to scalable, flexible architectures introduces new challenges. This review highlights recent advancements in flexible PSCs (F-PSCs), including the development of low-temperature-processed charge transport materials, flexible transparent electrodes, and encapsulation strategies that maintain mechanical robustness under deformation. Scalable deposition techniques, such as blade coating, slot-die coating, and spray coating, are also discussed, with respect to film uniformity, process control, and compatibility with roll-to-roll (R2R) manufacturing. The integration of solvent and additive engineering, along with interfacial modifications, is shown to be critical in optimizing film morphology and enhancing device performance. Notably, recent studies report flexible perovskite modules achieving PCEs exceeding 17% across active areas larger than 100 cm^2. Beyond the PCE, this review addresses critical issues in ensuring long-term operational stability, including mechanical reliability and environmental degradation from moisture, oxygen, light, and thermal stress. Strategies such as multi-cation perovskite formulations, advanced interfacial modification, and high-barrier encapsulants are evaluated for their role in enhancing long-term operational stability. Finally, we provide a forward-looking perspective on the technical gaps and collaborative efforts required, across materials science, engineering, and industrial scale-up, to enable the commercial application of F-PSCs.

Received 20th June 2025
Accepted 18th September 2025

DOI: 10.1039/d5se00873e

rsc.li/sustainable-energy

[a]*College of Engineering, Ming Chi University of Technology, New Taipei City 24301, Taiwan*

[b]*Organic Electronics Research Center, Ming Chi University of Technology, New Taipei City 24301, Taiwan. E-mail: huangyc@mail.mcut.edu.tw*

[c]*Department of Materials Engineering, Ming Chi University of Technology, New Taipei City 24301, Taiwan*

[d]*Department of Materials Science and Engineering, National Taiwan University, Taipei 10617, Taiwan. E-mail: suwf@ntu.edu.tw*

[e]*Center for Sustainability and Energy Technologies, Chang Gung University, Taoyuan 33302, Taiwan*

[f]*Research Center for Critical Issues, Academia Sinica, Taipei, 115201, Taiwan*

Hou-Chin Cha

Dr Hou-Chin Cha received his PhD in Mechanical Engineering from Chung Yuan Christian University, Taiwan, in 2006. He is currently an Assistant Research Fellow at the Organic Electronics Research Center, Ming Chi University of Technology. His research focuses on organic photovoltaics, perovskite solar cells, and organic photodetectors, with expertise in flexible device processing, transparent electrode development, flexible encapsulation, stability evaluation, and laser-assisted module fabrication. In recent years, he has emphasized scalable roll-to-roll and roll-to-sheet coating technologies.

Shih-Han Huang

Dr Shih-Han Huang is a Research Fellow at the Organic Electronics Research Center, Ming Chi University of Technology, Taiwan. He received his PhD from National Taiwan University in 2021. His research focuses on developing scalable formulations and manufacturing strategies for perovskite solar cells, with particular emphasis on solution processing and vapor-based deposition techniques.

1. Introduction

As countries worldwide commit to achieving net-zero carbon emissions by 2050, global electricity demand is expected to double within the next few decades. The global solar photovoltaic (PV) market is projected to grow from approximately USD 398.2 billion in 2024 to nearly USD 2.79 trillion by 2034, highlighting the rapid expansion and economic significance of PV technologies in the coming decade.[1] Meanwhile, crystalline silicon (c-Si) PV technologies continue to dominate the global market, accounting for around 90% of global production over the past two decades and maintaining a leading position in large-scale deployment.[2] With fossil fuels being progressively phased out, governments and industries are increasing their investments in renewable clean energy, driven by increasing sustainability awareness and supportive policy frameworks. Among various renewable technologies, solar energy stands out as a leading candidate. However, their inherent limitations, such as high production cost and mechanical rigidity, have motivated the search for alternative technologies. Recently, solar cells fabricated from organic–inorganic hybrid perovskite materials have been a rising star for the low-cost next generation of solar cells. Perovskite-structured materials (ABX_3) share a common crystal framework originally discovered by Gustav Rose in calcium titanate ($CaTiO_3$), where A-site cations (*e.g.*, MA^+, FA^+), B-site metal cations (*e.g.*, Pb^{2+}, Sn^{2+}), and X-site anions (*e.g.*, Cl^-, Br^-, I^-) contribute to their outstanding optoelectronic properties. These include strong light absorption, low exciton binding energy,[3,4] and long carrier lifetimes, which have driven PSC development from an initial PCE of just 3.8% to record-breaking levels. Perovskite solar cells (PSCs) have emerged as a promising next-generation PVs owing to their low-

Chia-Feng Li

Mr Chia-Feng Li received his BS degree in 2018 and his MS degree in 2020 from Ming Chi University of Technology. Since 2021, he has been pursuing his PhD in the Department of Materials Science and Engineering at National Taiwan University, under the supervision of Prof. Feng-Yu Tsai and Prof. Yu-Ching Huang. His research focuses on next-generation solar energy technologies, particularly organic photovoltaics, scalable perovskite solar cells, and module development.

Wei-Fang Su

Professor Su has a PhD from the University of Massachusetts, and is a postdoctoral fellow in Northwestern University. She was a research fellow at the Westinghouse Research and Development Center. She taught in National Taiwan University and became an Emeritus Professor in 2021. At present, she is a Visiting Chair Professor in Ming-Chi University of Technology. Her research is focused on the design, synthesis and processing of novel polymeric materials and nanomaterials for medical applications and electronic device/solar applications. She has published 268 SCI papers, 2 textbooks for polymers (2013 Springer) and solar cells (2012 Wiley) respectively, 32 US patents and 47 Taiwan patents.

Feng-Yu Tsai

Feng-Yu Tsai is a professor with and the chairperson of Department of Materials Science and Engineering (MSE) at National Taiwan University (NTU). He received his PhD degree in MSE from the University of Rochester, following which he worked as a process development engineer with Headway Technologies and as a senior process development engineer with DuPont Displays. He joined the faculty of NTU MSE in 2004. His research interests include atomic-scale thin film deposition mechanisms, their resultant material properties, and their manifestations in a wide variety of applications spanning from photovoltaics, thermoelectrics, and semiconductor devices, to hydrogen energy.

Yu-Ching Huang

Dr Yu-Ching Huang is a Professor in the Department of Materials Engineering at Ming Chi University of Technology (Taiwan) and a Jointly Appointed Associate Research Fellow at Academia Sinica (Taiwan). He received his PhD in 2010 at National Taiwan University (Taiwan). His research interests focus on organic and perovskite optoelectronic materials, photovoltaics and photodetectors, scalable manufacturing processes, and biomedical polymer applications. He has published more than 120 peer-reviewed papers (h-index 32) and 20 patents (Taiwan and U.S.).

Table 1 Comparative summary of solution-based coating methods for flexible perovskite solar cells, highlighting their advantages, disadvantages, material utilization, scalability, and suitability for large-area and flexible device fabrication

Coating method	Advantages	Disadvantages	Suitability for flexible substrate
Spin coating	Produces highly uniform films with excellent surface coverage at a small scale. It is simple, fast, and widely adopted in academic research, making it ideal for high-efficiency proof-of-concept devices and enabling systematic optimization of ink formulation and crystallization mechanisms	Very high material waste (>80%) occurs due to excess solution being spun off. The method is not scalable to large or continuous substrates and requires large ink volumes. It also has poor compatibility with roll-to-roll or continuous processes, and film thickness control becomes limited for large-area deposition	Mainly useful for lab-scale fabrication of flexible test cells and for studying new materials, but not applicable for large-area flexible PSC modules due to its lack of scalability
Blade coating	Blade coating features relatively low material waste compared to spin coating, while maintaining a simple setup that is compatible with ambient processing. Film thickness can be controlled by adjusting coating speed and blade height, making it scalable to medium-sized substrates and providing a good balance between simplicity and reproducibility	The method is highly sensitive to ink viscosity, coating speed, substrate roughness, and environmental conditions. Throughput is lower than slot-die coating, and there is a risk of film inhomogeneity, particularly at the substrate edges	Suitable for small- to medium-area flexible substrates and pilot-scale devices and often adopted as an intermediate step before scaling up to slot-die or roll-to-roll processes
Slot-die coating	Slot-die coating enables excellent thickness control and reproducibility across large areas. It provides very low material waste with high ink utilization and is highly scalable, being fully compatible with continuous roll-to-roll manufacturing. The method allows precise wet film deposition followed by controlled drying	It requires careful optimization of ink formulation, particularly viscosity, surface tension, and solvent volatility. Drying and crystallization must be tightly controlled to avoid defects, and the setup is more complex compared to blade coating	Slot-die coating is considered one of the most promising methods for large-area flexible PSC modules and is highly relevant for industrial production lines and commercialization
Spray coating	Spray coating is simple, low-cost, and compatible with ambient conditions. It can conformally coat textured, curved, or rough surfaces, which is advantageous for flexible or non-planar substrates, and the equipment is relatively inexpensive and scalable	Film uniformity is often limited, with defects such as pinholes and surface roughness being common. Thickness control is less precise compared to other methods, and post-treatments such as annealing or solvent engineering are usually required	Attractive for large-area flexible devices where surface conformity is critical, such as textiles or uneven substrates, although film quality issues remain a barrier for achieving high-performance PSCs
Inkjet printing	Inkjet printing enables digital, mask-free patterning and highly efficient material usage with minimal waste. It allows the fabrication of customized and pixelated device architectures and is compatible with localized deposition, making it suitable for wearable and portable electronic applications	The method suffers from low throughput, limiting its industrial relevance. Nozzle clogging and droplet coalescence can lead to nonuniform films, while film crystallization and uniformity require careful optimization of ink properties. Scalability is limited compared to slot-die coating	Inkjet printing is well-suited for patterned flexible devices, integrated sensors, and wearable or portable electronics, but is more appropriate for niche or specialized applications rather than large-area flexible PSC modules

cost solution processability, lightweight design, and ease of power conversion efficiency (PCE) improvement.[5] The unique properties of perovskite materials, such as low crystallization activation energy and high tolerance for compositional variability, enable facile thin-film deposition *via* scalable techniques.[6,7] These materials exhibit wide tunable bandgaps (1.5–3.2 eV), high defect tolerance (trap densities around 10^{15} cm^{-3}), and long charge carrier diffusion lengths exceeding 1 μm,[8] making them highly attractive for solar applications. Remarkably, within just a decade, single-junction PSCs have achieved a certified PCE of 27.0%,[9] despite persistent issues such as high defect densities and interfacial instabilities.[10,11] However, their success has so far been limited to lab-scale devices, and scalability to large-area modules remains a major challenge.[12] Nonetheless, as IDTechEx points out in its report perovskite photovoltaics 2023–2033, PSCs could complement or even replace conventional silicon-based solar cells in the future because of their low cost, high efficiency, scalable manufacturing capabilities, and potential to be both flexible and lightweight.[13]

Currently, most high-efficiency PSCs are primarily fabricated using spin coating methods at the laboratory scale, due to the

ability of spin coating to produce uniform, pinhole-free perovskite films with precise thickness control. Two spin coating strategies are employed for perovskite layer formation: one-step and two-step processes. In the one-step process, anti-solvents are often introduced to improve film formation. For example, Cheng's group used *N*,*N*-dimethylformamide (DMF) as the primary solvent and chlorobenzene (CB) as the anti-solvent to achieve highly uniform films.[14] Similarly, Seok's group employed *tert*-butyl alcohol (TB) as the anti-solvent in a mixture of dimethyl sulfoxide (DMSO) and gamma-butyrolactone (GBL) solvent system to improve film morphology.[15] Although the anti-solvent procedure can yield high-quality films, precise control over the anti-solvent step is difficult to scale up for large-area production. In contrast, the two-step spin coating method offers better control over perovskite morphology and interface formation.[16] However, it often suffers from incomplete phase conversion and pronounced edge effects, particularly as the coated area increases, further limiting its scalability. Overall, spin coating is limited by intrinsic drawbacks that hinder scale-up, including low material utilization, potential formation of surface defects and pinholes, and difficulty in achieving uniform coverage over large areas, all of which contribute to performance degradation in large-area devices.[17] To overcome these limitations, alternative scalable techniques such as blade coating, slot-die coating, spray coating, and inkjet printing have emerged as promising fabrication approaches. These techniques offer better potential for large-area uniformity, material usage efficiency, and process repeatability. To illustrate their relative merits, Table 1 provides a comparative summary of these solution-based coating methods, highlighting their advantages, disadvantages, material utilization, scalability, and suitability for large-area and flexible device fabrication. For instance, blade coating uses a controlled blade to spread the precursor solution evenly, slot-die coating relies on fluid dynamics to deposit uniform films with high precision, spray coating allows rapid film deposition by atomizing the precursor solution onto the substrate, and inkjet printing enables digital, mask-free patterning through the precise ejection of picoliter-scale droplets. However, further optimization is still needed in these scalable techniques, such as achieving consistent thickness, uniformity, and reproducibility.

This review provides a comprehensive overview of the progress and challenges in the development of flexible perovskite solar cells (F-PSCs), with a particular focus on scalable fabrication strategies. It begins by highlighting the significance of F-PSCs and recent advancements in the field, including the development of flexible tandem PSCs that aim to overcome single-junction efficiency limits through stacked absorber architectures, and the emergence of all-printed F-PSCs that enable fully solution-processed fabrication without vacuum deposition. This is followed by an in-depth discussion of issues related to scaling up to large-area devices. The review then examines three prominent scalable coating technologies—blade coating, slot-die coating, and spray coating—by first discussing their applications on rigid substrates and subsequently extending to flexible substrates, offering a comparative perspective on their process compatibility, film quality, and device performance. Furthermore, the review explores the transition from rigid to flexible substrate processing, including the selection of flexible substrates, development of electrodes, adoption of low-temperature processable charge transport materials, and encapsulation strategies, all of which are critical for ensuring mechanical flexibility and long-term operational stability of F-PSCs. Key stability concerns, both environmental and mechanical, are addressed in the context of real-world durability. In conclusion, this review outlines the current technical challenges and provides a forward-looking perspective on the commercialization of F-PSCs, emphasizing the need for materials innovation, scalable processing, and reliability testing to accelerate the realization of next-generation photovoltaic technology.

2. Flexible perovskite solar cells (F-PSCs)

2.1 Why are F-PSCs important

F-PSCs have gained increasing attention as a promising next-generation photovoltaic technology, not only due to their impressive PCEs but also because of their unique combination of mechanical flexibility, lightweight construction, and compatibility with scalable manufacturing techniques. These features collectively enable F-PSCs to meet application needs that conventional rigid solar technologies cannot fulfill, thereby expanding the scope and impact of solar energy utilization. One of the most compelling advantages of F-PSCs is their mechanical flexibility, which enables them to conform to curved, textured, or movable surfaces without compromising performance. This feature unlocks a wide range of application possibilities, including building-integrated photovoltaics (BIPV),[18] vehicle-integrated photovoltaics (VIPV),[19] and wearable electronics.[20] Unlike traditional rigid panels, F-PSCs can be seamlessly integrated into architectural components such as windows, façades, and lightweight roofing materials, transforming passive building surfaces into active energy generators. This architectural versatility is essential for the realization of smart, energy-autonomous buildings in densely populated urban environments. In the realm of mobile and wearable technologies, the ability to incorporate F-PSCs into fabrics, flexible substrates, or curved devices positions them as ideal energy sources for the rapidly growing fields of smart textiles, health monitoring systems, and the Internet of Things (IoT).[21] Their ability to deliver continuous, lightweight, and unobtrusive power makes them suitable for devices that demand compactness, mobility, and reliability, particularly in scenarios where access to traditional power sources is limited. Furthermore, the low weight and rollable nature of F-PSCs enable them to be easily transported and deployed in off-grid environments. This feature is particularly advantageous for emergency power supply systems, portable charging units, and renewable energy solutions in disaster relief, humanitarian missions, and remote infrastructure development. The practicality of F-PSCs in such contexts underscores their value beyond urban environments, helping to address global energy access challenges.

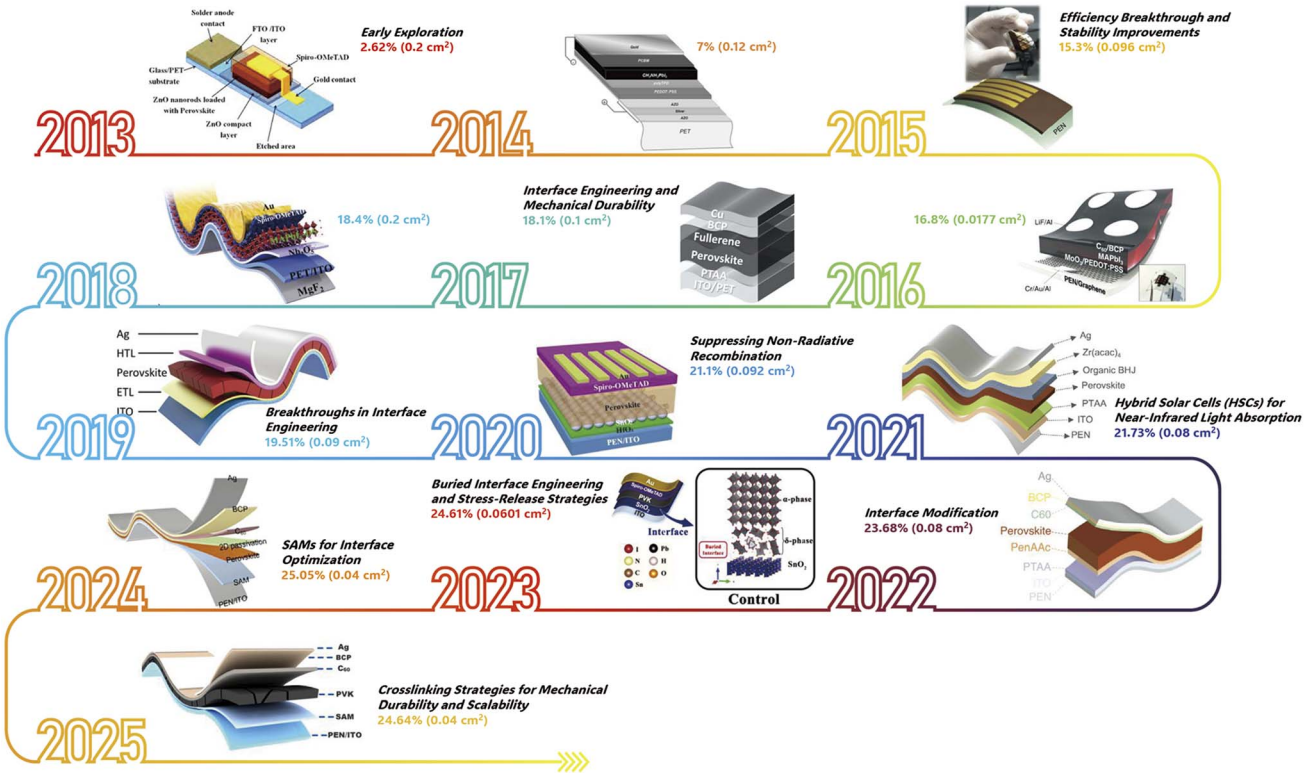

Fig. 1 The progress of power conversion efficiency in flexible perovskite solar cells from 2013 to April 2025.[24–36]

In addition to these functional benefits, F-PSCs align well with sustainability goals.[22] Their fabrication often relies on low-temperature, solution-based processes such as slot-die coating and roll-to-roll (R2R) manufacturing, which significantly reduce energy consumption and production costs compared to conventional high-temperature silicon-based methods. These scalable techniques support mass production on flexible substrates, paving the way for industrial-scale deployment and commercialization. The importance of F-PSCs is further amplified by the rapid progress in materials engineering and device architecture. Continuous innovation in encapsulation, barrier films, and interface engineering has led to marked improvement in both environmental stability and operational lifetime of flexible perovskite devices. As the field evolves, F-PSCs show promise for improved long-term stability compared to traditional photovoltaic technologies, making them a reliable option for long-term energy generation.[23] In summary, F-PSCs are not merely an incremental improvement but a paradigm shift in how solar energy can be implemented across diverse scenarios. Thanks to their versatility, ease of large-scale production, and strong performance, they play an essential role in accelerating the global transition toward more sustainable, locally deployable, and accessible energy systems.

2.2 Advancements in F-PSCs

The development of F-PSCs has progressed substantially since their initial investigation in 2013, with notable advancements achieved to date. Over the past decade, extensive research efforts have been dedicated to enhancing PCE, improving mechanical durability, and developing scalable fabrication techniques suitable for large-area manufacture. These advancements have progressively addressed many of the early-stage challenges that hindered the practical deployment of F-PSCs. A chronological overview of key technological milestones and performance improvements is illustrated in Fig. 1 and further discussed in the following sections.

2.2.1 Early exploration (2013–2014): overcoming fundamental challenges. During the early development of F-PSCs, significant efforts were directed toward integrating perovskite materials with flexible substrates such as polyethylene terephthalate (PET) and polyethylene naphthalate (PEN). However, several critical challenges quickly became apparent. The relatively high surface roughness of flexible substrates hindered the formation of high-quality perovskite films, leading to poor crystallization and film morphology, which in turn reduced device performance. In addition, commonly used transparent conductive layers like indium tin oxide (ITO) were prone to cracking under mechanical stress, which significantly affected electrical conductivity. Mechanical deformation during bending or flexing further accelerated device degradation, posing a serious barrier to the practical application of F-PSCs. At this early stage, the highest PCE was approximately 7%, reflecting both the infancy of the technology and its considerable room for further advancement.[24,25]

2.2.2 Efficiency breakthrough and stability improvements (2015–2016). Subsequent research efforts concentrated on optimizing the electron transport layer (ETL) to enhance charge extraction and improve perovskite film formation. Materials

such as titanium dioxide (TiO_2) and tin oxide (SnO_2) were systematically refined, leading to more efficient charge transport and improved perovskite crystallization. Concurrently, the introduction of hybrid organic–inorganic perovskites, particularly methylammonium lead iodide ($MAPbI_3$), resulted in significant efficiency improvements with PCEs reaching 15–17%.[26,27] To address the mechanical fragility of conventional ITO electrodes, alternative electrode materials such as metal grids[37] and carbon-based[38] electrodes were explored, offering improved mechanical durability and device flexibility without compromising device performance.

2.2.3 Interface engineering and mechanical durability (2017–2018). As research progressed, a concerted focus on interface engineering emerged to address key limitations in flexible PSCs. By minimizing defect states and suppressing non-radiative recombination, researchers developed self-healing interface materials incorporating hydrogen bonding and covalent interactions, which significantly improved the interfacial contact between the perovskite and electrode layers. In parallel, the incorporation of stretchable electrode materials such as silver nanowires (Ag NWs) and graphene provided improved mechanical flexibility and resistance to cracking under strain, directly addressing the mechanical instability of earlier devices. The synergistic effect of optimized interfaces and flexible electrodes not only pushed the PCE beyond 18% but also substantially enhanced the bending stability and mechanical durability of F-PSCs.[28,29]

2.2.4 Breakthroughs in interface engineering (2019). In 2019, notable advancements in interface engineering propelled the development of F-PSCs. Studies showed that precise control over the thickness and morphology of SnO_2-based ETLs could effectively reduce optical losses and enhance light absorption on PEN/ITO substrates. These improvements led to a record PCE of 19.51%, with devices maintaining 95% of their initial PCE after 6000 mechanical bending cycles.[30] Key advancements included enhanced charge transport, effective defect suppression, and increased open-circuit voltage (V_{OC}), all contributing to both improved PCE and mechanical reliability.

2.2.5 Suppressing non-radiative recombination (2020). In 2020, a novel passivation strategy using a herbal extract was introduced, where a small amount of artemisinin (0.22 mol%) was employed as a defect passivation agent. This approach effectively suppressed the formation of deep-level defects through lead ion (Pb^{2+}) complexation, leading to a significant improvement in PCE to 21.10% and enhanced device stability.[31] Under accelerated aging conditions, F-PSCs demonstrated exceptional long-term performance.

2.2.6 Hybrid solar cells (HSCs) for near-infrared light absorption (2021). To mitigate the limited absorption capabilities in the near-infrared (NIR) region, researchers developed hybrid solar cells (HSCs) by incorporating low-bandgap bulk heterojunction (BHJ) layers into inverted perovskite architectures. This innovation enabled remarkable PCEs of 23.80% for rigid HSCs and 21.73% for their flexible devices,[32] thereby highlighting their promise for wearable electronics and stable, long-term operation.

2.2.7 Large-area manufacturing and interface modification (2022). Further progress in interface engineering led to the development of pentylammonium acetate (PenAAc) surface treatments, which improved perovskite nucleation and crystallization. As a result, F-PSCs achieved a notable PCE of 23.68% in small-area devices and PCE of 21.52% for large-area devices (1.0 cm^2), while retaining 91% of their efficiency after 5000 bending cycles.[33] These advancements marked a critical step toward scalable and reliable manufacturing.

2.2.8 Buried interface engineering and stress-release strategies (2023). In 2023, attention turned to the role of buried interfaces in controlling perovskite film morphology and suppressing defect formation. The introduction of proline hydrochloride (PF) as a buried interlayer effectively stabilized the α-phase of formamidinium lead iodide ($FAPbI_3$) and mitigated stress-induced degradation. This breakthrough led to a record PCE of 24.61% (certified at 23.51%), with the devices meeting the stability standards set by the International Summit on Organic Photovoltaic Stability (ISOS). This achievement marks a significant milestone in the development of F-PSCs with long-term operational durability.[34]

2.2.9 Self-assembled monolayers (SAMs) for interface optimization (2024). In 2024, the implementation of asymmetric π-extended self-assembled monolayers (SAMs), such as (4-(9*H*-dibenzo[*a*,*c*]carbazol-9-yl)butyl)phosphonic acid (A-4PADCB), brought notable improvements at the interface between the flexible substrate and perovskite layer. These SAMs promoted better grain growth, enhanced film uniformity, and passivated interfacial defects. As a result, F-PSCs achieved a record PCE of 25.05% in small-area devices, and a certified PCE of 19.51% (with a measured PCE of 20.64%) for the large-area module.[35] These advancements significantly accelerated the commercialization prospects of large-area F-PSC technologies.

2.2.10 Crosslinking strategies for mechanical durability and scalability (2025). Recent developments have focused on enhancing mechanical robustness through crosslinking strategies. A novel crosslinking monomer, (2,5-dioxopyrrolidin-1-yl) 5-(dithiolan-3-yl)pentanoate (FTA), was introduced to chemically passivate defects and control perovskite crystallization. The resulting crosslinked FTA [CL(FTA)] structure effectively stabilized grain boundaries, reduced residual stress, and improved mechanical durability. Consequently, F-PSCs achieved a high PCE of 24.64% (certified PCE of 24.08%),[36] while a large-area module reached a PCE of 17.13%, underscoring their potential for industrial-scale production.

2.2.11 Development of flexible tandem PSCs. While significant advancements have been achieved in improving the efficiency, stability, and mechanical durability of F-PSCs, single-junction architectures are gradually nearing their theoretical efficiency limits. To overcome this performance plateau, tandem device architectures—especially those incorporating perovskite materials as one or both sub-cells—have emerged as a promising strategy. By stacking two photoactive layers with complementary absorption spectra, tandem solar cells can more efficiently harvest the solar spectrum and thus surpass the

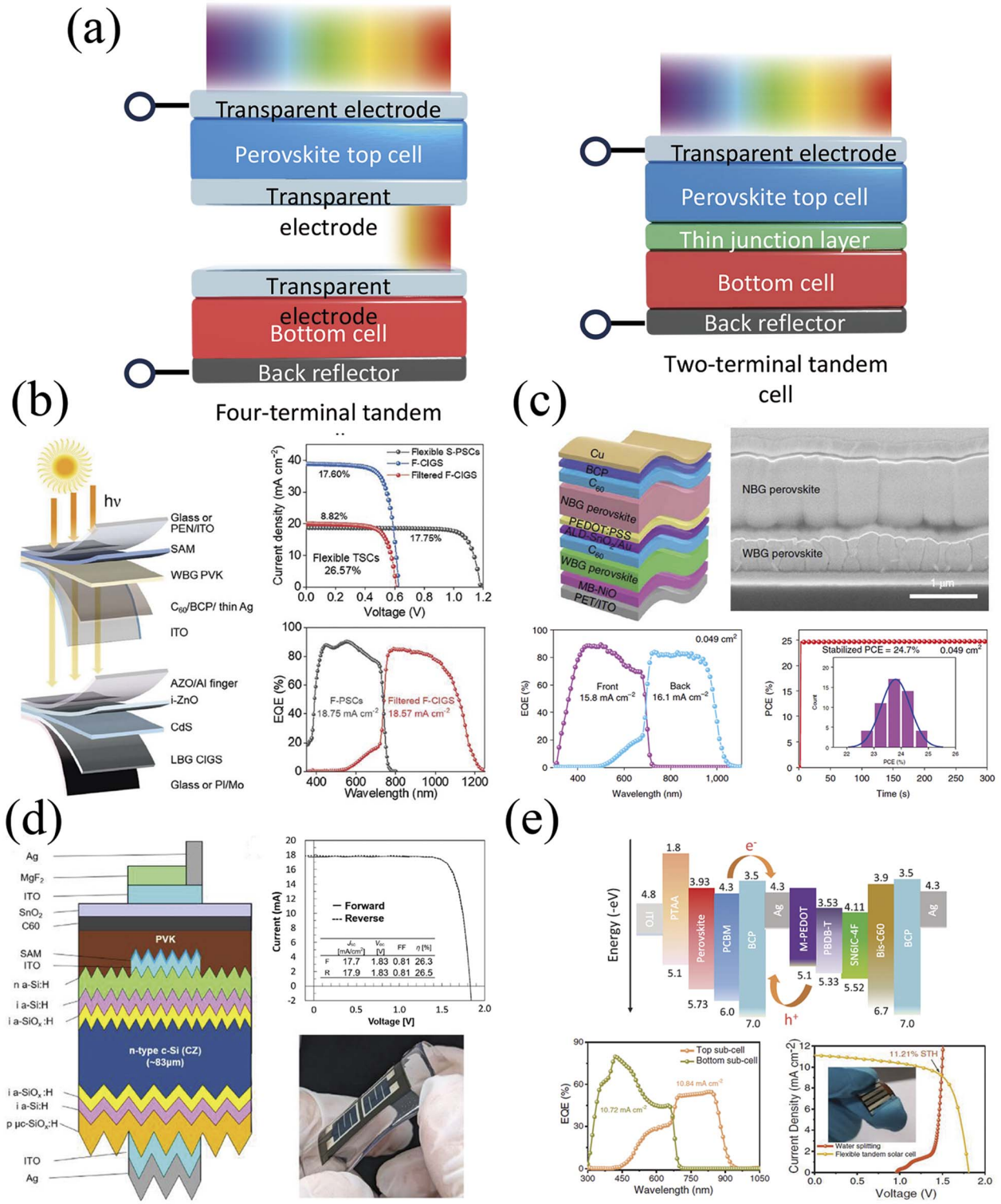

Fig. 2 (a) Schematic illustration of 4-terminal (4T) and 2-terminal (2T) perovskite tandem solar cell (TSC) architectures. (b) Structure of flexible perovskite (PVK)/CIGS 4T TSCs. Shown are the *J*–*V* curves of flexible CIGS (F-CIGS), filtered F-CIGS, and flexible single-junction perovskite solar cells (S-PSCs) with ARP surface modification. Also shown are the EQE spectra of ARP-treated S-PSCs and filtered F-CIGS, with integrated J_{SC} values of 18.75 and 18.57 mA cm^{-2}, respectively.[43] (c) Device structure and cross-sectional SEM image of a flexible all-perovskite tandem solar cell. The EQE spectra and stabilized power output of the champion flexible tandem cell are shown for a device with an aperture area of 0.049 cm^2.[50] (d) Schematic diagram and *J*–*V* characteristics of a flexible perovskite/thinned silicon tandem solar cell. Images of the fabricated flexible tandem device are also shown.[55] (e) Energy level alignment of a 2T perovskite–organic tandem solar cell. EQE spectra of the wide-bandgap perovskite top subcell and low-bandgap OPV bottom subcell are presented, along with the *J*–*V* curve of the flexible tandem device under simulated AM 1.5 G illumination. Inset: photograph of the flexible tandem device driving water splitting using NiFe LDH electrodes in a two-electrode configuration.[57]

Shockley–Queisser limit of single-junction devices. Although tandem integration has been successfully demonstrated on rigid substrates, adapting these architectures to flexible platforms introduces both new opportunities and challenges, including mechanical compatibility, interconnection design, and fabrication process integration. In recent years, various types of flexible tandem perovskite solar cells (F-TPSCs) have been reported, including monolithic two-terminal (2T) and mechanically stacked four-terminal (4T) configurations, as shown in Fig. 2(a). These flexible tandems span diverse material combinations such as perovskite/copper indium gallium selenide (PVSK/CIGS), all-perovskite tandems (PVSK/PVSK), perovskite/silicon (PVSK/Si), and perovskite/organic photovoltaics (PVSK/OPV). In the following sections, we review recent developments in F-TPSCs, with a focus on materials engineering, device architectures, and integration strategies adopted in 2T and 4T configurations. Special emphasis is placed on the interplay among flexibility, performance, and scalability, as well as the emerging role of tandem technologies in enabling next-generation lightweight, high-efficiency solar energy solutions.

2.2.11.1 Flexible perovskite/CIGS tandem solar cells. Early demonstrations of flexible perovskite/CIGS tandem solar cells were reported by Pisoni *et al.* (2017), who directly deposited perovskite layers onto flexible CIGS encapsulation front sheets, achieving stabilized efficiencies of 10.9% on 1.03 cm^2 and 13.2% on 0.15 cm^2 devices. By incorporating a transparent rear electrode (In_2O_3:H), they obtained near-infrared-transparent perovskite cells exceeding 12% efficiency, enabling flexible 4T tandem devices to achieve combined efficiencies of 18.2%.[39] Building upon this, Pisoni *et al.* (2018) introduced a multistage hybrid vacuum–solution deposition process to improve PbI_2 layer morphology and film uniformity, resulting in F-PSC efficiencies increasing from 14.2% to 15.8%. The use of amorphous indium zinc oxide (IZO) as a transparent conductive oxide enhanced mechanical durability, preserving over 80% efficiency after 1000 bending cycles at a 4 mm radius, while tandem efficiencies reached 19.6%.[40] Luo *et al.* (2023) advanced the field by optimizing flexible CIGS absorbers through a modified three-step co-evaporation process with controlled Ga distribution and Ag doping, achieving high crystallinity, enlarged grain size, and double GGI grading, yielding bottom cell efficiencies of 18.93% on polyimide substrates processed below 450 °C. Coupling this with a semitransparent flexible perovskite top cell (15.31%), they demonstrated fully flexible 4T tandems with a record PCE of 21.56%.[41] Zheng *et al.* (2024) fabricated the first monolithic perovskite/CIGS tandem on flexible conductive steel substrates, achieving a PCE of 18.1%, combining mechanical robustness with scalable tandem integration.[42] Tang *et al.* (2024) applied a dual passivation strategy targeting grain boundaries and interfaces in wide-bandgap perovskite top cells, which improved crystallinity, reduced non-radiative recombination, and enhanced charge transport, enabling a flexible 4T tandem efficiency of 26.57%, the highest reported to date, as shown in Fig. 2(b).[43] Tian *et al.* (2025) identified that the commonly used aluminum-doped ZnO (AZO) transparent conductive layer damages perovskite films and demonstrated that inserting an indium zinc oxide (IZO) interlayer protects the perovskite top cell, resulting in 21.24% efficiency and improved thermal stability; unencapsulated devices retained 80% of their initial efficiency after 120 minutes at ~90 °C under continuous maximum power point operation, whereas devices without the IZO degraded within 25 minutes.[44] Jeong *et al.* (2025) utilized a polyimide-coated soda-lime glass substrate with a lift-off process to suppress alkali diffusion, resulting in enhanced CIGS grain growth and carrier concentration, and achieved a certified PCE of 22.8% and a power-per-weight ratio of 6.15 W g^{-1}.[45] Tang *et al.* (2025) introduced [4-(7*H*-dibenzo[*c*,*g*]carbazol-7-yl)butyl]phosphonic acid (4PADCB) surface modification on RF-sputtered NiO_x films, improving band alignment and reducing voltage losses at the hole transport layer/perovskite interface, reaching a PCE of 22.8% and V_{OC} of 1.82 V.[46] Ying *et al.* (2025) developed an antisolvent-seeding approach to decouple SAM adsorption from dissolution and enhance perovskite crystallinity on rough flexible CIGS surfaces, achieving a certified PCE of 23.8% on devices (1.09 cm^2) with over 90% performance retention after 320 hours and 3000 bending cycles.[47] Collectively, these advances in absorber engineering, interface modification, substrate selection, and interlayer design have enabled substantial improvements in efficiency, mechanical durability, and thermal stability in flexible perovskite/CIGS tandem solar cells.

2.2.11.2 Flexible all-perovskite tandem solar cells. Several recent studies have advanced flexible all-perovskite tandem solar cells by addressing critical challenges in interface engineering, material stability, and scalable fabrication. Palmstrom *et al.* (2019) introduced a nucleophilic polymer nucleation layer enabling conformal atomic layer deposition of aluminum zinc oxide (AZO) as a recombination layer, preventing shunting and protecting bottom subcells; simultaneously, they tuned wide-bandgap perovskites *via* mixed A-site cations to improve stability, achieving efficiencies of 23.1% on rigid substrates (area not specified) and 21.3% on flexible substrates, respectively.[48] Lai *et al.* (2022) utilized SAMs as hole-selective contacts combined with post-deposition 2-thiopheneethylammonium chloride treatment to suppress recombination and achieve high-quality 1.77 eV wide-bandgap films, resulting in flexible 4T tandems with a PCE of 22.6% and 2-terminal tandems with a PCE of 23.8% and a record V_{OC} of 2.1 V.[49] Li *et al.* (2022) developed a molecule-bridged hole-selective contact using carbazole-based phosphonic acid self-assembled monolayers to enhance interfacial charge extraction and mechanical durability, with devices retaining performance after 10 000 bending cycles at a 15 mm radius, reaching a certified PCE of 24.4% on flexible devices (area not specified), as shown in Fig. 2(c).[50] Babu *et al.* (2022) demonstrated scalable blade-coating deposition of both wide- and narrow-bandgap layers on flexible substrates, producing 50 cm^2 4T tandem modules with a PCE of 15.3%; their robust two-step lamination encapsulation ensured thermal stability up to 800 h at 70 °C and outdoor T_{80} exceeding 2000 h under MPPT.[51] Pious *et al.* (2023) investigated SnF_2 additives in Pb–Sn narrow-bandgap perovskites, revealing the formation of a fluorinated tin oxide passivation layer and fluorine ion accumulation at interfaces, which reduced

recombination and improved quasi-Fermi level splitting; optimized SnF_2 concentrations led to flexible Pb–Sn single-junction PSCs with 18.5% efficiency and flexible 4T all-perovskite tandems with 23.1% PCE.[52] Geng *et al.* (2025) recently reported flexible all-perovskite tandem solar cells using a bilateral anchoring strategy at the NBG perovskite/PEDOT:PSS interface, where 2-bromoethylamine hydrobromide (2-BH) enhanced interfacial adhesion and suppressed Sn oxidation.[53] As a result, flexible narrow-bandgap single-junction devices achieved a PCE of 18.5% with 95% retention after 3000 bending cycles, and monolithic tandem cells reached a certified PCE of 24.01%. Together, these works underscore the critical roles of interface passivation, compositional engineering, and scalable processing in pushing flexible all-perovskite tandem solar cells toward higher efficiency and mechanical robustness.

2.2.11.3 Flexible perovskite/silicon tandem solar cells. Wang *et al.* (2024) demonstrated the first flexible perovskite/silicon tandem solar cell by enhancing the mechanical flexibility of an ultrathin (~30 μm) crystalline silicon bottom cell through wafer thinning and light-trapping texture optimization, while maintaining optical performance. The addition of a capping layer on the perovskite top cell shifted the neutral mechanical plane, further improving bending durability. The flexible tandem device achieved a certified stabilized efficiency of 22.8% with a power-to-weight ratio of 3.12 W g^{-1}, maintaining 98.2% of its initial efficiency after 3000 bending cycles at a 1 cm radius and 90.6% after 100 hours of maximum power point operation.[54] Shishido *et al.* (2025) advanced flexible perovskite/silicon tandems by integrating an inverted perovskite top cell onto a bendable 60 μm-thick microtextured silicon heterojunction (SHJ) bottom cell. The incorporation of a low-refractive-index doped layer enhanced optical management, boosting the SHJ cell efficiency to over 21%. Optimization of self-assembled monolayers on the textured surface led to a flexible tandem efficiency of 26.5% on devices with an active area not specified, as shown in Fig. 2(d). This work also suggests further improvements *via* current matching through bifacial SHJ designs and emphasizes the need for comprehensive mechanical durability evaluation.[55] More recently, Sun *et al.* demonstrated flexible perovskite/c-silicon monolithic tandem solar cells with textured surfaces by emphasizing the importance of perovskite phase homogeneity to simultaneously promote charge transfer and mitigate residual stress at the perovskite/Si interface.[56] This strategy enabled excellent mechanical stability with a bending curvature of 0.44 cm and yielded a certified PCE of 29.88% (steady-state 29.2%, 1.04 cm^2 aperture area), representing the highest performance reported for flexible perovskite-based photovoltaic devices to date.

2.2.11.4 Flexible perovskite/organic photovoltaics tandem solar cells. Li *et al.* (2020) demonstrated a monolithic perovskite–organic tandem solar cell combining a 1.74 eV wide-bandgap perovskite top cell with a 1.30 eV low-bandgap organic PBDB-T:SN6IC-4F bottom cell, achieving a PCE of 15.13% and a high V_{OC} of 1.85 V on a small active area device. The low-temperature fabrication process and material flexibility enabled the realization of flexible tandem devices with a PCE of

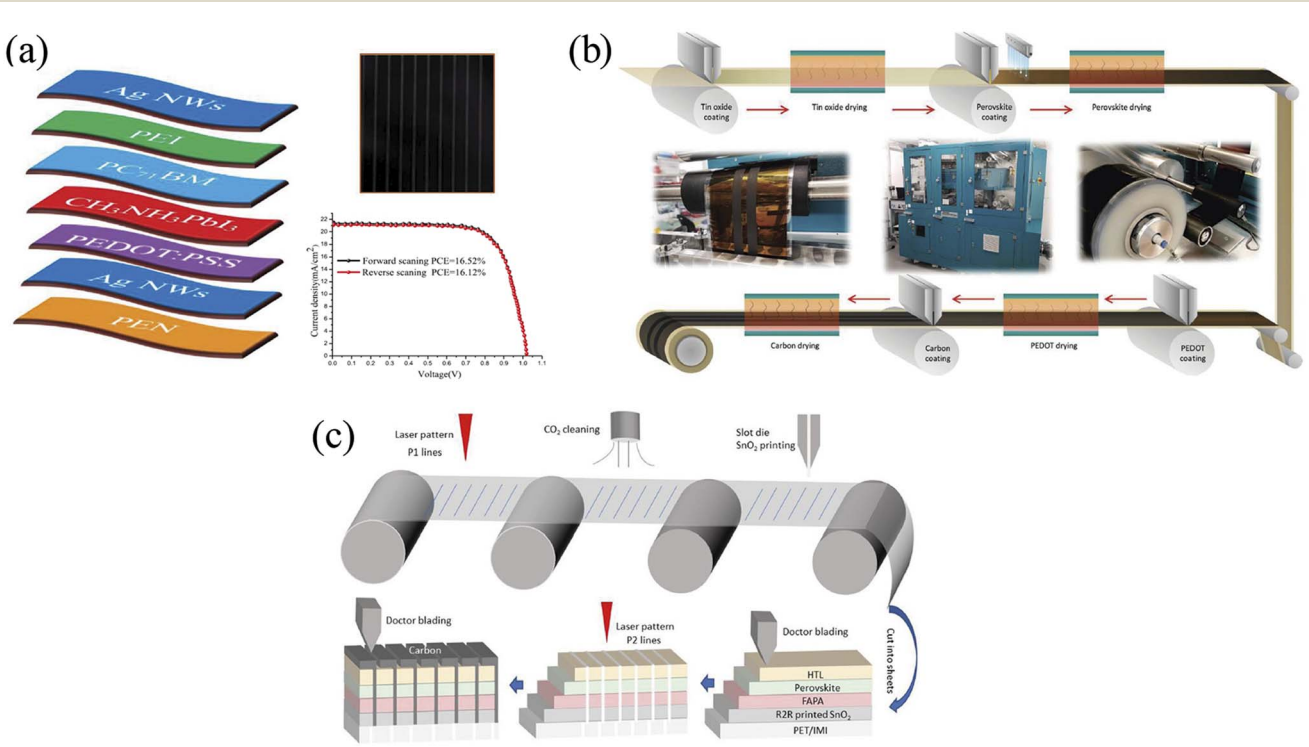

Fig. 3 (a) Structural diagram of the perovskite solar cell architecture. Photograph of a 10 cm × 12 cm perovskite solar cell. Hysteresis characteristics measured at the maximum power point.[58] (b) Schematic illustration of the R2R slot-die coating process used for fabricating perovskite solar cells, featuring a fully printable carbon top electrode.[59] (c) Workflow for manufacturing F-PSMs, including laser patterning, CO_2 snow jet cleaning, R2R slot-die coating, doctor blading, and stencil printing. F-PSCs follow a similar process but omit certain laser patterning steps.[60]

13.61%, retaining excellent optoelectronic performance. Additionally, the tandem cells were integrated into a photoelectrochemical water splitting system, reaching solar-to-hydrogen efficiencies of 12.30% (rigid) and 11.21% (flexible), as shown in Fig. 2(e).[57]

2.2.12 All-printed F-PSCs. Beyond advancements in small-area F-PSCs, one emerging technology that has demonstrated significant progress is fully printed F-PSCs, which are compatible with high-throughput R2R manufacturing. A critical challenge in scaling up such devices lies in controlling interfacial recombination losses that limit overall device performance. In 2021, Gao *et al.* successfully demonstrated fully inkjet-printed $CH_3NH_3PbI_3$ PSCs incorporating all functional layers—including a PEN/Ag NWs bottom electrode, PEDOT:PSS hole transport layer, $CH_3NH_3PbI_3$ absorber, $PC_{71}BM$ electron transport layer, PEI interfacial modifier, and Ag NWs top electrode. This comprehensive printing strategy enabled the formation of highly uniform and well-controlled films, leading to the fabrication of large-area devices up to 180 cm^2. Remarkably, the device with an active area of 120 cm^2 achieved a PCE of 16.78% ($V_{OC} = 1.02$ V, $J_{SC} = 21.96$ mA cm^{-2}, FF = 75%),[58] representing one of the highest PCEs reported for fully printed perovskite cells, as shown in Fig. 3(a). In addition, outstanding environmental stability was observed: unencapsulated devices retained 90% of their initial performance after six months under ambient conditions, while devices encapsulated with fluorinated thermoplastic polyurethane (FTPU) exhibited only a 5% degradation, underscoring the long-term reliability of this scalable, all-printed architecture for future commercial applications. In a groundbreaking advancement toward scalable manufacturing, Beynon *et al.* in 2023 demonstrated the first fully R2R coated perovskite solar cell, overcoming a long-standing limitation in printable back electrodes, as shown in Fig. 3(b). By employing a low-temperature n–i–p device architecture comprising SnO_2/perovskite/PEDOT/carbon, the team successfully replaced vacuum-deposited metal contacts with a fully solution-processable carbon electrode. This design enabled the formation of an ohmic contact between the p-type interlayer and the printable carbon electrode, mitigating interfacial incompatibilities and recombination losses. The resulting small-area devices exhibited power conversion efficiencies of 13–14%, comparable to their gold-contacted counterparts. Notably, the fully R2R-coated prototypes achieved a stabilized PCE of 10.8% without encapsulation, and demonstrated excellent operational durability, retaining 84% of their initial performance after 1000 hours under 70% relative humidity at 25 °C.[59] This work represents a pivotal step toward cost-effective, high-throughput production of perovskite photovoltaics *via* R2R processing. To address this, researchers introduced a fullerene-substituted alkylphosphonic acid dipole layer between the R2R-printed SnO_2 electron transport layer and the perovskite active layer. This strategic interface engineering reduced energy barriers and effectively suppressed buried interface recombination, enabling fully printed F-PSCs to achieve a PCE of 17.0% with negligible hysteresis and excellent mechanical durability, maintaining 95% of their initial performance after 3000 bending cycles. Furthermore, fully printed flexible perovskite solar modules (F-PSMs) with an aperture area of 20.25 cm^2 demonstrated a remarkable PCE of 11.6%,[60] as illustrated in Fig. 3(c). Notably, encapsulated F-PSMs exhibited excellent environmental stability, retaining 90% of their initial efficiency after 500 hours of damp-heat testing under ISOS-D3 conditions (65 °C, 85% RH). These advancements highlight the viability of fully printed architectures for large-area, flexible photovoltaic applications and underscore the importance of interfacial design in overcoming scalability barriers for next-generation perovskite solar technologies.

2.3 Issues of large-area F-PSCs

The development of large-area F-PSCs involves distinct technical challenges concerning material stability, mechanical reliability, and scalable process engineering. This section outlines five key issues that must be addressed to achieve industrial feasibility and ensure the long-term deployment of large-area F-PSCs.

2.3.1 Process scalability and cost-effective manufacturing. Scaling up from laboratory-scale devices to large-area flexible modules involves complex trade-offs among throughput, uniformity, and cost. Fabricating high-quality perovskite layers over flexible substrates using scalable methods such as blade coating or slot-die coating often results in non-uniform film thickness, inconsistent crystallinity, and interfacial defects. Moreover, flexible polymeric substrates generally cannot tolerate high-temperature post-processing, which necessitates the development of low-temperature or photonic annealing techniques. To ensure commercial feasibility, the overall production cost, including that of flexible substrates, encapsulation materials, and conductive electrodes, must be minimized while maintaining high yield and reproducibility. Although integration with R2R processing offers great potential for mass production, it remains technologically challenging due to these limitations.

2.3.2 Mechanical stability and stress-induced degradation. Unlike rigid devices, flexible solar cells are frequently exposed to mechanical stress such as bending, folding, or rolling. These repetitive mechanical deformations can lead to microcracks in the perovskite layer or delamination at material interfaces, which compromise device performance. The mechanical mismatch between brittle active layers and soft polymeric substrates further increases the risk of structural failure. To address this issue, researchers are exploring the use of stretchable or ductile transport layers, flexible electrodes such as silver nanowires or carbon nanotubes, and stress-tolerant encapsulation materials. Nevertheless, ensuring mechanical durability while maintaining electrical performance remains a significant challenge.

2.3.3 Intrinsic and environmental stability of perovskite materials. Perovskite materials are highly sensitive to external factors such as moisture, oxygen, ultraviolet (UV) light, and elevated temperatures. In flexible devices, the mechanical strain introduced during deformation can accelerate the formation of defects, which in turn amplifies environmental degradation pathways. Furthermore, flexible polymeric substrates typically

offer inferior barrier properties compared to rigid glass, leading to faster ingress of moisture and oxygen. This increases the risks of phase instability, ion migration, and interfacial degradation. To resist these issues, advanced encapsulation strategies employing multilayer barrier films or atomic layer deposition (ALD) coatings are essential. In parallel, material innovations aimed at developing environmentally stable perovskite compositions and robust interfacial layers are crucial for enhancing long-term operational stability.

2.3.4 Electrical performance and charge extraction in large areas. As the device area increases, maintaining uniform electrical performance becomes more difficult. Longer charge transport paths can lead to increased series resistance and reduced fill factors. Additionally, non-uniform depositions can cause spatial variations in current density and localized recombination losses. The selection of transparent conductive electrodes (TCEs) is particularly critical in flexible devices, which must combine high optical transparency, low sheet resistance, and mechanical flexibility. Traditional ITO is often unsuitable due to its brittleness. Alternatives such as metal nanowire networks, conductive polymers, or hybrid composites are promising, but scaling them up without compromising device efficiency remains a significant obstacle.

2.3.5 Interface engineering and layer compatibility on flexible substrates. Effective charge transport and device efficiency require optimal interfacial contact and energy-level alignment between successive layers. However, achieving this in flexible devices is more challenging due to the surface characteristics of polymeric substrates, which may exhibit high roughness, poor wettability, and limited chemical compatibility. These factors can hinder uniform film formation and weaken adhesion between layers. Furthermore, the limited heat tolerance of flexible substrates restricts the use of conventional solvent systems and annealing conditions. Interface engineering strategies such as self-assembled monolayers, surface modification treatments, and tailored buffer layers play a crucial role in promoting uniformity, adhesion, and charge transfer while preserving mechanical compliance. Balancing these demands with the requirements of scalable processing continues to be a critical area of research.

2.4 Key challenges of coating processes on flexible substrates

The development of scalable coating methods for flexible perovskite solar cells faces several critical challenges that must be addressed to enable reliable large-area manufacturing. Unlike rigid glass substrates, flexible polymeric substrates exhibit increased surface roughness, reduced thermal stability, and enhanced mechanical compliance, all of which complicate film formation and adhesion. These characteristics amplify the influence of solvent drying dynamics, interfacial compatibility, and mechanical strain distribution, making process optimization significantly more complex. The quality of the perovskite/transport layer interfaces is strongly influenced by the chosen coating method, as film formation dynamics directly affect wetting, adhesion, grain boundary distribution, and ultimately defect density. These interfacial properties, in turn, determine charge extraction efficiency, trap-assisted recombination, and the mechanical durability of F-PSCs. In this context, each coating technique, including blade coating, slot-die coating, spray coating, and inkjet printing, presents distinct limitations that require critical evaluation in terms of scalability, film uniformity, and defect control. A systematic analysis of these challenges provides a foundation for assessing which methodologies can be adapted for industrial roll-to-roll fabrication and for identifying targeted process innovations that may overcome the bottlenecks unique to flexible substrates.

2.4.1 Blade coating. The main challenge for blade coating lies in translating laboratory-scale demonstrations into continuous R2R manufacturing. At the lab scale, film thickness is easily tuned by the blade gap and coating speed, but under R2R conditions, the coating environment is far less controlled. Solvent evaporation becomes strongly influenced by air flow, substrate movement, and ambient humidity, leading to variability in crystallization dynamics. The shear-driven spreading of precursor inks promotes relatively smooth coverage but is highly sensitive to ink viscosity and substrate wettability. Insufficient wetting often induces interfacial voids and poor adhesion, which weaken mechanical robustness during bending. Grain boundary distribution is often less uniform, leading to localized trap formation unless solvent engineering or additives are employed. These interfacial shortcomings typically translate into reduced fill factor and accelerated efficiency loss under cyclic bending. In particular, R2R processes require higher throughput, where solvent volatility and drying uniformity are much harder to maintain compared with static coating. Moreover, flexible polymeric substrates introduce additional complexity because surface roughness and mechanical compliance affect wetting behavior, often resulting in film non-uniformities or discontinuities during bending. A critical comparison between blade coating in the laboratory and its R2R adaptation would therefore highlight the gap between proof-of-concept fabrication and scalable production, and underscore the need for innovations in solvent engineering, in-line drying control, and substrate surface modification strategies.

2.4.2 Slot-die coating. For slot-die coating, the most critical aspects that need deeper discussion include the stability of the liquid meniscus, substrate preheating, and in-line drying control. Meniscus stability is governed by coating speed and ink rheology, and instability often results in thickness fluctuations and nonuniform edge coverage. Substrate preheating is often employed to adjust drying kinetics and improve nucleation, but excessive heating may accelerate solvent evaporation and induce pinhole formation. In-line drying methods, such as N_2-knife or IR-assisted heating, help regulate the wet-to-dry transition, yet their effectiveness depends strongly on solvent composition and coating width. Another important consideration is the adaptability of slot-die coating to different perovskite compositions: formamidinium-based, mixed-halide, or triple-cation systems each require unique solvent environments with distinct viscosities and drying rates. Without careful optimization, achieving uniform large-area films remains

difficult. The controlled meniscus and continuous flow typically yield highly uniform films with low interfacial roughness. However, variations in drying rate across wide flexible substrates can generate interfacial stress and nonuniform grain boundaries. Appropriate preheating and solvent engineering mitigate these issues, resulting in reduced trap density and more stable interfaces under mechanical strain. Consequently, slot-die coated devices often exhibit higher reproducibility and longer bending lifetimes compared with blade-coated devices, making this method particularly attractive for scalable fabrication. Overall, slot-die coating offers high scalability but requires precise integration of process parameters to ensure reproducibility across different material systems.

2.4.3 Spray coating. The scalability of spray coating depends strongly on the control of spray parameters, which directly determine film morphology and uniformity. Nozzle type is central: pneumatic nozzles generate broader droplet distributions, whereas ultrasonic nozzles produce more uniform and finer droplets. Carrier gas pressure regulates the velocity and density of deposition, and the nozzle–substrate distance influences droplet impact dynamics and film coverage. Improper parameter tuning can result in nonuniform thickness, coffeering morphology, or excessive porosity. In addition, solvent evaporation during droplet flight and impact governs nucleation and grain growth, making it difficult to achieve uniform crystallization across large flexible substrates. Droplet-based deposition often produces rougher interfaces due to splashing, droplet coalescence, and incomplete film merging. These irregularities increase trap density and weaken adhesion to underlying transport layers. Optimizing spray parameters (nozzle type, distance, carrier pressure) and applying *in situ* heating can significantly improve film–substrate interaction and reduce defect-assisted recombination. Nevertheless, without precise control, spray-coated films tend to show increased leakage current, larger variability in performance, and poor durability under repeated mechanical strain. Without systematic optimization, significant inhomogeneity appears in large-area modules. A thorough understanding of the interplay between spray parameters and film formation is therefore essential for engineering spray coating toward reliable large-area flexible PSC fabrication.

2.4.4 Inkjet printing. For inkjet printing, three aspects deserve more critical analysis, including ink formulation, substrate compatibility, and printhead reliability. Ink formulation requires a careful balance of viscosity, surface tension, and solvent volatility to ensure stable droplet ejection while preventing the formation of satellite drops. Substrate compatibility is equally important, since polymeric substrates with different surface energies can cause either droplet spreading or dewetting, both of which result in film non-uniformities. Printhead clogging remains a persistent problem because perovskite precursors may crystallize at the nozzle, especially under ambient conditions. These issues directly affect printing resolution, defect density, and device reproducibility. The digital deposition of discrete droplets can cause local thickness variation and interfacial roughness at droplet boundaries, which are prone to defect formation and charge trapping. Proper ink formulation combined with surface energy modification

Table 2 Post-deposition steps, impacts, challenges, and possible solutions for F-PSCs

Post-deposition step	Impact on flexible substrates	Challenges	Possible solutions
Ink formulation (solvent and additive engineering)	Governs wetting behavior, nucleation uniformity, and stress distribution during bending	Flexible substrates often exhibit higher surface roughness and lower surface energy, resulting in incomplete wetting and dewetting	Surface energy modification, mixed-solvent systems with controlled polarity, and functional additives to tune nucleation and enhance film continuity
Anti-solvent treatment	Promotes rapid crystallization, reducing pinholes and improving coverage	During dynamic coating on flexible substrates, synchronization of anti-solvent application is difficult; uneven dripping leads to nonuniform film crystallization	Vapor-assisted crystallization, in-line gas quenching, and programmable spraying with precise timing relative to the coating front
Thermal annealing	Essential for grain growth and defect passivation; governs stress relaxation on bendable substrates	Flexible polymers deform or shrink at elevated temperatures (>150 °C), resulting in cracks or interfacial delamination	IR-assisted annealing, and low-temperature chemical annealing routes compatible with polymer substrates
Solvent annealing/vapor treatment	Enhances crystal orientation, reduces grain-boundary density, and improves ductility	Excess solvent vapor may cause swelling or chemical attack of polymer substrates; achieving spatially uniform exposure on large-area films is difficult	Controlled humidity/solvent chambers, inert-gas dilution, and short-pulse vapor dosing optimized for polymer stability
Interface modification	Reduces trap density, improves adhesion under bending, and buffers mechanical stress	Interlayers must be ultrathin, flexible, and resistant to cracking; some SAMs may dissolve in coating solvents	Nanometer-thick cross-linked polymer interlayers, robust SAMs, and mechanically compliant treatments such as elastomeric coatings

improve wetting uniformity and interfacial adhesion. Printhead clogging, however, often leads to inconsistent film quality. These interfacial issues directly impact reproducibility, often resulting in lower efficiency and accelerated mechanical degradation compared with slot-die and blade coating. Despite its advantages in patterning precision and material efficiency, inkjet printing remains limited in throughput and long-term stability. Beyond these intrinsic challenges, the realistic potential of inkjet printing should be evaluated in comparison with other scalable methods such as blade coating and slot-die coating. Although inkjet offers distinct advantages in patterning precision and material utilization, it remains constrained by limited throughput and cost-effectiveness. A comparative discussion on manufacturing cost, scalability, and interfacial defect formation would clarify where inkjet printing can realistically compete, and where conventional scalable methods remain superior.

Taken together, the choice of coating method plays a decisive role in defining interfacial roughness, trap density, adhesion, and mechanical stability. Among these methods, slot-die coating generally offers the most favorable balance between interfacial smoothness, defect suppression, and durability, whereas spray coating and inkjet printing require more extensive optimization to mitigate their inherent interface-related drawbacks. Interface engineering strategies, including the use of SAMs, polymeric interlayers, and surface treatments, remain indispensable to further reduce interfacial defects and ensure that coated films achieve both high electronic performance and reliable mechanical robustness on flexible substrates.

Post-deposition engineering plays a decisive role in defining the microstructural quality and operational stability of perovskite films fabricated on flexible substrates. Each processing step, from ink formulation to interface modification, directly influences nucleation, crystallization kinetics, film continuity, and stress management during bending. However, transferring these processes from rigid glass to polymer supports introduces additional challenges, including low surface energy, high roughness, poor thermal tolerance, and susceptibility to solvent-induced damage. Table 2 summarizes the impacts, challenges, and possible solutions of the key post-deposition steps for flexible perovskite devices. To overcome these barriers, a combination of tailored approaches is required. Ink formulation strategies can be optimized through surface energy tuning and additive engineering. Anti-solvent treatments must be adapted to dynamic coating processes by employing vapor-phase or programmable methods. Annealing protocols need to shift from conventional thermal heating toward rapid photonic or low-temperature chemical methods that are compatible with flexible polymers. Solvent and vapor annealing need to balance crystal orientation improvement with substrate safety, which requires precise control of exposure environments. Finally, interface modification is indispensable for maintaining adhesion and reducing defect densities, where robust interlayers and self-assembled systems provide mechanical compliance. In summary, the careful integration of these post-deposition strategies enhances perovskite film performance and simultaneously addresses the intrinsic weaknesses of polymer substrates. This comprehensive approach paves the way for scalable, durable, and high-performance F-PSCs.

3. Various coating technologies for PSCs

Although PSCs have achieved remarkable PCEs, their typical device area remains below 1 cm^2, which is significantly smaller than that of commercial silicon solar cells. To enable commercialization, scalable and high-yield production techniques are essential for fabricating large-area devices. This requirement is not only critical for the mass production of PSCs but also for emerging applications such as tandem solar cells and BIPV, where large-area uniformity and process stability are of particular importance. To address these needs, various scalable coating methods have been developed, such as blade coating, slot-die coating, and spray coating. These solution-based techniques offer precise control over film thickness, allow for continuous deposition, reduce material waste, and improve production throughput. Early research efforts have primarily focused on applying these methods to rigid substrates such as glass, which offers excellent thermal stability and surface uniformity, providing favorable conditions for high-quality perovskite film formation. Building on these advancements, recent studies have extended these scalable processes to flexible substrates, aiming to transfer the benefits of large-area, low-cost manufacturing to F-PSCs. However, the mechanical properties and lower thermal tolerance of flexible substrates introduce additional challenges in terms of film uniformity, adhesion, and stability. For F-PSCs, interface engineering on polymeric substrates is essential not only for electronic optimization but also for ensuring layer compatibility with mechanically compliant substrates. Interfacial layers improve adhesion between the perovskite and underlying flexible substrates, suppress interfacial defects, and promote uniform crystallization, which together minimize the risk of fracture during bending and enhance charge transport pathways. By tailoring both the surface energy and mechanical compliance at critical interfaces, such strategies reduce delamination, maintain film continuity, and preserve PCE under repeated deformation. This demonstrates that achieving high PCE on flexible substrates requires addressing both interfacial chemistry and mechanical compatibility through deliberate interface engineering. By simultaneously enhancing mechanical stability and facilitating effective charge extraction, interfacial layers are essential for the realization of high-performance F-PSCs. Consequently, optimizing these scalable coating techniques for flexible devices has become a key focus in advancing the industrialization of F-PSCs. This review highlights recent progress in scalable deposition methods, discussing their development from rigid to flexible substrate applications, and examining the advantages, limitations, and critical factors that influence their implementation in commercial PSC manufacturing.

3.1 Blade coating

Blade coating has made notable progress in fabricating PSCs on glass substrates due to its simplicity, low cost, and scalability. This technique enables the deposition of uniform and

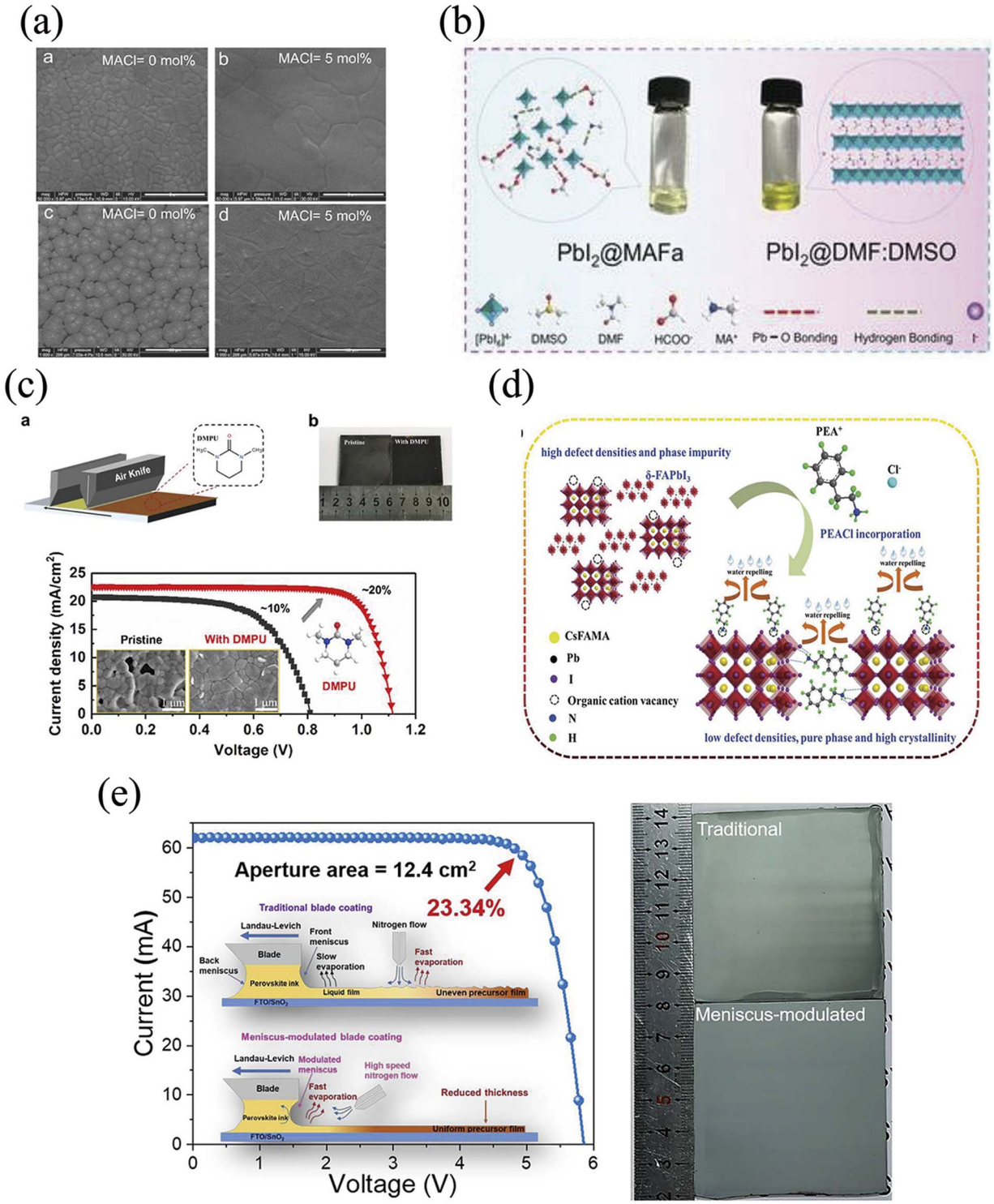

Fig. 4 (a) Morphological comparison of doctor-bladed perovskite films with and without 5 mol% MACl additive. The $MA_{0.6}FA_{0.38}Cs_{0.02}PbI_{2.975}Br_{0.025}$ thin films exhibit significantly improved surface smoothness and grain uniformity upon MACl incorporation. The scale bars are 2 μm and 100 μm, respectively.[62] (b) Photographic images of PbI_2@MAFa and PbI_2@DMF:DMSO precursor solutions, accompanied by a schematic diagram illustrating molecular interactions within each solution system. The PbI_2@MAFa solution leads to better crystallization behavior and improved film quality.[68] (c) A schematic illustration of the blade coating process used for fabricating FA-dominated perovskite films is presented, alongside the molecular structure of the *N*,*N*′-dimethylpropyleneurea (DMPU) additive. Photographs of the film backsides, with and without DMPU, highlight the enhancement in film uniformity and coverage achieved through DMPU incorporation.[69] (d) A schematic representation of the effects of PEACl modification is shown, demonstrating the suppression of the nonperovskite δ-phase, effective defect passivation, and improved water repellency. These features collectively enhance device stability and performance.[70] (e) Comparison between traditional blade coating and the meniscus-modulated blade coating technique. The schematic diagrams highlight key differences in fluid control and film formation. Photographs of 6 cm × 6 cm $FAPbI_3$ films fabricated using both methods clearly show the superior film uniformity achieved *via* the meniscus-modulated approach.[72]

crystalline perovskite films, significantly improving device performance. However, achieving precise control over film thickness, uniformity, and stability, particularly for large-area applications, remains a challenge. To address these limitations, recent research has focused on optimizing solvent engineering, anti-solvent treatment, and compositional modifications. For instance, Yang *et al.* extended the narrow processing window of anti-solvent treatment by using a mixed *N*-methyl-2-pyrrolidone (NMP)/DMF solvent, allowing processing within approximately 8 minutes. Their approach achieved PCEs of 18.55% (0.12 cm^2), 17.33% (1.2 cm^2), and 13.3% for a 12.6 cm^2 four-cell module, respectively.[61] Building on this, Tang *et al.* improved the perovskite composition by introducing cesium ion (Cs^+) and bromide ion (Br^-) into a $(MAPbI_3)_{0.6}(FAPbI_3)_{0.4}$ system, forming $MA_{0.6}FA_{0.38}Cs_{0.02}PbI_{2.975}Br_{0.025}$. With methylammonium chloride (MACl) as an additive, they achieved smooth, pinhole-free films and a stable PCE of 19.3%[62] (Fig. 4(a)). Xu *et al.* developed an NMP/*N*-methyl-2-pyrrolidinium ion ($NMPH^+$) solvent system that enhanced lead(II) iodide (PbI_2) solubility and stabilized α-$FAPbI_3$. Their method yielded PCEs of 21.35% (small-area), 17.07% (12.32 cm^2), and 14.17% (55.44 cm^2), respectively.[63] Two-step deposition has also proven effective. By sequentially depositing PbI_2/DMSO and formamidinium iodide (FAI)/isopropyl alcohol (IPA), researchers exploited strong coordination between DMSO and Pb^{2+} to form intermediate PbI_2–DMSO complexes, facilitating the formation of high-quality α-$FAPbI_3$ films.[64] Compositional engineering has played a critical role in enhancing stability and performance. Cs^+ incorporation into FA-based perovskites lowers the δ-to-α phase transition temperature, enhancing phase stability and moisture resistance.[65] Additives such as MACl can delay crystallization, promoting larger grain sizes and better film uniformity, thereby improving device performance.[66,67] Hui *et al.* introduced methylammonium formate (MAF) *via* a two-step process to further stabilize α-$FAPbI_3$. Combined with MACl, they achieved a high PCE of 24.1%. The unencapsulated devices retained 80% of their initial PCE after 500 hours under 85 °C thermal stress (Fig. 4(b)).[68] Li *et al.* utilized *N*,*N*′-dimethylpropyleneurea (DMPU) to enhance film morphology and passivate grain boundaries. Their 10 cm^2 module achieved a PCE of 17.71% and demonstrated excellent thermal and moisture stability (Fig. 4(c)).[69] To suppress surface defects, hydrophobic additives have also been applied. Wu *et al.* incorporated phenylethylammonium chloride (PEACl) into a CsFAMA-based triple-cation precursor, enhancing α-$FAPbI_3$ stability and defect passivation. This strategy resulted in a PCE of 22.0% with improved operational stability (Fig. 4(d)).[70] Interface engineering has also contributed significantly. Li *et al.* added a surfactant-like zinc phthalocyanine (ZnPc) compound into $MAPbI_3$, enabling better crystal growth and surface passivation. This approach allowed the formation of large-area (up to 16 cm^2) perovskite films, achieving a PCE of 18.3% (1.96

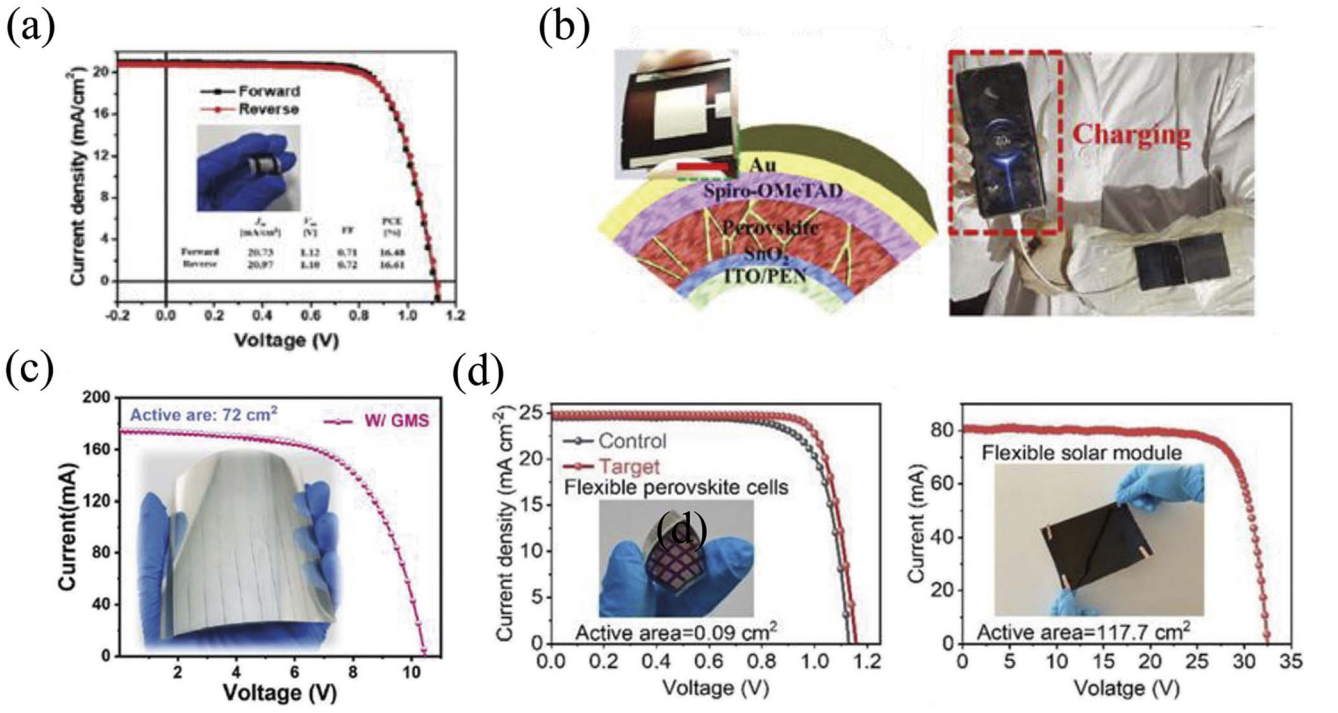

Fig. 5 (a) *J*–*V* curves of large-area F-PSCs (1 cm^2) utilizing a poly(3,4-ethylenedioxythiophene):poly(styrene sulfonate) (PEDOT:PSS) (35 nm)/PTAA bilayer as the hole transport layer. The insets show a photograph of the device and its key performance parameters.[73] (b) Schematic illustration of the F-PSC device architecture. The inset displays a photograph of a large-area flexible PSC (scale bar: 1 cm), and additional photos demonstrate its application as a wearable power source.[75] (c) *J*–*V* curves of blade-coated large-area F-PSMs with an active area of 100 cm^2.[77] (d) *J*–*V* curve of the champion flexible PSC with an active area of 0.09 cm^2, along with the *J*–*V* curve of an F-PSM featuring an active area of 117.7 cm^2.[78]

cm^2) and 20.5% (0.1 cm^2), respectively.[71] Notably, Huang *et al.* achieved the highest blade-coated PSC efficiency to date using a meniscus-modulated blade coating technique (Fig. 3(e)). They optimized a high-concentration DMF/NMP-based precursor and applied high-speed nitrogen flow to control crystallization, improving film uniformity and grain size. This method resulted in a record PCE of 25.31% (0.09 cm^2) and 23.34% (12.4 cm^2), with a certified PCE of 23.09%, demonstrating the scalability and potential of blade coating for high-performance PSCs.[72]

Blade coating has demonstrated significant progress in the fabrication of PSCs on glass substrates. However, transitioning to flexible substrates introduces new challenges. Flexible substrates such as PET and PEN typically exhibit lower thermal stability and higher surface roughness, both of which can compromise film uniformity and crystallinity. Moreover, ensuring reliable mechanical durability and effective encapsulation is critical for the practical deployment of F-PSCs. To address these challenges, recent research has focused on optimizing processing conditions, selecting suitable flexible substrates, and developing scalable coating strategies to improve the performance and stability of F-PSCs. For instance, Wang *et al.* introduced thiourea (TU) as an additive in the perovskite precursor solution to regulate crystal growth, resulting in improved film density and morphology on rough substrates. This approach enhanced interface engineering and led to a PCE of 19.41% and a record fill factor (FF) of 81%, as shown in Fig. 5(a).[73] In addition to morphology control, defect passivation has emerged as a crucial strategy. Additives such as ammonium chloride (NH_4Cl) can slow down nucleation and improve surface coverage, enabling the formation of small-area F-PSCs with PCEs of up to 19.72%, and large-area modules reaching 15.86%.[74] Mechanical robustness is another key concern. To this end, Xue *et al.* developed a temperature-responsive shape-memory polyurethane (SMPU) that can self-heal grain boundary cracks. By enhancing grain connectivity and passivating defects, SMPU effectively alleviated mechanical stress. As a result, blade-coated F-PSCs retained over 80% of their initial PCE after 6000 bending cycles at an 8 mm radius, achieving a peak PCE of 21.33%, as illustrated in Fig. 5(b).[75] To facilitate ambient and scalable fabrication, Jafarzadeh *et al.* proposed a DMF-free two-step deposition method using DMSO and IPA as solvents. PET/ITO flexible substrates were laminated onto glass carriers for sheet-to-sheet blade coating, yielding F-PSMs with PCEs of 6.58% (18.55 cm^2) and 3.92% (82.45 cm^2), respectively.[76] The strong coordination between DMSO and perovskite precursors enhanced solubility and crystallization, while air knife drying and a heated coating stage helped offset the low volatility of DMSO. To further improve film uniformity, Gong *et al.* introduced glycerol monostearate (GMS) as a dispersant in DMF/NMP-based ink. GMS stabilized perovskite colloidal particles, prevented aggregation, and enhanced crystallization control. This enabled the fabrication of a 72 cm^2 blade-coated F-PSM with a PCE of 15.87%, as shown in Fig. 5(c).[77] Pushing the boundaries of ambient blade-coating fabrication, a recent study developed a $Cs_{0.05}FA_{0.95}PbI_3$ perovskite ink based on a DMF/NMP solvent system, incorporating 1-butyl-3-methylimidazolium thiocyanate (BPySCN) to fine-tune crystallization dynamics. This formulation enabled the fabrication of a large-area (117.0 cm^2) flexible n–i–p PSM with a PCE of 17.52% and a high specific power density of 1969.1 W kg^{-1},[78] as shown in Fig. 5(d).

Although blade coating has demonstrated remarkable progress in fabricating both small- and large-area PSCs on rigid glass substrates, its adaptation to flexible substrates continues to face persistent and multifaceted challenges. The impressive efficiencies and stabilities achieved through solvent engineering, interface modification, and compositional tuning highlight the potential of blade coating for scalable manufacturing. Nevertheless, the technique remains highly sensitive to various processing parameters such as substrate temperature, coating speed, ambient environment, and solvent volatility, which can hinder reproducibility and device uniformity, especially in industrial-scale production. Despite recent innovations such as the use of shape-memory polymers and surface passivation strategies that have improved the mechanical durability of flexible devices, intrinsic limitations of flexible substrates, including lower thermal stability and higher surface roughness, still obstruct optimal crystallization and long-term operational stability. A clear performance gap remains between rigid PSCs, which can achieve efficiencies of up to 25.31%,[72] and their flexible counterparts, whose efficiencies typically remain below 22%.[73–75] To bridge this gap and move blade coating toward commercial viability, future research should prioritize the development of standardized inline-compatible coating systems specifically designed for flexible substrates. These systems should incorporate feedback mechanisms for real-time film quality control. Furthermore, engineering solvent systems with tunable rheological properties, implementing low-temperature annealing strategies, and designing universal additives that balance crystallization dynamics with mechanical resilience are crucial steps toward enhancing both performance and stability. The successful transition of blade coating from a promising laboratory-scale technique to a robust and scalable manufacturing process relies on interdisciplinary collaboration among materials science, process engineering, and device physics.

3.2 Slot-die coating

Slot-die coating is a precise thin-film deposition technique widely used in PSC fabrication. Ink is delivered through a syringe pump to a coating head, forming an upstream and a downstream meniscus that control film formation. Integrated into R2R systems, slot-die coating enables high material utilization and large-area uniformity, making it suitable for multiple device layers, including the perovskite layer, hole transport layer (HTL), and ETL. Vak *et al.* first demonstrated slot-die-coated PSCs, achieving over 11% PCE with a sequential deposition method using nitrogen-assisted drying.[79] Hwang *et al.* later reported a fully slot-die-coated PSC, attaining 11.96% efficiency.[80] Despite its uniformity, challenges such as pinholes and cracks persist, necessitating drying optimization.[81] Rapid solvent evaporation often leads to precursor aggregation, particularly on metal oxide substrates.[82] Cotella *et al.* addressed this by

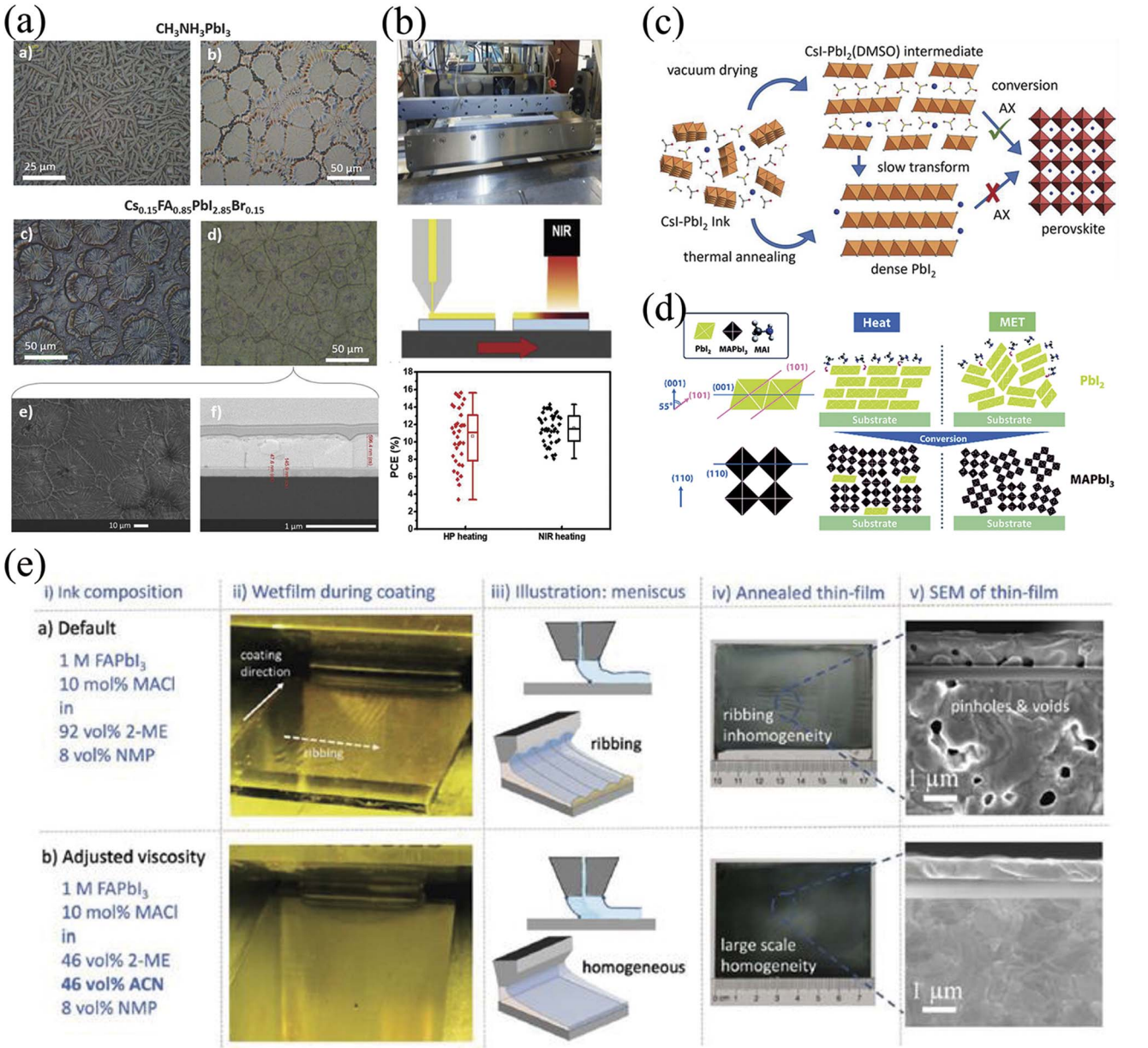

Fig. 6 (a) Microstructures of perovskite layers observed under an optical microscope, including $CH_3NH_3PbI_3$ layers dried at 140 °C using slow and fast temperature ramping, as well as $Cs_{0.15}FA_{0.85}PbI_{2.85}Br_{0.15}$ layers dried under similar conditions. The figure also includes an SEM image of the $Cs_{0.15}FA_{0.85}PbI_{2.85}Br_{0.15}$ layer processed with fast ramping, and a cross-sectional FIB-SEM image showing SnO_2 and perovskite layers coated on PET/ITO substrates.[84] (b) Slot-die coating machine integrated with NIR heating, along with performance statistics of devices processed under different heating conditions.[86] (c) Formation of a porous semi-amorphous $CsI-PbI_2$ (DMSO) precursor phase after vacuum drying the deposited $CsI-PbI_2$ ink. This structure is unstable and gradually converts into dense PbI_2 over time. In contrast, thermal annealing of the wet $CsI-PbI_2$ ink leads to the formation of highly crystalline, dense PbI_2, which, due to its compactness, cannot be completely converted into perovskite through slot-die coating.[88] (d) Schematic comparison of the relative orientations of PbI_2 films fabricated by MET and conventional heat treatment, along with the corresponding $MAPbI_3$ films.[91] (e) Comparison of thin-film homogeneity using two different precursor inks: 0% and 46% ACN in a 2-methoxyethanol (2-ME)/ACN mixed solvent. Column (ii) shows as-coated wet perovskite films; column (iii) presents schematic drawings of the meniscus and ribbing phenomena; column (iv) displays annealed film images; and column (v) includes SEM top-view and cross-sectional images of the perovskite films after annealing.[97]

preheating the substrate and using a cold air knife to promote lateral crystal growth, yielding comparable performance to spin-coated devices.[83] Thermal processing also plays a key role, with Galagan *et al.* showing that slow heating results in needle-like crystals, while fast heating forms plate-like structures, as illustrated in Fig. 6(a).[84] To overcome the limitations of conventional annealing, Huang *et al.* explored NIR annealing and achieved a PCE of 11.4%.[85] By modifying the precursor with n-butanol, uniform slot-die deposition was achieved over a 12 cm × 12 cm area within 20 seconds, improving device

performance.[86] A fully printed PSC module with an area of 4 cm × 4 cm attained 10.34% PCE, as shown in Fig. 6(b). Gas-blowing-assisted drying, such as high-pressure nitrogen extraction (HPNE), further enhances film quality. Du *et al.* optimized slot-die coating conditions to achieve a stable PCE of 19.4% in a 40 mm × 40 mm module.[87] Anti-solvent bathing offers another approach, although scalability remains challenging. Two-step sequential deposition, first applied to TiO_2-mesoporous PSCs, involves slot-die coating of PbI_2, followed by MAI infiltration. Gas quenching, which simulates spin coating, enhances porosity but necessitates sealed storage,[80,88] as illustrated in Fig. 6(c). Heo *et al.* improved PCE by incorporating MAI into the PbI_2 precursor.[89] Extending this approach to triple-cation perovskites, R2R slot-die coating has been successfully employed under ambient conditions, yielding a maximum PCE of 13.0%.[90] In place of gas quenching, Kim *et al.* developed the medium extraction technique (MET), which efficiently removes DMSO from PbI_2-DMSO films and leads to a PCE of 18.3% on 10 cm × 10 cm substrates, as shown in Fig. 6(d).[91] Additives also play a crucial role in improving perovskite films. Bu *et al.* used potassium hydroxide (KOH) to treat the SnO_2 ETL, eliminating hysteresis and enabling the formation of a 0.16 cm^2 PSC device with 20.50% PCE.[92] Lewis base additives, such as diphenyl sulfoxide (DPSO), stabilized precursor films, allowing slot-die-coated PSMs to reach 16.63% PCE over 20.77 cm^2.[93] Rana *et al.* employed a fluorinated phenylphosphonate to enhance cesium formamidinium (CsFA) perovskites, achieving 19.28% PCE over 58.5 cm^2 with improved stability.[94] Post-passivation strategies, including amino acid-based passivation[95] and benzylammonium iodide (BAI) treatment,[96] further improved crystallization and charge extraction, pushing module efficiencies above 20%. Li *et al.* highlighted the need to optimize precursor solutions and process parameters for scaling up perovskite absorber deposition.[97] By introducing acetonitrile (ACN) into a 2-methoxyethanol (2-ME)-based $FAPbI_3$ precursor solution, they reduced issues such as non-uniform thickness and ribbing effects, as shown in Fig. 6(e). This non-uniformity, if not leveled before solidification, persists in the final film. Scanning electron microscopy (SEM) analysis revealed defects such as grain irregularities and voids. With an optimized ACN content of 46%, they achieved a certified PCE of 22.3% and a tandem mini-module with an area greater than 12 cm^2 and an efficiency exceeding 17%. A quantum dot (QD) Solar cell also achieved 23.2% efficiency with slot-die coating, demonstrating its scalability for industrial production.[98]

In recent years, slot-die coating technology has shifted from glass substrates to flexible ones to meet the demands of flexible devices. To enhance the quality of perovskite layers, various fabrication strategies have been explored, all aimed at controlling the crystallization dynamics of perovskite materials.

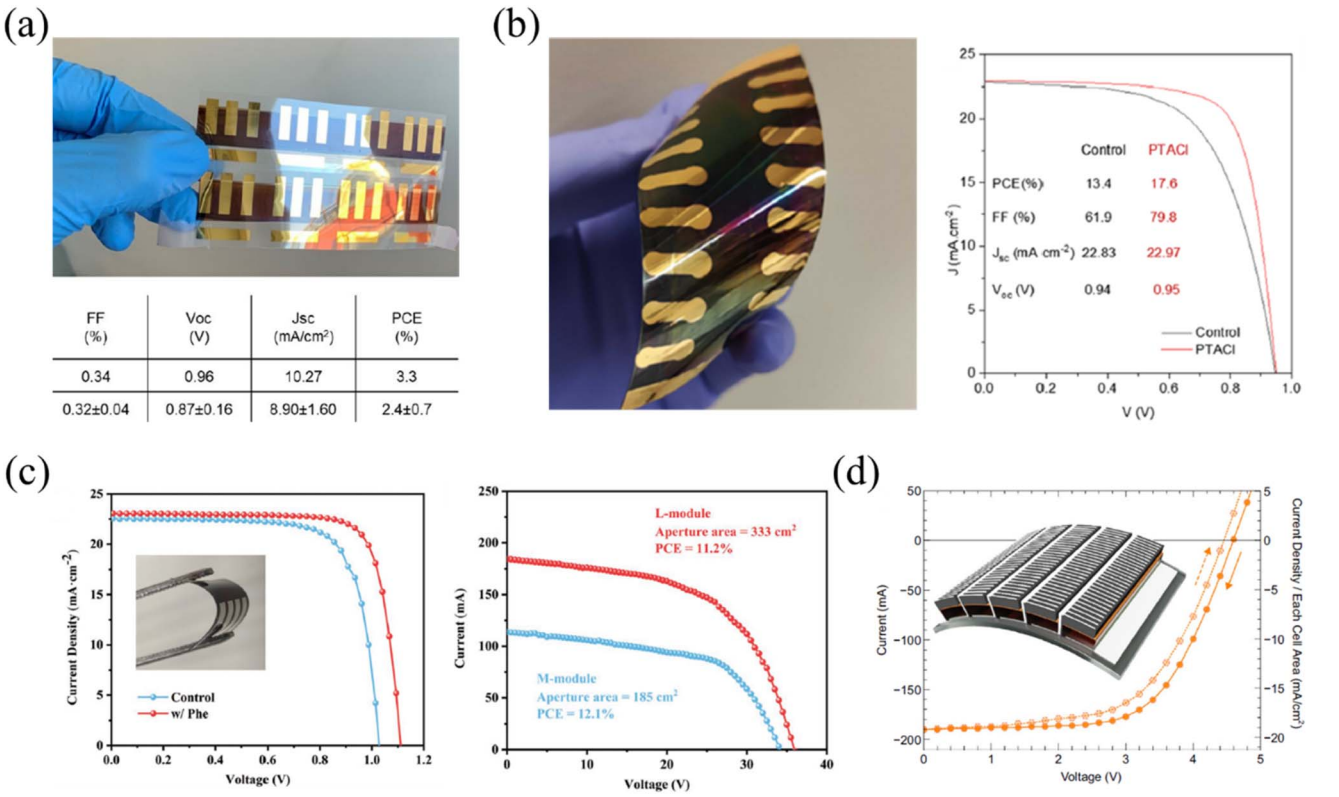

Fig. 7 (a) *J*–*V* characteristics of a fully slot-die coated device with a gold top electrode, fabricated and measured in an uncontrolled humid air environment (relative humidity: 65% and 75%). The best photovoltaic performance parameters and the average values obtained from 9 devices are shown.[99] (b) Photograph of F-PSCs fabricated on a 3.25 cm × 7.5 cm substrate, each with 0.049 cm^2 active pixels, along with the *J*–*V* curve of the champion device.[102] (c) Statistical distributions of photovoltaic parameters for F-PSCs with and without phenylethylammonium (PEA) additive.[103] (d) *J*–*V* curve of an R2R fabricated perovskite module. The inset shows a schematic diagram of the module structure.[104]

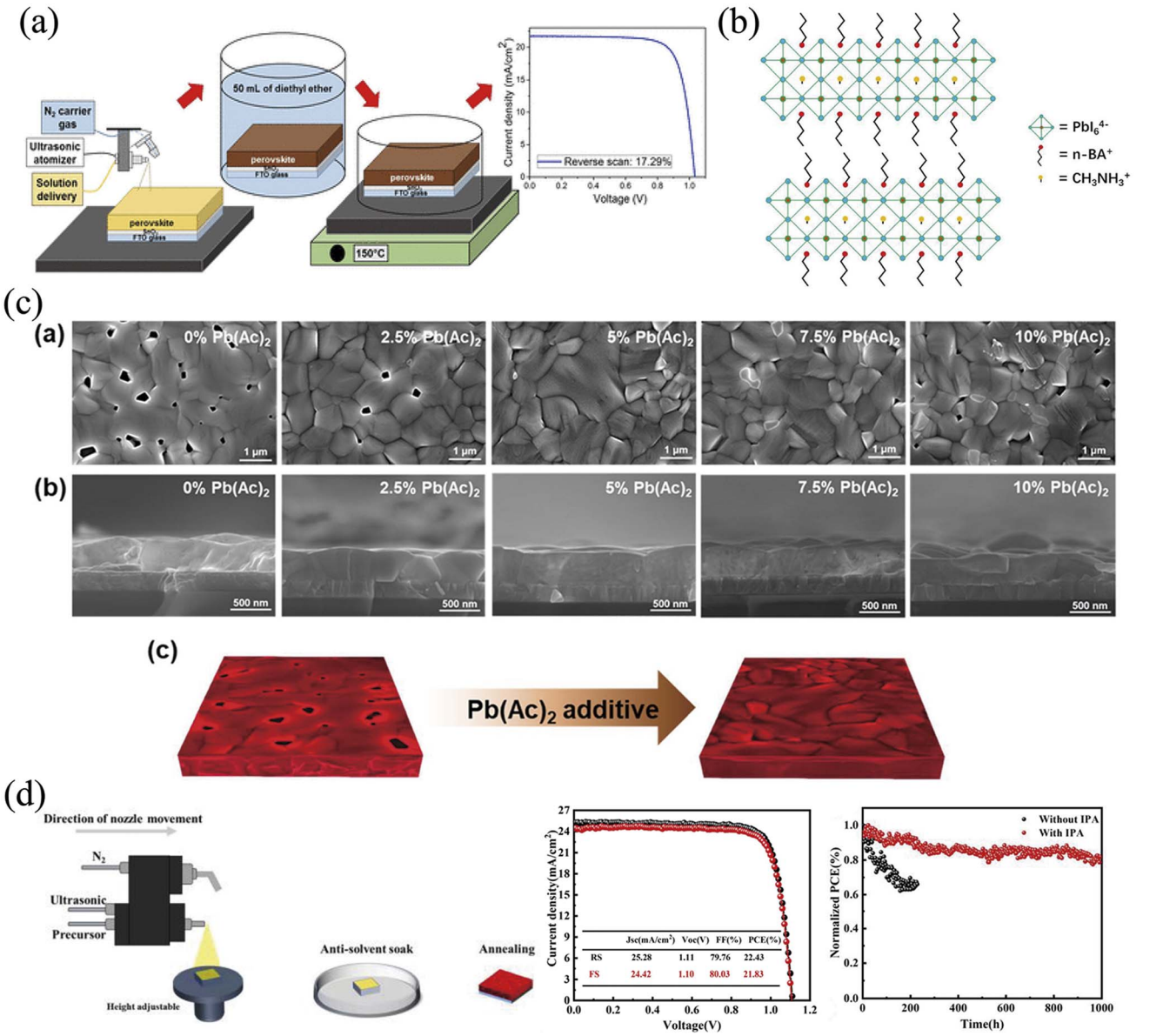

Fig. 8 (a) The use of a chlorine-containing perovskite ink with a broad processing window, combined with antisolvent extraction. This approach yielded perovskite films with relatively rougher surfaces compared to those produced by spin coating. The corresponding devices achieved a maximum PCE of 17.3%, with an average PCE of 16.3% across 24 devices.[112] (b) The schematic crystal structure of the Ruddlesden–Popper phase $(BA)_2(MA)_3Pb_4I_{13}$.[115] (c) SEM images (top-view and cross-sectional) of spray-deposited $CsPbI_2Br$ perovskite films incorporating varying amounts of $Pb(Ac)_2$. A schematic comparison of $CsPbI_2Br$ films with and without the $Pb(Ac)_2$ additive is also provided.[120] (d) A co-solvent strategy in which IPA is added to the perovskite precursor to modify the local microenvironment during ultrasonic spray coating (USC). The champion device achieved a PCE of 22.43% (active area: 0.13 cm^2) and retained 80% of its initial efficiency after 1000 hours of continuous illumination.[121]

Bisconti *et al.* explored slot-die coating as a scalable one-step method, successfully preparing high-quality perovskite films on flexible PET substrates,[99] as shown in Fig. 7(a). To reduce the use of toxic solvents, the research team employed a methylamine (MA)-assisted strategy, partially replacing ACN and 2-ME, resulting in an environmentally friendly perovskite ink containing 70% ethanol (EtOH). This ink was successfully applied to both rigid and flexible substrates, with rigid devices achieving a PCE of over 19.0%.[100] Kiani *et al.* used a mixed EtOH/ACN (1 : 1) solvent to prepare $MAPbI_3$-based F-PSCs *via* slot-die coating, achieving a PCE of 10%.[101] In the latest research on flexible devices, researchers prepared $MAPbI_3$ perovskite inks using pure DMF as the solvent and applied the slot-die coating technique, successfully demonstrating a fully scalable fabrication process for flexible n–i–p structured PSCs with a PCE of 17.6%,[102] as shown in Fig. 7(b). Bu *et al.* used KOH to treat the SnO_2 ETL, eliminating hysteresis and enabling the formation of a flexible 16.07 cm^2 PSC module with a PCE of 14.89%.[92] Slot-die coating equipped with a gas quenching system was utilized to deposit the perovskite layer, promoting

rapid crystallization and uniform film formation. The process was optimized for F-PSCs, with the resulting device exhibiting a PCE of 20.21% for an active area of 0.1 cm^2.[103] Afterward, a 2,2′,7,7′-tetrakis(*N*,*N*-di-*p*-methoxyphenylamine)-9,9′-spirobifluorene (spiro-OMeTAD) HTL was applied, and a molybdenum oxide (MoO_x)/copper (Cu) mixed electrode was deposited *via* thermal evaporation, as shown in Fig. 7(c). The first demonstration of fully R2R-fabricated PSMs was carried out by Weerasinghe *et al.*[104] The research team deposited all functional layers, except for the PET/transparent conductive oxide (TCO) electrode substrate, at room temperature using industrially applicable manufacturing methods such as slot-die coating, reverse gravure printing, and screen printing. Furthermore, they successfully replaced the expensive vacuum-deposited metal electrode with a carbon/silver (Ag) hybrid electrode. The resulting small-area R2R-coated flexible devices achieved a PCE of 15.5%, while the series-interconnected solar cell module (with an active area of 50.0 cm^2) reached a PCE of 11.0%, as shown in Fig. 7(d).

Slot-die coating has emerged as a promising technique in the fabrication of PSCs, offering advantages such as high material utilization, uniform large-area coating capability, and strong compatibility with R2R manufacturing. Although numerous studies have highlighted its potential for high efficiency and scalable production, several key challenges must still be overcome before widespread industrial adoption can be realized. One major issue is the control of crystallization dynamics, which continues to limit the reproducibility and long-term stability of slot-die-coated films. Despite the introduction of various drying strategies, such as cold air knives, gas extraction, and gas quenching, as well as precursor modifications involving Lewis bases, less toxic solvents, and functional additives, uniform film formation over large areas remains difficult. Defects such as voids, pinholes, and incomplete crystallization persist, indicating that the complex interplay among processing parameters (*e.g.*, substrate temperature, coating speed, drying environment) is still not fully understood or optimized. Another challenge lies in the transition from rigid to flexible substrates. Although progress has been made, F-PSMs typically lag behind their rigid counterparts in terms of efficiency and operational stability. Issues such as mechanical stress, electrode compatibility, and durability under bending stress remain unresolved. This highlights the need for innovations in materials and device architectures, such as elastic conductive layers, advanced thermal management strategies, and robust flexible encapsulation techniques, to enable reliable performance on flexible platforms. Lastly, while impressive device efficiencies have been achieved on small-area (<1 cm^2) and intermediate-area (>10 cm^2) modules, true R2R integration that meets industrial scalability requirements is still a work in progress. Challenges such as system-level machine design, stable ink delivery, and continuous process control must be addressed. To date, most high-performance demonstrations rely on lab-scale, batch-processing conditions that fall short of replicating the demands of continuous production environments.

3.3 Spray coating

Spray coating is a scalable and low-temperature deposition technique that is well-suited for the fabrication of large-area perovskite films.[105] This method enables uniform film formation through four main steps: ink droplet generation, deposition, coalescence into a wet film, and drying. Various atomization techniques, such as high-flow gas, ultrasonic vibrations, and ink cavitation, have been adopted to support industrial-scale production.[106] Compared with conventional antisolvent drop-casting, spray coating not only reduces antisolvent usage but also accelerates supersaturation, enhances nucleation uniformity, and improves film quality over large areas. Ultrasonic spray coating (USC) further refines droplet size distribution, airflow control, and spray cone stability, making it a cost-effective approach for PSC fabrication.[105] Initially, spray coating was applied only in the second deposition step to improve surface morphology, resulting in increasing PCEs from 10.2% to 12.5%.[107] Later, researchers extended this approach to a one-step process by directly depositing $MAPbI_3$ precursor solutions. Rapid drying and crystallization during this process enhanced film uniformity and led to a PCE of 11%,[108] which was further improved to 11.3% by optimizing the ink formulation.[109] Chou *et al.* adjusted the precursor concentration to fabricate active layers with an area of approximately 3 cm^2, achieving a PCE of 12.3%.[110] Silvano's team incorporated gas-quenching into the USC process, which improved crystallization and yielded a PCE of 16.88%.[111] Uličná *et al.* developed a cost-effective USC system suitable for large-area deposition and achieved a PCE of 17.3% using chloride-containing inks,[112] as illustrated in Fig. 8(a). In addition to one-step fabrication, spray coating has also been applied to replace conventional dripping methods in two-step PSC fabrication. For instance, Huang *et al.* optimized the spray deposition of PbI_2 and achieved PCEs of 16.0% for 0.1 cm^2 devices and 13.1% for 1 cm^2 devices.[113,114] Liu *et al.* developed a reproducible spray-coating method for two-dimensional PSCs, achieving a PCE of 10.4%,[115] as shown in Fig. 8(b). Environmentally friendly approaches to spray coating have also been introduced. Sansoni *et al.* successfully deposited perovskite films on textured silicon substrates without using toxic solvents, demonstrating excellent optoelectronic properties.[116] Furthermore, additive engineering and post-deposition passivation strategies have significantly enhanced the performance of spray-coated PSCs. Gao *et al.* improved device efficiency to 18.2% by incorporating binary additives,[117] and Cai *et al.* further optimized spray conditions to achieve a PCE of 20.6%.[118] Chen *et al.* applied an antisolvent spray treatment using methylamine acetate (MAAc) and a small-molecule additive, resulting in a PCE of 17.18%.[119] Yu *et al.* developed a scalable one-step crystallization approach for $CsPbI_2Br$ films by introducing lead(II) acetate ($Pb(Ac)_2$) and employing vacuum extraction, which led to a PCE of 10.06% (Fig. 8(c)).[120] Xu *et al.* implemented a co-solvent strategy by adding IPA into the perovskite precursor solution, thereby modifying the local microenvironment during USC.[121] By optimizing the DMF : NMP : IPA volume ratio to 11 : 2 : 1, they successfully fabricated high-quality $FAPbI_3$ films. This strategy enhanced crystallinity,

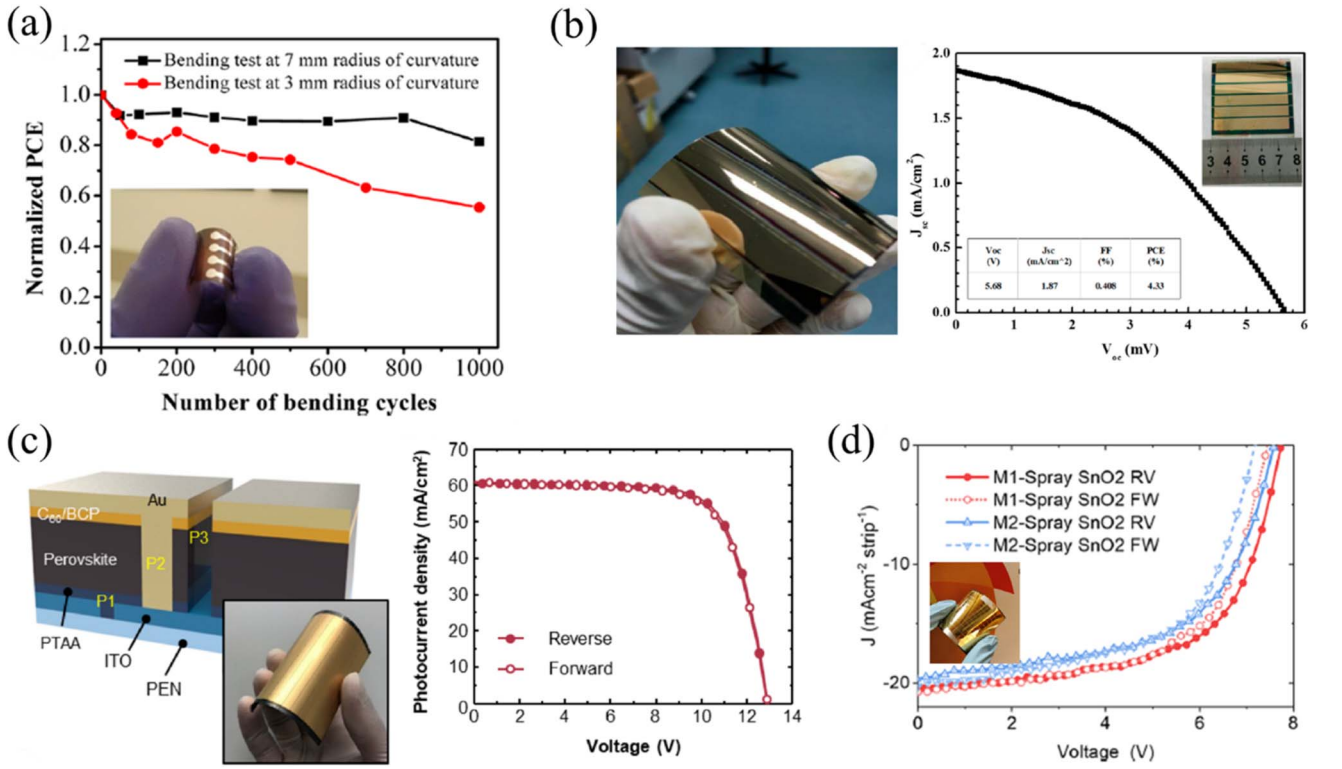

Fig. 9 (a) Normalized PCE of flexible devices after bending tests with radii of curvature of 7 mm and 3 mm. The inset shows a photographic image of the flexible devices.[106] (b) Photographic image of a flexible device with a large area of 5.0 cm × 5.0 cm, along with the *J*–*V* characteristics of a typical F-PSC (active area: 13.5 cm^2) measured without a mask. The inset shows a typical F-PSM.[124] (c) Schematic cross-sectional view and photograph of a F-PSM, accompanied by the *I*–*V* curves of a flexible perovskite mini-module with an active area of 35.1 cm^2.[125] (d) *J*–*V* curves of a F-PSM fabricated with spray-coated SnO_2 films. The inset displays a photograph of the F-PSM.[127]

suppressed the formation of PbI_2 and the undesired δ-phase, and improved overall film stability.[122,123] The resulting champion PSC achieved a PCE of 22.43% with an active area of 0.13 cm^2 and maintained 80% of its initial efficiency after 1000 hours of continuous illumination (Fig. 8(d)).[121]

Building on the success of spray-coating techniques for PSCs on rigid glass substrates, recent studies have demonstrated their feasibility for flexible substrates, enabling the formation of scalable and high-performance F-PSCs. Das *et al.* developed a high-throughput ultrasonic spray-coating method, applying it to PET substrates coated with TiO_2 and ITO. The resulting F-PSCs achieved a PCE of 8.1% and retained 60% ~90% of their peak PCE after over 1000 bending cycles,[106] as shown in Fig. 9(a), highlighting the potential of ultrasonic spray-coating for high-performance F-PSC fabrication. In some cases, the entire PSCs can be fabricated using spray-coating alone. Zhou *et al.* deposited TiO_2 nanoparticles onto polymer substrates *via* ultrasonic spray-coating, optimizing the spray parameters to achieve uniform thin films. The resulting F-PSCs, fabricated on PEN/ITO substrates, achieved a PCE of 10.87% with an active area of 0.4 cm × 0.4 cm.[124] They further demonstrated process scalability by fabricating large-area F-PSCs measuring 5 cm × 5 cm, as shown in Fig. 9(b), underscoring the potential of spray-coating for scalable manufacturing. A 2022 study introduced the "Film-Growth-Megasonic-Spray-Coating" (FGMSC) system, which utilizes ultrafine perovskite precursor droplets (<10 μm) for continuous, uniform deposition on large-area flexible substrates.[125] Focusing on a perovskite composition of $(CsPbI_3)_{0.02}(FA_{0.2}MA_{0.2}Pb(I_{2.8}Br_{0.2}))_{0.98}$, the study employed a gamma-butyrolactone (GBL) : DMF : DMSO solvent system (1 : 0.8 : 0.2). Despite the high boiling points and low vapor pressures of these solvents, high-quality perovskite films were produced without the use of an air knife. By carefully controlling the precursor droplet supply and implementing multiple spray-coating steps, the FGMSC system enhanced process scalability and efficiency while addressing challenges in film uniformity and rapid drying. Ultimately, a F-PSM with an active area of 35.1 cm^2 achieved a PCE of 16.10%,[125] as shown in Fig. 9(c). Huang *et al.* proposed a low-temperature (<150 °C) spray-coated compact TiO_2 (c-TiO_2) process, yielding devices with an average PCE of 13.95%.[126] Zhou *et al.* also applied ultrasonic spray-coating to deposit TiO_2 nanoparticle layers, resulting in flexible PSCs with a PCE of 14.32% on ITO glass and 10.87% on ITO-PEN substrates.[124] In another approach, Taheri *et al.* combined laser scribing optimization with automated spray-coating of SnO_2 layers. By varying laser power and evaluating cell interconnections, they determined the optimal parameters, achieving flexible PSCs with spray-coated SnO_2 layers that delivered nearly 15.3% PCE under 1 sun

illumination, which is comparable to that of devices fabricated *via* spin-coating,[127] as shown in Fig. 9(d).

Based on the above literature review, spray coating has undoubtedly demonstrated significant potential and versatility in the fabrication of both PSCs and F-PSCs. Its strengths lie in scalable processing, cost reduction, and improved environmental compatibility. However, to fully transition this technique toward commercial application and industrial deployment, several critical aspects still warrant deeper investigation and optimization. First, process reproducibility and film uniformity remain major challenges. Although many studies have improved crystallization through strategies such as gas quenching, additive engineering, solvent system tuning, and post-treatment methods, the intrinsic nature of spray coating—being influenced by factors including spray cone angle, substrate temperature gradients, solvent evaporation rates, and droplet size distribution—makes it more difficult to ensure consistent film quality over large areas. This underscores the need for future research to focus on systematic modeling of processing parameters and the development of multivariable control strategies to enhance process predictability and stability. Second, although recent results for flexible devices highlight the promising potential of spray coating, most high-efficiency outcomes are still limited to small-area devices and often rely on stable rigid glass substrates. Long-term stability, mechanical durability under repeated bending, and encapsulation compatibility of F-PSCs still require further verification. Future studies could benefit from incorporating multilayer material engineering strategies within the spray-coating process, such as graded layer designs, interfacial modifications, or spatial thickness control, to improve the overall mechanical and environmental robustness of the devices. Moreover, while innovative systems such as the FGMSC have been introduced to enhance continuous coating capabilities, most current developments remain at the laboratory scale and have not yet been validated on integrated R2R manufacturing platforms. Greater collaboration with equipment manufacturers is recommended to develop modular, high-throughput spray-coating systems and to conduct long-term trials under industrial roll-to-roll conditions to evaluate scalability and compatibility with real-world production.

4. Transitioning from rigid to flexible substrates in PSC processing

The shift from rigid to flexible substrates in PSCs represents a significant advancement toward the realization of lightweight, portable, and adaptable photovoltaic technologies. Unlike conventional glass-based PSCs, F-PSCs must endure mechanical deformations while maintaining high efficiency and long-term operational stability. This transition requires comprehensive modifications across various aspects of device fabrication, including material selection, processing techniques, and structural design. Flexible substrates present unique challenges in film deposition and mechanical integrity. Due to their limited thermal tolerance, low-temperature processing methods must be employed to ensure high-quality perovskite film formation without compromising substrate stability. In addition, the selection of electrode materials becomes critical, as ITO, commonly used in rigid devices, lacks the mechanical flexibility necessary for sustained durability under bending or deformation. Therefore, the development of alternative transparent conductive materials that combine mechanical resilience with sufficient electrical conductivity is essential for the advancement of F-PSC technology. Beyond structural considerations, the charge transport layers must also be adapted to support efficient charge extraction while remaining compatible with flexible substrates. Many conventional hole and electron transport materials require high-temperature annealing, prompting the need for low-temperature-processable alternatives. These alternative materials must not only facilitate effective carrier transport but also maintain their functionality under mechanical stress. Furthermore, robust encapsulation strategies are vital to protect the perovskite layer from environmental factors such as moisture and oxygen, while simultaneously accommodating mechanical deformation without causing performance degradation. Effective encapsulation ensures device stability and longevity, which are particularly important for practical deployment. This section explores the critical factors influencing the transition to F-PSCs, with a focus on the properties of flexible substrates, the selection of suitable electrode materials, the development of low-temperature charge transport layers, and encapsulation techniques. Together, these elements form the foundation for the successful fabrication of durable and efficient F-PSCs.

4.1 Flexible substrates

An ideal flexible substrate must meet several key criteria that significantly influence the performance, stability, and manufacturability of PSCs. It must exhibit sufficient mechanical durability to withstand the stresses encountered during both device fabrication and daily operation.[128] Flexibility is also essential, particularly for R2R processing, which is critical for large-scale production.[129] Additionally, the substrate should possess chemical resistance to perovskite solvents and endure high-temperature processing without deformation. Transparent substrates are preferred as they enable greater light harvesting, thereby enhancing the photovoltaic performance. To ensure long-term operational stability, excellent barrier properties against moisture and oxygen are necessary. Furthermore, flexible substrates typically exhibit higher surface roughness compared to rigid ones, which can adversely affect subsequent layer deposition. Therefore, selecting a suitable substrate is vital for improving both the PCE and the long-term reliability of F-PSCs.[130] Currently, three primary categories of flexible substrates are utilized in F-PSC fabrication: polymers, metals, and flexible glass, each presenting distinct advantages and limitations.

Polymer substrates, such as PET and PEN, are widely favored for their cost-effectiveness, high transparency, and flexibility.[131] However, their relatively low glass-transition temperatures (approximately 70 °C for PET and 120 °C for PEN) restrict their

suitability for high-temperature processing.[132] To address this, Skafi *et al.* developed a dual low-temperature process (≤100 °C) for fabricating stable F-PSCs on PET substrates,[133] while Chen *et al.* achieved similar results using 120 °C annealing on PEN substrates.[134] Polyimide (PI) offers superior thermal stability (from −200 °C to 400 °C), but its relatively low optical transparency and higher cost are notable drawbacks.[135] Colorless polycarbonate (PC) exhibits excellent heat resistance but has inferior corrosion resistance compared to PET, PEN, and PI, which limits its use in F-PSC applications.[136] Skafi *et al.* reported the first perovskite solar cells on PC substrates by introducing a blade-coated planarizing layer with a commercial ambient-curable resin, reducing roughness from 1.46 μm to 23 nm and simultaneously enhancing solvent resistance.[137] Using customized transparent ITO electrodes (78% average visible transmittance (AVT), 25 Ω sq^{-1}, bending radius 20 mm), the devices reached 13.0% PCE and maintained 80% of their initial PCE after 1776 h of ISOS-D-1 testing, demonstrating the potential of PC substrates for commercial integrating F-PSCs. Additionally, PI and PC substrates show lower compatibility with TCO electrodes than PET and PEN.[138] Recent advances have explored the development of ultra-lightweight polymer-based F-PSCs. For instance, Zhang *et al.* reported a device with a PCE of 14.19% and a high power-to-weight ratio of 23.26 W g^{-1} using a 1.4 μm-thick PET substrate.[139] Other studies have enhanced performance through interfacial engineering and novel charge transport layers, achieving PCEs up to 22.41% alongside optimized power-to-weight ratios.[140] Metal foil substrates, such as titanium and copper foils, offer high thermal resistance, low permeability to moisture and oxygen, and excellent mechanical durability. Their conductive nature simplifies the device architecture by serving as both the substrate and a functional electrode. However, their opacity necessitates the use of transparent top electrodes for light harvesting.[141] Lee *et al.* first demonstrated F-PSCs fabricated on titanium foil, achieving a PCE exceeding 6%, although performance was limited by the high resistance of an ultra-thin silver top electrode.[142] Heo *et al.* later improved device performance by integrating a graphene-based transparent electrode, resulting in efficiencies exceeding 15%.[143] While metal substrates are promising for large-area flexible solar panels, further optimization of the transparent top electrode is necessary to improve conductivity and light transmittance. Lee *et al.* successfully fabricated ITO-free F-PSCs on 127 μm-thick titanium foil, and Feleki *et al.* introduced an all-inorganic transport layer system that demonstrated excellent mechanical durability after 1000 bending cycles.[142,144] Flexible glass substrates, when thinned to a few hundred micrometers, provide a balance between flexibility and the benefits of conventional glass, including chemical stability and superior barrier properties.[145] Tavakoli *et al.* pioneered the use of 50 μm-thick willow glass, achieving a PCE of 12.06% and retaining device performance after 200 bending cycles at a bending radius of 4 cm.[146] Dai *et al.* applied blade coating to fabricate a 42.9 cm^2 perovskite module on flexible glass, obtaining a PCE of 15.86%.[74] Despite these advancements, scalability and long-term reliability remain challenges for widespread deployment. Studies on flexible willow glass substrates (FWGSs) have demonstrated promising stability and superior moisture and oxygen barrier properties while retaining the intrinsic advantages of glass, thereby positioning FWGSs as a strong candidate for R2R processing. In one notable case, FWGS-based PSCs demonstrated a PCE of 22.6% after 1600 bending cycles at a bending radius of 20.5 mm, offering a 55% higher specific power compared to PET-based devices.[147]

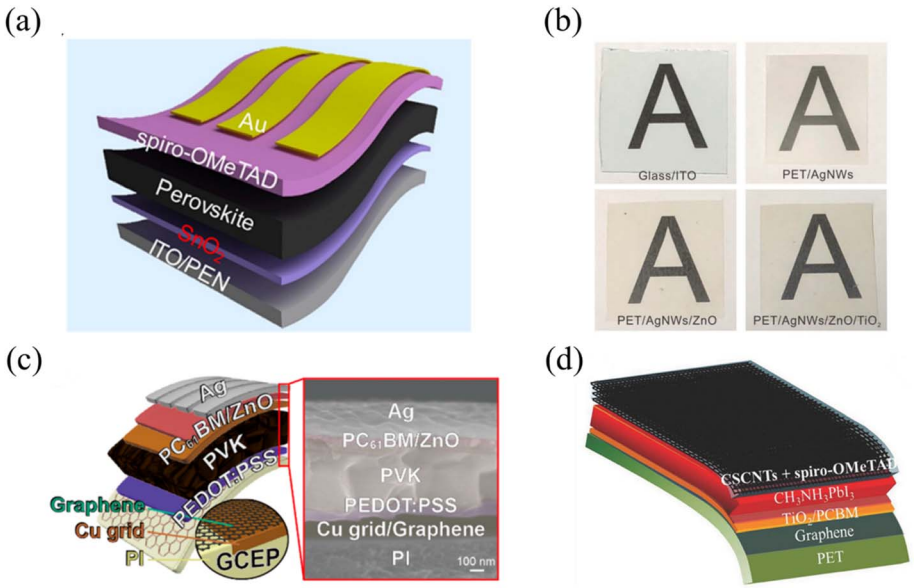

Fig. 10 (a) Schematic illustration of SnO_2-based flexible planar perovskite solar cells (SnO_2-F-PSCs).[150] (b) Photographs comparing various flexible substrates with a conventional glass/ITO substrate.[158] (c) Structure of F-PSCs employing an electrode platform composed of a conductive elastomeric polymer (CEP) film and graphene sheet (GCEP), along with the corresponding cross-sectional scanning electron microscopy (SEM) image.[159] (d) Device architecture of flexible PSCs utilizing all-carbon electrodes.[171]

However, bending rigidity remains a major constraint—glass must be significantly thinner than polymer alternatives to achieve comparable flexibility, which complicates handling and large-scale fabrication.[148] Beyond flexible glass, zirconia (ZrO_2) substrates have also been investigated for photovoltaic applications.[149] Zirconia features exceptional thermal stability (up to 1000 °C), low thermal expansion, and outstanding resistance to moisture and oxygen ingress. However, its high cost, considerable weight, and relatively high surface roughness (~25 nm) present significant challenges. If these issues can be addressed, zirconia may emerge as a viable alternative for the fabrication of high-performance F-PSCs.

4.2 Electrodes

The development of F-PSCs typically relies on plastic substrates coated with TCO. Among these, ITO is widely used due to its high transmittance in the visible spectrum and low sheet resistance, as shown in Fig. 10(a).[150] However, its brittleness limits durability under repeated mechanical stress, making the search for alternative transparent electrodes a key research focus.[151] Various materials, including Ag NWs, conductive polymers, graphene, and carbon nanotubes (CNTs), have been explored for their potential to combine high conductivity, optical transparency, and mechanical flexibility.[152,153] Pandey *et al.* highlighted the impact of bottom electrode sheet resistance on F-PSC performance.[154] They fabricated inverted PSCs on PEN, PET, and glass substrates with an ITO/PEDOT:PSS/perovskite/C_{60}/BCP/Ag structure, comparing devices with active areas of 0.1 cm^2 and 1 cm^2. For small-area devices, substrate sheet resistance had minimal effect, except for PET-ITO (98 Ω $\square^{-1}$). However, in 1 cm^2 devices, increased series resistance significantly reduced the short-circuit current density and fill factor, leading to lower PCEs on PET-ITO (49 Ω $\square^{-1}$, 98 Ω $\square^{-1}$) compared to PEN-ITO (12 Ω $\square^{-1}$) and glass-ITO (3.8 Ω $\square^{-1}$). This performance drop was evident in the V_{OC} region of the *J–V* curves. To enhance ITO properties, Kim *et al.* developed high-quality ITO electrodes on PET using plasma arc ion plating.[155] The method produced ITO films with a sheet resistance of 15.75 Ω $\square^{-1}$ and transmittance above 83%, outperforming conventional sputtered ITO. F-PSCs utilizing these electrodes achieved a PCE of 16.8%. Despite these advances, ITO's brittleness remains a challenge for flexible applications.[156] Metallic electrodes, such as nanogrids and nanowires, offer a promising alternative to TCOs, as illustrated in Fig. 10(b) and (c).[157–159] Li *et al.* developed an ultrathin silver grid electrode coated with PH1000, achieving a smooth surface with an RMS roughness of 2.0 nm and a sheet resistance of 3 Ω $\square^{-1}$.[160] F-PSCs fabricated with this electrode (PET/Ag grid/PH1000/PEDOT:PSS/$MAPbI_3$/phenyl-C_{61}-butyric acid methyl ester (PCBM)/aluminum (Al)) demonstrated a PCE of 14.0% with minimal hysteresis and retained 95% efficiency after 5000 bending cycles (5 mm radius). Sun *et al.* introduced a plasmon-enhanced Ag periodic grid electrode, fabricated using polystyrene microsphere templates and reactive ion etching.[161] The electrode exhibited 66% transmittance and 19 Ω $\square^{-1}$ sheet resistance, enabling F-PSCs to achieve a PCE of 16.47% with 90% efficiency retention after 1500 bending cycles (3 mm radius). While Ag NWs are attractive for their flexibility and conductivity, their chemical instability in perovskite environments and poor adhesion remain concerns.[128,162,163] Lee *et al.* addressed this by designing an amorphous aluminum-doped zinc oxide (a-AZO)/Ag NWs/AZO electrode, which achieved 88.6% transmittance at 500 nm and a sheet resistance of 11.86 Ω $\square^{-1}$.[164] F-PSCs using this electrode exhibited superior bending resistance, maintaining stable performance at a 12.5 mm radius. Carbon-based electrodes, such as graphene and CNTs, have emerged as viable alternatives due to their excellent electrical properties, flexibility, stability, and low cost.[165–170] Luo *et al.* fabricated fully carbon-based F-PSCs using chemical vapor deposition (CVD)-grown graphene as the bottom electrode and cross-stacked CNTs as the top electrode (Fig. 10(d)).[171] While single-layer graphene offered higher transmittance, double-layer graphene achieved the best performance, yielding a PCE of 11.9%. These devices retained 90% efficiency after 1000 hours of operation at 60 °C under 1-sun illumination. Tran *et al.* developed a low-temperature (150 °C) plasma-assisted thermal CVD method for directly synthesizing graphene on polyethersulfone (PES) substrates with a Ti buffer layer.[172] Using an AZO/Ag/AZO composite counter electrode, they demonstrated improved bifacial photovoltaic output. In our recent work, we developed perovskite solar cells with screen-printed carbon top electrodes (C-PSCs) as a cost-effective alternative electrode. By introducing poly(3-hexylthiophene) (P3HT) into the antisolvent CB, we enhanced perovskite crystallization, reducing defect density and improving charge transport. This resulted in a significant PCE improvement of 11%, with the low-temperature C-PSCs achieving 10.90% and retaining 90% of their initial efficiency after 1200 hours in ambient air.[173]

4.3 Selection of low-temperature processable charge transport materials

The charge transport layer (CTL) plays a vital role in perovskite solar cells by enabling efficient charge extraction and transport of electrons or holes. An ideal CTL should exhibit high electrical conductivity, optical transparency, suitable energy level alignment with the perovskite absorber, and strong chemical and environmental stability. These characteristics not only contribute to high PCE but also improve long-term device stability—key factors for commercial viability. In the development of flexible and scalable perovskite solar cells, especially those fabricated on temperature-sensitive substrates, low-temperature processable CTL materials are essential. Such materials enable compatibility with plastic substrates, reduce thermal damage during fabrication, and support roll-to-roll or printing-based manufacturing. The following sections introduce various hole and electron transport materials that can be processed at low temperatures, highlighting their properties and recent advancements.

4.3.1 Hole transport materials. To address the thermal constraints of flexible substrates and enable scalable manufacturing, the development of low-temperature-processable HTLs has attracted significant attention.

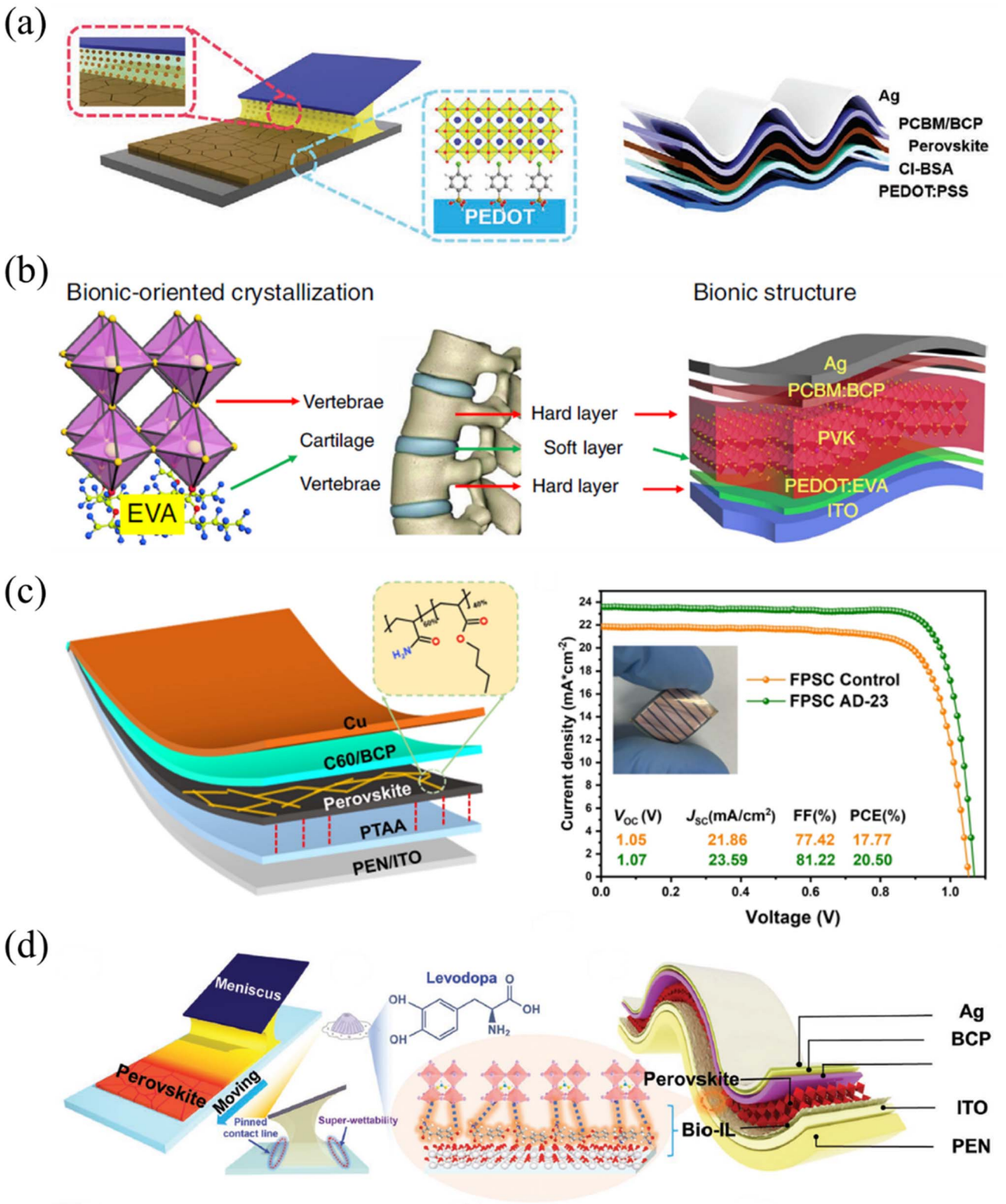

Fig. 11 (a) Schematic illustration of the nucleation, growth, and conversion processes involved in the fabrication of final F-PSCs.[175] (b) Bio-inspired structural concept showing the analogy between vertebrae and perovskite solar cells, emphasizing the application of nature-inspired design principles.[176] (c) Device architecture of the F-PSC along with the corresponding *J*–*V* characteristics, illustrating its photovoltaic performance.[179] (d) Schematic representation of the flexible printing process for PSCs, featuring a meniscus-guided blade-coating technique for perovskite film deposition at a blade speed of 5 mm s^{-1}, and the associated bio-inspired design and device structure of the printed PSC.[182]

Materials such as PEDOT:PSS, poly[bis(4-phenyl)(2,4,6-trimethylphenyl)amine] (PTAA), NiO_x, and spiro-OMeTAD have been widely investigated for their compatibility with solution-based or low-temperature deposition methods, offering promising alternatives to conventional high-temperature or doped organic HTLs. Recent studies have also focused on improving the performance and stability of these materials, especially in the context of scalable fabrication techniques such as blade coating, slot-die coating, and spray coating.

PEDOT:PSS was the first HTL used in inverted F-PSCs. Yang *et al.* employed PEDOT:PSS in a low-temperature, solution-based process and achieved a PCE of 9.2%.[174] Later, Chen's group introduced MAAc as an ink additive and 4-chlorobenzenesulfonic acid (Cl-BSA) for defect passivation, significantly improving both performance and stability. Their flexible device (1.01 cm^2) achieved a remarkable PCE of 18.12%,[175] as shown in Fig. 11(a). Meng *et al.* further enhanced mechanical robustness by adopting a design inspired by biological structures. They employed a conductive and adhesive poly(3,4-ethylenedioxythiophene):ethylene vinyl acetate (PEDOT:EVA) as the HTL, acting as an "articular cartilage"-like buffer layer to absorb and redistribute mechanical stress. Finite element simulations confirmed that PEDOT:EVA effectively reduced localized stress on the perovskite layer during bending. Moreover, it promoted oriented crystallization of the perovskite layer. As a result, flexible devices reached PCEs of 19.87% (1.01 cm^2) and 17.55% (31.20 cm^2), retaining over 85% of their initial efficiency after 7000 bending cycles,[176] as shown in Fig. 11(b).

Despite these improvements, PEDOT:PSS still presents drawbacks such as its acidic and hygroscopic nature, which may corrode electrodes and degrade the perovskite layer, ultimately limiting device stability. Additionally, its relatively low work function restricts the V_{OC} of the inverted F-PSCs. To overcome these limitations, PTAA has emerged as a promising alternative due to its low-temperature solution-processability, excellent moisture resistance, and chemical stability.[177] A bilayer structure of PEDOT:PSS and PTAA has shown enhanced carrier extraction and transport, achieving PCEs of 19.41% (0.09 cm^2) and 16.61% (1 cm^2), with excellent mechanical and environmental stability.[73] Furthermore, ultrathin PTAA layers (2–10 nm) deposited *via* thermal evaporation have optimized energy level alignment with the perovskite, enabling inverted F-PSCs to reach a PCE of 17.27%, with negligible hysteresis and superior stability.[178] Currently, PTAA-based HTLs hold the record for the highest PCE (20.50%) among inverted F-PSCs,[179] as illustrated in Fig. 11(c).

Nickel oxide (NiO_x), an inorganic HTL, is another widely studied material due to its earth abundance, intrinsic p-type conductivity, high optical transparency, and low hygroscopicity. Najafi *et al.* demonstrated flexible PEN/ITO devices incorporating room-temperature-processed NiO_x and zinc oxide (ZnO) nanoparticle transport layers, achieving a PCE of 16.6% and a stabilized efficiency of 16.1%. These devices retained over 90% of their initial performance after 500 hours (triple-cation perovskite) and over 85% after 1000 hours ($MAPbI_3$), highlighting excellent stability.[180] Compared to organic HTLs, NiO_x offers advantages in cost and scalability, especially when deposited *via* sol–gel or nanoparticle ink-based slot-die coating. Wang *et al.* enhanced NiO_x nanoparticle films using hydrogen iodide treatment, improving the PCE from 17.86% to 20.51%. Their flexible module also achieved 16.15% efficiency.[181] In a bio-inspired approach, Fan *et al.* addressed evaporation-induced thickness variations by introducing a dopamine-based adhesion strategy. Levodopa was incorporated into the NiO_x layer to form a bio-inspired interfacial layer (Bio-IL), improving both mechanical and environmental stability. This approach enabled a F-PSM (14.63 cm^2, $Cs_{0.05}MA_{0.07}FA_{0.88}PbI_{2.76}Br_{0.24}$) to achieve a PCE of 16.87%,[182] as shown in Fig. 11(d).

4.3.2 Electron transport materials. To enable scalable fabrication and integration into flexible devices, considerable efforts have been devoted to developing low-temperature-processable ETLs. Traditional ETLs such as compact and mesoporous TiO_2 typically require high-temperature sintering, limiting their compatibility with flexible substrates. In response, alternative materials such as SnO_2, ZnO, and PCBM have garnered increasing attention due to their favorable energy alignment, good electron mobility, and potential for low-temperature or solution-based processing. Recent studies have shown that these ETLs can be effectively deposited using scalable coating techniques such as blade coating, slot-die coating, and spray coating, demonstrating promising photovoltaic performance in both rigid and flexible PSCs.

For example, Xue *et al.* employed blade coating to deposit a compact SnO_2 nanoparticle film (2.67 wt%) at a blade-to-substrate distance of 100 μm, followed by thermal annealing at 120 °C in ambient air. The HTL, spiro-OMeTAD, was also processed at low temperature, resulting in a device fabrication process that did not exceed 130 °C. This low-temperature approach enabled flexible PSCs to achieve a peak PCE of 21.33%.[75] To improve film uniformity and reduce void formation, low-surface-tension solvents such as IPA have been introduced. Wu *et al.* applied this strategy in an R2R slot-die coated SnO_2 layer using an IPA-containing ink formulation (I3), achieving a PCE of 14.36% (V_{OC} = 1.06 V, J_{SC} = 19.43 mA cm^{-2}, FF = 69.30%). In contrast, the IPA-free device (I0) yielded only 10.23%, highlighting the beneficial role of IPA in enhancing ETL film quality and reducing interfacial recombination. Slot-die coating was used to deposit the SnO_2 ETL, with annealing temperatures maintained at 120 °C to avoid thermal damage to the flexible substrate. This careful thermal control allowed successful integration into F-PSCs, yielding PCEs of 12.1% and 11.2% for devices with large active areas of 167 cm^2 and 300 cm^2, respectively.[103] In another study, Taheri *et al.* utilized automated spray coating for the SnO_2 layer combined with optimized laser scribing to enhance cell interconnections. By tuning the laser power, the resulting F-PSCs achieved a PCE of nearly 15.3% under AM1.5 G illumination, which was comparable to that of devices fabricated using spin-coated ETLs.[127] Despite these advancements, challenges remain—particularly regarding the surface roughness of polymer substrates. Surface protrusions can rival the thickness of the entire functional layer stack, negatively impacting film coverage and quality. To mitigate this issue, researchers introduced a phase-transfer agent

Table 3 A summary of representative PSCs and PSMs on rigid substrates with active areas greater than or equal to 1 cm^2, fabricated using various techniques including blade coating, slot-die coating, and spray coating. The table compares device structures, active areas, and optoelectronic properties—such as open-circuit voltage (V_{OC}), short-circuit current density (J_{SC}), fill factor (FF), and power conversion efficiency (PCE)—along with providing the corresponding references

Deposition method	Structure	V_{OC} (V)	J_{SC} (mA cm^{-2})	FF (%)	PCE (%)	Active area (cm^2)	Ref.
Blade coating	FTO/c-TiO_2/perovskite/spiro-OMeTAD/Ag	1.111	21.38	72.9	17.33	1.2	61
	ITO/PTAA/$FAPbI_3$/PCBM/BCP/Ag	7.35	3.27	71	17.07	12.32 (module)	63
	ITO/PTAA/$FAPbI_3$/PCBM/BCP/Ag	14.20	1.92	52	14.17	55.44 (module)	63
	FTO/SnO_2/$Cs_{0.15}FA_{0.85}PbI_{2.55}Br_{0.45}$/spiro-OMeTAD/Au	6.687	3.7	72	17.71	10 (module)	69
	FTO/SnO_2/KCl/$FAPbI_3$/PTABr/spiro-OMeTAD/Au	5.855	25.03	79.6	23.34	12.4 (module)	72
	FTO/SnO_2/KCl/$FAPbI_3$/PTABr/spiro-OMeTAD/Au	9.535	24.61	78	22.88	22.4 (module)	72
	ITO/PEDOT:EVA/perovskite/PCBM/BCP/Ag	1.18	22.91	82	22.16	1.01	176
	ITO/PTAA/perovskite/PCBM/BCP/Ag	4.62	5.12	66.2	15.65	10.08 (module)	184
	FTO/c-TiO_2/m-TiO_2/perovskite/Co(II) and Co(III)/Au	1.09	22.64	73.66	18.26	1.96	185
	ITO/PTAA/$MA_{0.6}FA_{0.4}PbI_3$/C_{60}/BCP/Ag	5.81	4.249	78	19.25	17.9 (module)	186
	ITO/PTAA/$MA_{0.6}FA_{0.4}PbI_3$/C_{60}/BCP/Ag	16.07	1.527	78	19.15	50.1 (module)	186
	ITO/PTAA/$MAPbI_3$/fullerene(C_{60})/BCP/Cu	17.24	72.5	68.9	14.9	57.2 (module)	187
	FTO/ZnO-SnO_2/perovskite/CuPc/Au	8.06	3.05	72.5	17.82	18 (module)	188
	FTO/ZnO-SnO_2/perovskite/CuPc/Au	13.16	1.70	74.3	16.6	47 (module)	188
	ITO/PTAA/BCP/$FA_{0.9}Cs_{0.1}PbI_3$/C_{60}/BCP/Cu	9.413	2.87	80.32	21.78	26.9 (module)	189
	FTO/NiO_x/Al_2O_3/MeO-4PACz/$FA_{0.85}Cs_{0.15}PbI_{2.85}Br_{0.15}$/PEAI/$C_{60}$/BCP/Cu	5.82	4.78	81.29	22.66	11.09 (module)	190
	FTO/NiO_x/Al_2O_3/MeO-4PACz/$FA_{0.85}Cs_{0.15}PbI_{2.85}Br_{0.15}$/PEAI/$C_{60}$/BCP/Cu	16.13	1.593	78.4	20.14	113 (module)	190
	FTO/SnO_2/$(FAPbI_3)_{1-x}$($MAPbBr_3$)x/spiro-OMeTAD/Au	6.71	3.47	71	16.54	10 (module)	191
	FTO/SnO_2/$(FAPbI_3)_{1-x}$($MAPbBr_3$)x/spiro-OMeTAD/Au	11.83	1.8	62	13.32	53.6 (module)	191
	FTO/SnO_2/PbI_2:THTO/FAI:MACl/spiro-OMeTAD/Au	6.65	3.72	75	18.65	25 (module)	192
	FTO/TiO_2/SnO_2/PVSK/spiro-OMeTAD/Au	10.4	2.381	72.236	17.89	37.05 (module)	193
	ITO/SnO_2/$FA_{1-x}MA_xPb(I_{1-y}Br_y)_3$/spiro-OMeTAD/Ag	6.82	3.64	78.47	19.45	11.35 (module)	194
	FTO/SnO_2/$FAPbI_3$/spiro-MeOTAD/Au	10.81	2.232	70.5	17.01	25 (module)	195
	FTO/SnO_2/$MAPbI_3$/spiro-MeOTAD/Au	7.83	2.89	77.9	17.62	10 (module)	196
	FTO/SnO_2/$FAPbI_3$/spiro-OMeTAD/Au	9	3.14	77.55	21.9	15.64 (module)	197
	FTO/SnO_2/$FAPbI_3$/spiro-OMeTAD/Au	9.016	3.188	76.52	22	15.64 (module)	198
	Bottom: glass/ITO/NiO/VNPB/$Cs_{0.35}FA_{0.65}Pb_{1.8}Br_{1.2}$/$C_{60}$/$SnO_2$/ Au top: PEDOT:PSS/$FA_{0.7}MA_{0.3}PbI_{0.5}Sn_{0.5}$ I_3/C_{60}/SnO_2/Ag	8.04	3.55	75.9	21.7	20.25 (2T module)	199
	ITO/NiO_x/MeO-2PACz/PbI_2:$(FAI)_{0.3}$:$(CsI)_{0.15}$/FAI:MACl/C_{60}/BCP/Cu	22.3	0.81	63.49	12.6	121 (module)	200
Slot-die coating	FTO/NiO_x/perovskite/PCBM/PEI/Ag (our work)	5.73	2.85	63.34	10.34	16 (module)	86
	FTO/TiO_2/$FA_{0.91}Cs_{0.09}PbI_3$/spiro-OMeTAD/Au	4.55	44.8	76.2	19.6	7.92 (module)	87
	FTO/c-TiO_2/SnO_2/PVSK/spiro-OMeTAD/Au	6.42	3.08	74.2	14.7	12 (module)	88
	FTO/SnO_2/$Cs_{0.05}MA_{0.4}FA_{0.55}Pb(I_{0.96}Br_{0.04})_3$/spiro-OMeTAD/Au	6.48	3.16	74.1	15.2	12 (module)	88
	FTO/NiMgLiO/$FA_{0.83}Cs_{0.17}PbI_{2.83}Br_{0.17}$/LiF/$C_{60}$/BCP/Bi/Ag	1.08	21.8	78.9	18.5	1	93
	FTO/NiMgLiO/$FA_{0.83}Cs_{0.17}(PbI_2)_{0.83}Br_{0.17}$/LiF/$C_{60}$/BCP/Bi/Ag	1.08	0.434	76.4	17.2	20.77 (module)	93
	FTO/SnO_2/perovskite/spiro-OMeTAD/Au	13.70	0.109	75.04	19.28	58.5 (module)	94
	ITO/PTAA/perovskite/C_{60}/BCP/Ag	3.15	7.3125	63.87	14.7	14.4 (module)	96
	ITO/MeO-4PACz/$FAPbI_3$/LiF/C_{60}/SnO_2/Cu	1.088	24.92	83.10	22.54	2.2	97
	ITO/MeO-4PACz/$FAPbI_3$/LiF/C_{60}/SnO_2/Cu	8.36	3.06	66.8	17.1	12.7 (module)	97
	FTO/NiO_x/SRE/perovskite/PCBM/BCP/Ag	20.74	1.143	78.4	18.6	174 (module)	201
	FTO/SnO_2/perovskite/PMMA/CuSCN/Au	8.71	2.78	61.0	14.8	9 (module)	202
	ITO/NiO_x(with LS1)/$MAPbI_3$/PCBM/BCP/Ag	6.503	3.024	75.73	14.90	19.16 (module)	203
	ITO/c-TiO_2/$CH_3NH_3PbI_{3-x}Cl_x$/spiro-OMeTAD/Au	21.2	17.3	67.9	10	168.75 (module)	204
	FTO/SnO_2/KPb_2Br_5-CsFA/spiro-OMeTAD/Au	14.23	1.74	64.86	16.22	57.5 (module)	205

Table 3 (*Contd.*)

Deposition method	Structure	V_{OC} (V)	J_{SC} (mA cm^{-2})	FF (%)	PCE (%)	Active area (cm^2)	Ref.
	FTO/SnO_2/$Cs_{0.05}(MA_{0.17}FA_{0.83})_{0.95}Pb(I_{0.83}Br_{0.17})_3$/PEAI/spiro-OMeTAD/Au	18.15	1.42	62.8	16.13	186.1 (module)	206
	ITO/SnO_2/TACA-ZrO_2 NPs/$Cs_{0.03}FA_{0.97}PbI_3$/spiro-OMeTAD/Au	9.156	3.189	80.21	23.42	23.23 (module)	207
	ITO/SnO_2/TACA-ZrO_2 NPs/$Cs_{0.03}FA_{0.97}PbI_3$/spiro-OMeTAD/Au	16.629	1.73	77.38	22.26	87.45 (module)	207
	FTO/urea-NiO_x/$Cs_{0.05}(FA_{0.95}MA_{0.05})_{0.95}Pb(I_{0.95}Br_{0.05})_3$/BzMIMBr/$C_{60}$/BCP/Cu	19.84	1.16	74.65	17.18	196 (module)	208
	FTO/NiO_x/$FA_{0.91}Cs_{0.09}PbI_3$/PCBM/BCP/Ag	1.13	24.02	82.49	22.44	1	209
	FTO/NiO_x/$FA_{0.91}Cs_{0.09}PbI_3$/PCBM/BCP/Ag	30.92	141.2	79.14	19.74	175 (module)	209
Spray coating	ITO/PEDOT:PSS/$CH_3NH_3PbI_3$/C_{60}/BCP/Ag	0.83	21.94	67.6	12.3	1	110
	FTO/TiO_2/$MAPbI_3$/spiro-OMeTAD/Au	1.032	18.59	68.2	13.09	1	113
	FTO/TiO_2/$MA_{0.7}FA_{0.3}PbI_3$/spiro-OMeTAD/Au	4.381	4.80	72	15.14	10.36 (module)	210
	ITO/NiO_x/$MAPbI_3$/C_{60}/BCP/Ag	1.02	20.16	57.26	11.89	1	211

(phenyltrimethylammonium chloride, PTACl) into SnO_2 inks to improve nanoparticle distribution and film uniformity. With this modification, a flexible device fabricated using a blade-coated ETL and HTL, a slot-die coated perovskite layer, and an evaporated top electrode in an n–i–p structure achieved a PCE of 17.6% over a 0.1 cm^2 area.[102]

In addition to SnO_2, low-temperature spray-coating methods have also been explored for TiO_2-based ETLs. Huang *et al.* developed a sub-150 °C spray-coating process for compact TiO_2, which yielded PCEs of 14.30% for rigid PSCs and 8.52% for their flexible counterparts.[126] Similarly, Zhou *et al.* employed ultrasonic spray coating to deposit TiO_2 nanoparticle layers, achieving efficiencies of 14.32% on ITO-glass and 10.87% on ITO-PEN substrates.[124] In another notable advancement, a bilayer ETL structure composed of SnO_2 and mesoporous TiO_2 was introduced, resulting in a device PCE of 14.8%, approximately 30% higher than that of a device using SnO_2 alone (11.4%). This fabrication strategy was further scaled up to produce a 12 cm^2 flexible module in which all layers were patterned by laser scribing (P1, P2, and P3), achieving a module PCE of 8.8%.[183]

While significant progress has been made in the development of low-temperature-processable HTLs and ETLs for F-PSCs, several critical challenges remain that could hinder large-scale commercialization and long-term device stability. For example, although PEDOT:PSS has been widely used as an HTL due to its ease of processing and reasonable performance, its intrinsic acidity and hygroscopicity pose serious threats to device longevity by accelerating the degradation of the perovskite layer and electrode materials. Despite recent innovations, such as chemical doping, biomimetic interfacial designs (*e.g.*, PEDOT:EVA), and bilayer structures incorporating PTAA, there is still a pressing need to assess the long-term durability of these systems under realistic environmental and mechanical stress conditions. Similarly, while PTAA-based HTLs have demonstrated record efficiencies and enhanced environmental stability, their high cost and batch-to-batch variability raise concerns about feasibility for large-scale production. Thus, further efforts are needed to develop alternative HTLs that retain the solution-processability and tunable energy levels of organic materials, while offering the robustness and stability typically associated with their inorganic counterparts. On the ETL side, materials such as SnO_2 and ZnO have shown considerable promise due to their compatibility with low-temperature and scalable deposition techniques like blade coating, slot-die coating, and spray coating. However, the inherent surface roughness of flexible substrates such as PET and PEN can impede the formation of uniform ETL layers, leading to poor interfacial contact and increased defect density. While strategies like solvent engineering, nanoparticle surface modification, and the incorporation of interfacial additives (*e.g.*, PTACl) have shown potential in addressing these challenges, there is currently a lack of standardized evaluation protocols for assessing film uniformity and scalability over large areas. To overcome these limitations, future research should focus on the development of transport layers with self-leveling or self-healing properties, enhanced tolerance to substrate-

Table 4 A summary of representative F-PSCs and F-PSMs based on various fabrication techniques, including blade coating, slot-die coating, and spray coating. The table compares device structures, active areas, and optoelectronic properties—such as open-circuit voltage (V_{OC}), short-circuit current (J_{SC}), fill factor (FF), and power conversion efficiency (PCE)—along with providing the corresponding references

Deposition method	Structure	V_{OC} (V)	J_{SC} (mA cm^{-2})	FF (%)	PCE (%)	Active area (cm^2)	Ref.
Blade coating	PEN/ITO/PEDOT:PSS/PTAA/$MAPbI_3$/PCBM/BCP/Ag	1.09	21.98	81	19.41	0.09	73
	PEN/ITO/PEDOT:PSS/PTAA/$MAPbI_3$/PCBM/BCP/Ag	1.10	20.97	72	16.61	1	73
	MgF_2/willow glass/ITO/PTAA/$MAPbI_3$/C_{60}/BCP/Cu	1.092	22.83	79.1	19.72	0.052	74
	MgF_2/willow glass/ITO/PTAA/$MAPbI_3$/C_{60}/BCP/Cu	13.142	19.71	73.5	15.86	42.9 (module)	74
	PEN/ITO/SnO_2/perovskite/spiro-OMeTAD/Au	1.18	24.21	74	21.33	0.1	75
	PEN/ITO/SnO_2/perovskite/spiro-OMeTAD/Au	1.14	23.84	73	19.81	1.01	75
	PET/ITO/SnO_2/$Cs_{0.15}FA_{0.85}PbI_{3-x}Br_x$/PTAA/Au	1.03	19.18	71.4	14.08	0.09	76
	PET/ITO/SnO_2/$Cs_{0.15}FA_{0.85}PbI_{3-x}Br_x$/PTAA/Au	6.43	2.58	39.69	6.58	25 (module)	76
	PET/ITO/SnO_2/$Cs_{0.15}FA_{0.85}PbI_{3-x}Br_x$/PTAA/Au	10.36	0.58	33.49	3.92	94 (module)	76
	PET/ITO/Meo-2PACz/perovskite/PEAI/PCBM/BCP/Ag	1.173	24.96	83.51	24.45	1.01	77
	PET/ITO/Meo-2PACz/perovskite/PEAI/PCBM/BCP/Ag				15.87	72 (module)	77
	PET/ITO/SnO_2/perovskite/PEAI/spiro-OMeTAD/Au	1.16	24.85	79.9	23.01	0.09	78
	PET/ITO/SnO_2/perovskite/PEAI/spiro-OMeTAD/Au	32.49	0.69	78.5	17.52	117.7 (module)	78
	PET/PEDOT:PSS/Cl-BSA/perovskite/PCBM/BCP/Ag	1.10	22.13	74.44	18.12	1.01	175
	PET/ITO/PEDOT:EVA/perovskite/PCBM/BCP/Ag	1.18	21.26	79	19.87	1.01	176
	PET/ITO/PEDOT:EVA/perovskite/PCBM/BCP/Ag	4.73	5.34	68	17.55	31.20 (module)	176
	PEN/PEDOT:PSS/NiO_x/perovskite/PCBM/Ag	1.09	22.32	78.26	19.04	1.01	181
	PEN/ITO/Bio-IL/perovskite/PCBM/BCP/Ag	1.11	23.50	80.76	21.08	0.1	182
	PEN/ITO/Bio-IL/perovskite/PCBM/BCP/Ag	1.08	21.59	77.94	18.12	1.01	182
	PEN/ITO/Bio-IL/perovskite/PCBM/BCP/Ag	5.39	4.52	69.26	16.87	14.63	182
Slot-die coating	PET/ITO/SnO_2/$Cs_{0.15}FA_{0.85}PbI_{2.85}Br_{0.15}$/spiro-OMeTAD/Au	1.03	20.7	72	15.2	0.09	84
	PET/ITO/SnO_2/perovskite/spiro-OMeTAD/Au	1.090	20.48	76	17.18	0.16	92
	PET/ITO/poly-TPD/$MAPbI_3$/PCBM/Au	0.96	10.27	34	3.3	0.16	99
	PET/ITO/Cu:NiO_x/$MAPbI_3$/PCBM/BCP/Ag	1.13	21.75	79.4	19.56	0.09	100
	PET/ITO/SnO_2/$MAPbI_3$/spiro-OMeTAD/Au	0.958	16.6	62.9	10.01	0.03	101
	PET/ITO/PTACl-SnO_2/$MAPbI_3$/spiro-OMeTAD/Au	0.95	22.97	79.8	17.6	0.049	102
	PET/ITO/PTACl-SnO_2/$MAPbI_3$/spiro-OMeTAD/Au	0.97	21.7	60.2	12.7	1	102
	PET/ITO/SnO_2/perovskite/spiro-OMeTAD/MoO_x/Cu	1.11	23.04	78.92	20.21	0.1	103
	PET/ITO/SnO_2/perovskite/spiro-OMeTAD/MoO_x/Cu	34.2	0.61	57.7	12.1	185 (module)	103
	PET/ITO/SnO_2/perovskite/spiro-OMeTAD/MoO_x/Cu	35.9	0.55	56.8	11.2	333 (module)	103
	PET/TCE/SnO_2/$FAI_{0.45}MA_{0.55}PbI_3$/HTAB/P3HT/carbon	1.02	19.9	76.1	15.5	0.08	104
	PET/TCE/SnO_2/$FAI_{0.45}MA_{0.55}PbI_3$/HTAB/P3HT/carbon	4.59	3.88	62.3	11.0	49.5	104
	PET/ITO/SnO_2/perovskite/spiro-OMeTAD/Au	6.542	3.30	69	14.89	16.07 (module)	92
	MgF_2/PET/ITO/perovskite/PCBM/BCP/Ag	1.09	24.5	79.7	21.3	0.09	201
	PEN/ITO/SnO_2/perovskite/spiro-OMeTAD/Ag	0.98	16.82	63.99	10.57	0.07	212
Spray coating	PET/ITO/TiO_2/$MAPbI_{3-x}Cl_x$/spiro-OMeTAD/Ag	1.03	15.3	51.4	8.1	0.065	106
	PEN/ITO/TiO_2/$CH_3NH_3PbI_3$/spiro-OMeTAD/Au	0.945	20.68	55.6	10.87	0.16	124
	PEN/ITO/TiO_2/$CH_3NH_3PbI_3$/spiro-OMeTAD/Au	5.68	1.87	40.8	4.33	13.5 (module)	124
	PEN/ITO/PTAA/perovskite/C_{60}/BCP/Cu	1.07	22.17	76.27	18.14	0.078	125
	PEN/ITO/PTAA/perovskite/C_{60}/BCP/Cu	12.92	1.73	72.19	16.10	35.1 (module)	125
	PEI/ITO/TiO_2/perovskite/spiro-MeOTAD/Ag	0.892	18.82	50.76	8.52	0.1	126
	PET/ITO/SnO_2/perovskite/spiro-OMeTAD/Au	0.989	20.39	76	15.3	0.1	127
	PET/ITO/SnO_2/perovskite/spiro-OMeTAD/Au	7.72	2.55	60.8	12	16.84 (module)	127
	PET/ITO/SnO_2/perovskite/spiro-OMeTAD/Au	7.57	2.45	57.7	11.7	21.84 (module)	127

induced roughness, and improved mechanical adhesion. Moreover, integrating R2R-compatible fabrication techniques with *in situ* diagnostic tools could improve layer-by-layer quality control, thereby facilitating the transition from lab-scale demonstrations to manufacturable device architectures. Lastly, comprehensive techno-economic analyses are crucial to evaluating the practical viability of emerging materials and processing techniques, ensuring that enhancements in device performance and stability do not compromise scalability or affordability.

To provide a comprehensive overview of recent advancements in scalable PSC technologies, Table 3 summarizes representative PSCs and PSMs fabricated on rigid substrates with active areas ≥1 cm^2. The table focuses on key scalable coating techniques—blade coating, slot-die coating, and spray coating—by comparing device structures, active areas, and key optoelectronic parameters, including V_{OC}, J_{SC}, FF, and PCE. This comparison highlights the performance trends associated with each deposition method. Complementarily, Table 4 presents representative examples of F-PSCs and F-PSMs utilizing the same scalable coating approaches. It emphasizes the

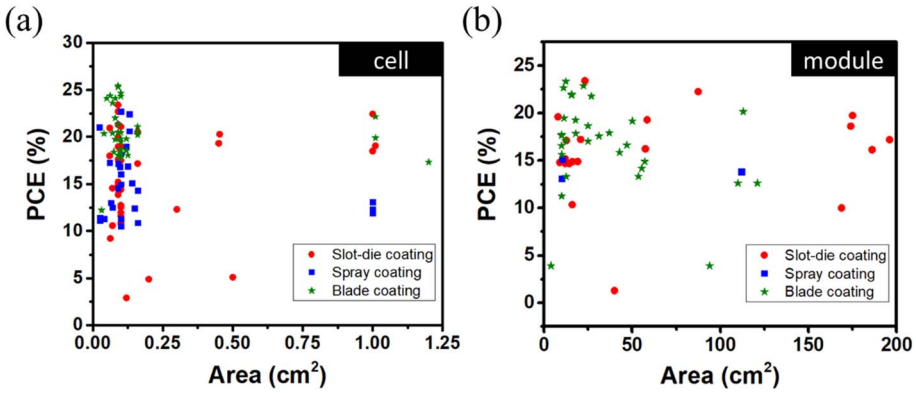

Fig. 12 PCE distribution of (a) PSC devices and (b) PSC modules as a function of active area, fabricated using three scalable deposition techniques reported in the literature: slot-die coating, spray coating, and blade coating.

adaptability of these techniques to flexible substrates and benchmarks their corresponding device configurations, active areas, and photovoltaic performance metrics. Together, these two tables provide a side-by-side comparison between rigid and flexible device development, offering insights into the scalability, versatility, and performance potential of each coating strategy. Fig. 12 illustrates the distribution of PCEs for cells and modules as a function of active area, categorized by the three large-area deposition techniques: blade coating, slot-die coating, and spray coating. Among these, blade coating exhibits the most consistent and outstanding performance. For active areas smaller than 1 cm^2, device efficiencies reach up to 25%, while module efficiencies remain stable between 10% and 20%, even as the active area increases to approximately 200 cm^2. In contrast, slot-die coating achieves similarly high efficiencies in small-area devices (up to 25% for areas <0.5 cm^2), but its performance declines significantly with increasing module size—particularly for active areas larger than 100 cm^2. Spray coating, on the other hand, generally exhibits lower overall efficiency, and the available data are limited, especially for large-area applications, making it difficult to draw definitive conclusions regarding its scalability. In summary, both blade coating and slot-die coating stand out as the most promising technologies for the scalable fabrication of high-efficiency small-area devices and large-area modules due to their process stability and performance reproducibility. In contrast, spray coating still requires further optimization to unlock its full potential for large-area solar cell manufacturing.

4.4 Encapsulation

The performance of PSCs is determined not only by their PCE but also by their operational stability and lifetime, given the intrinsic sensitivity of perovskite materials to moisture and oxygen.[213,214] To enhance device stability, effective encapsulation techniques are essential. While conventional rigid PSCs typically use glass plates sealed with thermosetting epoxy resin, such methods are unsuitable for F-PSCs, prompting the need for novel encapsulation materials and strategies. An ideal encapsulation material should possess high optical transmittance, excellent barrier properties (*i.e.*, low oxygen and water vapor transmission rates), UV resistance, chemical stability, mechanical flexibility, and long-term durability. ALD is one promising approach due to its excellent film uniformity and barrier performance, making it suitable for flexible electronics. However, its high-cost limits large-scale adoption. Alternative encapsulation techniques include thermal sealing with polymer adhesives, which form durable encapsulation layers upon heating, and thin-film encapsulation methods such as physical vapor deposition (PVD), which effectively block oxygen and moisture. Plasma-enhanced chemical vapor deposition (PECVD) can deposit multilayer barriers like silicon oxide and silicon nitride, greatly enhancing long-term stability. Plasma-enhanced atomic layer deposition (PEALD) also offers precise thickness control and dense films, making it suitable for ultra-thin, high-performance barriers. Encapsulation methods for flexible devices can generally be classified into two categories: single-layer and multilayer thin-film encapsulation.[215,216]

4.4.1 Single-layer thin-film encapsulation. This method employs a single inorganic layer as the barrier. While it is straightforward to implement, its effectiveness is often limited by defects and pinholes that allow oxygen and moisture to penetrate. A representative material in this category is aluminum oxide (Al_2O_3), deposited *via* ALD, which offers excellent uniformity and can be processed at low temperatures. Al_2O_3 films have demonstrated a water vapor transmission rate (WVTR) as low as 1.7×10^{-5} g per m^2 per d.[217] However, due to surface defects, single-layer encapsulation may still permit the ingress of oxygen or moisture. In contrast, multilayer encapsulation combines an inorganic layer with an organic one, such as poly(1,3,5-trimethyl-1,3,5-trivinylcyclotrisiloxane) (pV3D3), to mitigate defects in the inorganic barrier and enhance overall device stability. Organic materials are considered promising candidates for creating long-lasting and low-cost F-PSCs. For instance, Ma *et al.* successfully utilized paraffin wax as an encapsulation material to achieve durable PSCs.[218] Their study showed that paraffin wax can be processed at temperatures below 100 °C to form a stable barrier. After encapsulation, the device retained 80% of its initial PCE after 1000 hours of

exposure. This solvent-free encapsulation method presents strong potential for the large-scale production of F-PSCs.

4.4.2 Multilayer thin-film Encapsulation. Multilayer thin-film encapsulation typically integrates alternating inorganic and organic layers. The inorganic components, such as Al_2O_3, silicon dioxide (SiO_2), silicon nitride (Si_3N_4), and silicon oxynitride (SiO_xN_y), act as barriers that block moisture and oxygen ingress, while the organic layers, such as polyurethane (PU), polyethylene-1-octene (POE), and pV3D3, help to mitigate defects in the inorganic layers and enhance the overall reliability of the device. This encapsulation strategy has been widely applied in organic optoelectronic devices, significantly extending their operational lifetimes under ambient conditions. For instance, encapsulated F-PSCs have retained approximately 80% of their initial PCE for over 400 hours before showing noticeable degradation.[213] Furthermore, studies have demonstrated that F-PSCs with multilayer encapsulation maintained 97% of their initial PCE after 300 hours of exposure at 50 °C and 50% relative humidity (RH).[219] To further improve moisture resistance, PEN is considered a more suitable flexible substrate than PET due to its lower WVTR. Additionally, carbon-based materials—known for their hydrophobicity, flexibility, and electrical conductivity—have been proposed as alternative encapsulants, offering a promising pathway toward more durable F-PSCs. Continuous research efforts are being directed toward the development of novel encapsulation materials and techniques to further extend device longevity. If multilayer encapsulation can be implemented in a cost-effective manner while providing high-performance barrier properties, it will become a critical step toward realizing durable and affordable F-PSCs.[220]

The advancement of F-PSCs heavily relies on overcoming key challenges related to encapsulation techniques. One of the primary issues is selecting the appropriate flexible substrate that balances mechanical robustness with minimal impact on device efficiency. This requires innovations in low-temperature processing and encapsulation methods to protect the devices from environmental degradation, such as moisture and oxygen infiltration. Flexible substrates, such as polymers, are prone to permeability, making effective encapsulation critical to maintaining device performance and longevity. Multilayer encapsulation, which combines inorganic layers (*e.g.*, Al_2O_3, SiO_2) with organic layers (*e.g.*, polyurethane, pV3D3), offers a promising solution to enhance the barrier properties of encapsulation systems. These multilayer systems are capable of reducing defects in the inorganic layers, thereby improving the overall durability of the F-PSCs. In addition to material selection, interface engineering plays a crucial role in improving encapsulation reliability by enhancing charge transport and reducing interfacial defects that could lead to degradation over time. To meet the requirements for large-scale production, scalable fabrication methods such as roll-to-roll processing are essential for producing uniform encapsulation layers efficiently. However, challenges remain in ensuring consistent layer quality and uniformity to guarantee high throughput in mass production. Addressing these encapsulation challenges is crucial for improving the overall stability of F-PSCs, ensuring their viability for practical applications.

5. Stability

The long-term stability of PSCs is crucial for commercialization and practical use. While PSCs achieve high efficiency, their environmental and mechanical stability remains a key challenge. Environmental stability refers to resistance against moisture, heat, light, and oxygen, which can degrade the perovskite and other materials. As discussed, encapsulation plays a vital role in mitigating these effects. Mechanical stability, particularly for flexible devices, ensures PSCs maintain functionality under bending or stretching. Enhancing both environmental and mechanical stability is essential for developing efficient, durable, and reliable PSCs suitable for real-world applications. This section explores key strategies and advancements in improving PSC stability.

5.1 Environmental stability

To ensure the long-term stability of F-PSCs in practical applications, verifying their environmental durability is crucial.

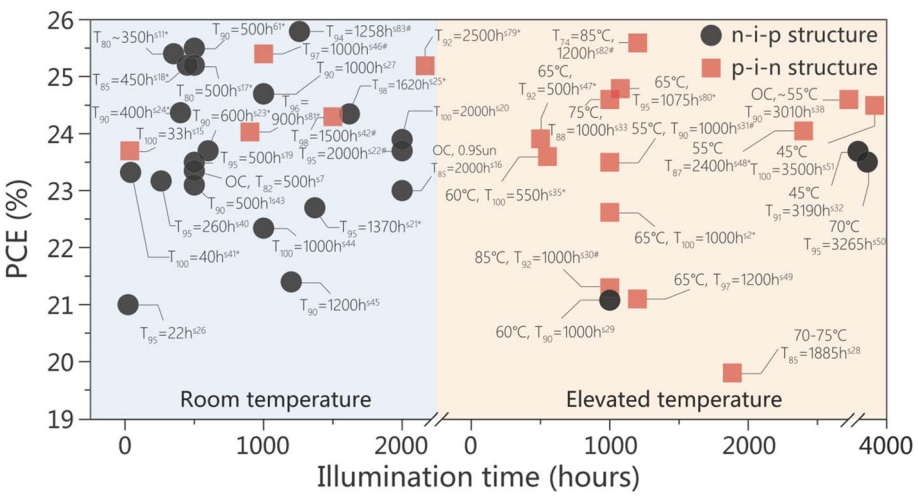

Fig. 13 The state of the art of perovskite stability under continuous illumination.[224]

Researchers have developed standardized testing methods to assess PSC performance under various environmental conditions, such as humidity, UV exposure, high and low temperatures, and temperature cycling. Humidity tests simulate high-moisture environments to assess the degradation of perovskite materials due to water exposure. UV exposure tests evaluate the damage caused by UV radiation on the organic components of the materials. High-temperature tests simulate hot environments to examine the impact of elevated temperatures on the material's structure and efficiency, while low-temperature tests evaluate performance under cold conditions. Temperature cycling tests simulate daily or seasonal temperature fluctuations, assessing the thermal stability of the materials. These tests help researchers understand performance degradation and provide insights into strategies to enhance the reliability and long-term stability of PSCs in real-world applications. Standardized stability testing protocols, such as those outlined in International Electrotechnical Commission (IEC) 61215 and ISOS, are widely adopted for evaluating PSC stability.[221–223] As shown in Fig. 13, most studies focus on device-level stability data,[224] with limited research on module-level stability. Nevertheless, several investigations have successfully enhanced PSC performance in accelerated aging tests by optimizing material properties and structural designs. Defects located at grain boundaries in perovskite films act as non-radiative recombination centers due to the presence of under-coordinated Pb^{2+} ions, halide vacancies, and dangling bonds. These defects introduce trap states within the bandgap that capture carriers, accelerating trap-assisted recombination and lowering the quasi-Fermi level splitting, which in turn reduces VOC and overall PCE. Moreover, grain boundaries provide pathways for ion migration—especially halide ions—further compromising operational stability. To mitigate these issues, diverse passivation strategies are widely employed. Organic ammonium halides (*e.g.*, phenethylammonium iodide) can form hydrogen bonds or ionic interactions with under-coordinated Pb^{2+} or halide vacancies, thereby reducing trap densities. Fullerene derivatives (*e.g.*, PCBM, ICBA) function as electron-accepting passivators that neutralize charged defects, while Lewis bases such as thiophene or pyridine derivatives coordinate directly with Pb^{2+} centers, effectively suppressing defect-assisted recombination. Collectively, these passivation interactions chemically stabilize grain boundaries, enhance charge transport continuity, and improve resistance to mechanical cracking, which is especially crucial for flexible perovskite devices. For example, Han *et al.* introduced a bifunctional organic molecule, 5-ammonium valeric acid (5-AVA) iodide, at the grain boundaries of $MAPbI_3$ crystals. This approach localized the perovskite crystals at the nanoscale, suppressed decomposition and reconstruction, and made ionic migration reversible. PSCs using this $(5\text{-AVA})_xMA_{1-x}PbI_3$ active layer demonstrated stable operation for over 9000 hours at the maximum power point (MPP) at 55 °C ± 5 °C with no significant degradation, successfully meeting the IEC 61215:2016 qualification standards.[222] In 2022, Saule Technologies achieved significant advancements in small perovskite cells. These cells retained 84% of their initial efficiency after 1000 hours at the MPP under 0.6 sun, and showed no degradation after 1000 hours at 85 °C, highlighting improvements in thermal stability and long-term performance.[225] In 2023, Microquanta Semiconductor and Wuxi Utmolight Technology made considerable strides in module-level stability. Microquanta developed standard perovskite modules with multi-layer encapsulation, passing IEC 61215 and IEC 61730 tests, demonstrating reliability under conditions such as UV exposure, damp heat, and temperature cycling.[226] Similarly, Wuxi Utmolight Technology fabricated modules with an area of 0.72 m^2 using advanced encapsulation materials and laser scribing techniques, minimizing interface defects and reducing vulnerability to environmental degradation. These modules also passed IEC 61215 and IEC 61730 certifications in November 2023, showcasing exceptional stability and strong commercial potential.[227]

5.2 Mechanical stability

Mechanical properties are critical for F-PSCs, but mechanical stability remains a challenge, especially for transparent electrodes and perovskite layers. TCOs like ITO and fluorine-doped tin oxide (FTO) are commonly used on polymer substrates, but they are brittle. After several bending cycles, cracks can form, degrading the device. Additionally, convex bending of perovskite layers can cause damage.[228] Cracks in perovskite films reduce conductivity and mechanical stability. In this context, standardized testing methodologies have recently been introduced, such as the consensus protocol proposed by Fukuda *et al.* for characterizing the mechanical performance of flexible photovoltaics under bending tests.[229] This complements the established ISOS protocols for stability testing of PSCs and provides a valuable framework for ensuring consistent evaluation across different studies. Recently, designs aimed at mitigating bending damage by promoting mechanical strain distribution have shown potential for practical applications.[176,230] Various ultra-flexible transparent electrodes have been developed to replace TCOs, focusing on the bending radius and test cycles. ITO-based devices typically cannot withstand bending radii smaller than 5 mm, while flexible perovskite solar cells without ITO electrodes can endure radii even below 1 mm. This is due to the brittleness of the ITO layer, where cracks negatively affect the perovskite layer, resulting in lower PCE. Enhancing bending resistance requires improvements not only in functional layers and substrates but also in the perovskite layer itself. Inspired by spinal structures, Meng *et al.* proposed a biomimetic design to enhance F-PSC flexibility by absorbing and distributing stress. They used PEDOT:EVA as the HTL, likening it to articular cartilage for its flexibility and adhesion. Simulations of stress distribution showed that PEDOT:EVA reduced local stress on the perovskite layer during bending, compared to traditional PEDOT:PSS. Additionally, the ionic nature of halide perovskites gives them high tolerance to strain, making them suitable for flexible electronics.[176] However, this "flexibility" also makes PSCs mechanically fragile, posing challenges for long-term durability. Various strategies, compositional, structural, grain boundary, and interfacial engineering, have been developed to improve performance and mechanical stability.[151,152,231] Compositional engineering involves substituting

elements or ions within the perovskite structure to enhance mechanical and electronic properties. Examples include mixed-cation or mixed-halide perovskites, where different cations or halides improve stability and performance.[232–234] Structural engineering optimizes the micro- and nanostructures of the perovskite layer, such as thickness, porosity, and morphology, to better distribute mechanical stress and prevent cracks or delamination. Since halide perovskites are polycrystalline, grain boundaries are often weak points for failure.[235,236] Interfacial engineering focuses on improving interfaces between the perovskite layer and adjacent layers, where stress often accumulates, leading to delamination. Approaches include using interfacial modification layers or selecting materials with better mechanical compatibility with perovskites.[237] Recently, Dong *et al.* proposed strategies to protect the perovskite layer under bending conditions. By introducing an insulating elastic material, trimethyl-triethynylcyclotrisiloxane, they achieved grain boundary encapsulation, which suppressed carrier recombination and ion migration, improving durability. After 10 000 bending cycles, the cell retained over 73% of its initial PCE.[238] The device achieved a bending radius as small as 2.5 mm, one of the best values for flexible perovskite solar cells based on ITO substrates.

Environmental stability has seen improvements with the use of additives like 5-AVA to enhance perovskite material durability. Continued research should focus on optimizing these additives for broader scalability. The advancements in module-level stability by companies like Microquanta and Wuxi Utmolight, especially through improved encapsulation, emphasize the importance of developing more reliable encapsulation materials for F-PSCs. On the mechanical side, the brittleness of traditional transparent conductive oxides, like ITO, remains a major challenge. The future of F-PSCs lies in exploring alternative electrode materials that provide greater flexibility while maintaining high performance. Strategies such as grain boundary engineering and interfacial modifications have shown potential in improving the mechanical durability of the perovskite layer under bending stress. Moving forward, greater focus should be placed on developing materials that combine both environmental and mechanical stability to ensure the long-term reliability of F-PSCs for commercial use.

6. Challenges and outlook

Despite the significant attention that PSCs and related organic optoelectronic devices have gained in both academic and industrial circles due to their high efficiency and low-cost characteristics, challenges still remain in their commercialization and large-scale application. These challenges extend beyond processing difficulties to include issues such as material stability, structural integrity, and the potential for flexible applications. Below, we explore these key challenges and potential solutions.

6.1 Large-area fabrication

Achieving uniformity and reproducibility of thin films is crucial for device performance in large-area fabrication. Processes like blade coating, slot-die coating, and spray coating often face difficulties in achieving consistent film thickness and crystal structure, primarily due to uneven solvent evaporation rates and changes in solution flow dynamics. For example, during blade coating, uneven surface tension of the substrate (*i.e.*, the Marangoni effect) can lead to variations in solvent concentration, affecting the crystal nucleation and structural integrity of the films. To address this, researchers are focusing on optimizing solution formulations with additives such as surfactants or stabilizers and exploring localized heating techniques to control solvent evaporation post-coating.

6.2 Non-uniform crystal nucleation: challenges and monitoring

Non-uniform crystal nucleation remains a fundamental obstacle in perovskite film fabrication, as rapid solvent evaporation or excessively concentrated precursor solutions often induce high defect densities, grain boundary formation, and internal voids. These microstructural imperfections compromise both efficiency and stability. Recent studies have demonstrated that solution additives such as DMSO or ethylene glycol monomethyl ether can effectively slow down nucleation kinetics, thereby reducing defect density. In parallel, advanced monitoring strategies including real-time crystallization tracking using synchrotron X-ray diffraction are being developed to synchronize annealing processes with nucleation dynamics, offering more precise control over film quality and long-term performance.

6.3 Chemical insights into ink formulation

Perovskite ink formulation dictates the entire transformation pathway from solution complexes to intermediate adducts and final perovskite phases. Coordinating solvents (*e.g.*, DMSO, DMF, NMP) together with Lewis-base additives form transient complexes with PbX_2, thereby delaying uncontrolled nucleation and promoting uniform film formation. The donor number, volatility, and coordination strength of solvents collectively determine the supersaturation trajectory during solvent evaporation, which in turn governs nucleation density and subsequent grain growth behavior. Moreover, mixed-halide and mixed-cation systems introduce additional coupling between ionic speciation and solvent–solute interactions, thereby modulating defect chemistry such as halide vacancy formation and trap density. This chemical perspective underscores that precise ink formulation is essential for minimizing defect generation at the earliest stages of film formation.

6.4 Crystallization control strategies during film formation

Beyond ink design, controlling the conversion of intermediate phases into the final perovskite lattice is equally crucial. Anti-solvent quenching or gas-/vacuum-assisted extraction rapidly increases supersaturation, generating dense nucleation while mitigating coffee-ring effects; however, excessively fast extraction may entrap residual solvent and induce microvoid formation. Thermal annealing, including gradient or stepwise protocols, facilitates solvent removal, collapse of intermediates, and oriented grain growth, yet overheated or nonuniform

annealing can induce stress, phase segregation, and interfacial debonding, effects amplified on flexible substrates due to a coefficient of thermal expansion mismatch. Alternatively, humidity- or solvent-vapor-assisted annealing provides a wider processing window by moderating nucleation and growth kinetics while reducing pinhole density, though it requires stricter control of ambient conditions. Collectively, these crystallization control strategies highlight the delicate balance between processing kinetics, defect mitigation, and mechanical reliability.

6.5 Flexible substrate issues

For large-area devices on flexible substrates (such as PI or PET), differences in thermal expansion coefficients between the substrate and thin film can cause cracking or wrinkling during thermal treatment, compromising the device's structural integrity. To mitigate these thermal expansion issues, rapid photothermal annealing techniques, such as intense pulsed light annealing or near-infrared heating, can precisely control the substrate's heating process. Additionally, introducing elastic interface layers, such as polydimethylsiloxane (PDMS) films, can effectively reduce stress transfer between the film and substrate, thereby enhancing the stability and structural strength of devices on flexible substrates.

6.6 Environmental stability

Environmental stability is a critical factor affecting the long-term performance of perovskite solar cells, especially due to the material's sensitivity to moisture, oxygen, and UV light, which can lead to degradation. For example, humidity can cause PbI_2 and MAI to decompose, forming unstable intermediate phases that affect the lattice structure and reduce PCE. Researchers have suggested using double-cation or multi-cation systems, like Cs^+/FA^+ mixtures, to improve lattice stability and reduce moisture sensitivity. The use of hydrophobic polymer encapsulation materials, such as poly(vinylidene fluoride-*co*-hexafluoropropylene) (PVDF-HFP),[239] has also shown promise in improving moisture resistance.

6.7 Photo-stability and ion migration

In addition to environmental stability, photo-stability and ion migration remain significant challenges for PSC commercialization. Under light or external electric fields, migration of iodide and lead cations can redistribute the internal electric field, leading to performance degradation. To address this, stable lattice design strategies, such as using passivating agents like TiO_2, aim to stabilize grain boundaries and reduce ion migration. Interface-sensitive modifiers (*e.g.*, small-molecule SAMs, PEI, polymeric buffers) lower interfacial energy barriers for nucleation on polymer substrates, improving wetting and adhesion while passivating under-coordinated Pb^{2+}/halide defects. Post-deposition chemical treatments (*e.g.*, organic ammonium halides, Lewis bases, fullerene derivatives) passivate grain boundaries and reduce Shockley–Read–Hall recombination, thereby improving V_{OC} and bending durability by mitigating crack initiation at intergranular weak points.

6.8 Mechanical flexibility

Lastly, the mechanical flexibility of PSCs remains a major challenge, especially when used on flexible substrates. The brittleness of the perovskite film can lead to cracking, particularly under repeated bending. Researchers are optimizing the directional alignment of crystal grains to form columnar structures, improving resistance to cracking. Additionally, metal passivating agents like zinc-based compounds are being explored to enhance the toughness of grain boundaries and improve the mechanical flexibility of the films. To address the brittleness of the ITO transparent conductive layer, alternative flexible conductive materials, such as oxide/conductive polymer composite films like PEDOT:PSS/Ag NW, are being investigated. Furthermore, introducing low-modulus polymer buffer layers, such as PU-based composites, can reduce stress concentration during bending, enhancing the overall mechanical stability of the interface layer and electrodes.

6.9 Key challenges for F-TPSCs and all-printed F-PSCs

As F-TPSCs continue to advance, their future development hinges on resolving key challenges in device architecture, material stability, and scalable processing. The 2T monolithic structure offers compact integration and lower series resistance but requires strict current matching and reliable interconnection layers to prevent performance losses. In contrast, 4T mechanically stacked tandems allow independent sub-cell optimization and material diversity, yet face issues such as optical losses at the interlayer and increased device thickness. Material selection also critically influences performance and flexibility. Perovskite/CIGS and perovskite/Si tandems benefit from mature bottom-cell technologies but pose challenges in interfacial engineering and mechanical robustness. All-perovskite and perovskite/OPV tandems offer low-temperature, flexible processing routes but still lag behind in long-term stability and efficiency. In parallel, all-printed flexible perovskite solar cells have emerged as a promising alternative to vacuum-based processing. By using fully solution-based techniques—including inkjet and digital printing—for every functional layer, recent demonstrations have achieved large-area modules exceeding 16% efficiency, with strong mechanical durability and air stability. To realize practical deployment, future efforts must focus on improving interfacial contact, transparent electrode resilience, and compatibility with roll-to-roll, low-temperature manufacturing without compromising device lifetime.

7. Conclusion

The future development of PSCs depends on innovations across multiple technologies and interdisciplinary collaboration, especially in the area of F-PSCs. Although F-PSCs offer advantages such as lightweight design and high efficiency, their commercial applications still face significant obstacles, particularly in mechanical stability, durability, and the realization of flexible integration. Overcoming these challenges requires advancements in materials, processing techniques, and

structural designs to enable commercialization and large-scale adoption. Material innovation would be a key driver, with a focus on developing stable, efficient, and environmentally friendly materials. For F-PSCs, it is essential to create perovskite materials that are compatible with flexible substrates by enhancing intrinsic stability and reducing structural damage during deformation or bending. Research on hybrid cation perovskites and inorganic perovskite materials is expected to significantly improve the long-term performance and stability of flexible devices. In parallel, the development of flexible tandem PSCs represents a promising route to surpass the efficiency limits of single-junction architectures by stacking complementary absorbers. Despite the challenges in current matching, interlayer engineering, and mechanical integration, recent progress has demonstrated the feasibility of high-efficiency flexible tandem designs, which will be instrumental in future high-performance applications. Breakthroughs in processing technologies also play a crucial role in accelerating commercialization. Developing scalable, low-cost, and environmentally friendly fabrication methods such as solution processing and vacuum-free techniques can reduce production costs and enable high-efficiency, large-area manufacturing. In particular, all-printed F-PSCs, which rely entirely on solution-based printing methods for each functional layer, have emerged as a key strategy to achieve fully roll-to-roll-compatible, low-temperature fabrication for flexible devices. Compared to rigid substrates, flexible substrates present greater challenges in coating uniformity and mechanical strength, making these areas critical for future technological development. In terms of application expansion, F-PSCs hold great potential for use in wearable electronics, BIPV, and flexible displays. Realizing these applications will not only drive the advancement of F-PSC technology but also contribute to broader adoption of green energy solutions. However, to meet the demands of these fields, F-PSCs must achieve higher standards in terms of lightweight design, durability, and mechanical flexibility. Finally, integrating the industrial supply chain is essential for driving commercialization. Strengthening collaboration between academia and industry can accelerate equipment development, material supply chain integration, and standardization, all of which are vital for scaling up production. Cross-disciplinary collaboration and the sharing of technological knowledge would help overcome current processing challenges and boost the commercialization potential of F-PSCs. In conclusion, while challenges remain, the future of F-PSCs is full of promise. These challenges are not limited to materials and processing techniques but also include the need to improve stability, durability, and efficiency while maintaining mechanical flexibility. Future research must address these areas through collaborative and interdisciplinary efforts to drive technological advancement. With continuing breakthroughs, perovskite solar cells are poised to become a leading technology in the global transition toward sustainable energy.

Conflicts of interest

There are no conflicts to declare.

Data availability

No primary research results, software or code have been included and no new data were generated or analysed as part of this review.

Acknowledgements

The authors gratefully acknowledge the support from the National Science and Technology Council of Taiwan under Grant No. NSTC 112-2628-E-131-001-MY4, NSTC 114-2222-E-131-002 and NSTC 114-2622-E-131-007. All authors contributed to the literature review, scientific discussions, and manuscript preparation.

References

1 https://www.cervicornconsulting.com/solar-photovoltaic-market.
2 https://www.perovskite-info.com/perovskite-solar?utm_source=chatgpt.com.
3 K. X. Steirer, P. Schulz, G. Teeter, V. Stevanovic, M. Yang, K. Zhu and J. J. Berry, Defect tolerance in methylammonium lead triiodide perovskite, *ACS Energy Lett.*, 2016, **1**, 360–366.
4 S. D. Stranks, G. E. Eperon, G. Grancini, C. Menelaou, M. J. Alcocer, T. Leijtens, L. M. Herz, A. Petrozza and H. J. Snaith, Electron-hole diffusion lengths exceeding 1 micrometer in an organometal trihalide perovskite absorber, *Science*, 2013, **342**, 341–344.
5 M. De Bastiani, V. Larini, R. Montecucco and G. Grancini, The levelized cost of electricity from perovskite photovoltaics, *Energy Environ. Sci.*, 2023, **16**, 421–429.
6 T. Bu, L. K. Ono, J. Li, J. Su, G. Tong, W. Zhang, Y. Liu, J. Zhang, J. Chang and S. Kazaoui, Modulating crystal growth of formamidinium–caesium perovskites for over 200 cm2 photovoltaic sub-modules, *Nat. Energy*, 2022, **7**, 528–536.
7 C. Chen, J. Chen, H. Han, L. Chao, J. Hu, T. Niu, H. Dong, S. Yang, Y. Xia and Y. Chen, Perovskite solar cells based on screen-printed thin films, *Nature*, 2022, **612**, 266–271.
8 D. Shi, V. Adinolfi, R. Comin, M. Yuan, E. Alarousu, A. Buin, Y. Chen, S. Hoogland, A. Rothenberger, K. Katsiev, Y. Losovyj, X. Zhang, P. A. Dowben, O. F. Mohammed, E. H. Sargent and O. M. Bakr, Low trap-state density and long carrier diffusion in organolead trihalide perovskite single crystals, *Science*, 2015, **347**, 519.
9 https://www.nrel.gov/pv/cell-efficiency.html, 2024.
10 H. Min, D. Y. Lee, J. Kim, G. Kim, K. S. Lee, J. Kim, M. J. Paik, Y. K. Kim, K. S. Kim and M. G. Kim, Perovskite solar cells with atomically coherent interlayers on SnO2 electrodes, *Nature*, 2021, **598**, 444–450.
11 Y. Zhao, F. Ma, Z. Qu, S. Yu, T. Shen, H.-X. Deng, X. Chu, X. Peng, Y. Yuan and X. Zhang, Inactive (PbI2) 2RbCl stabilizes perovskite films for efficient solar cells, *Science*, 2022, **377**, 531–534.

12 N.-G. Park and K. Zhu, Scalable fabrication and coating methods for perovskite solar cells and solar modules, *Nat. Rev. Mater.*, 2020, **5**, 333–350.
13 **https://www.idtechex.com/en/research-article/perovskite-pv-resolving-the-stability-challenge/27295**, 2022.
14 M. Xiao, F. Huang, W. Huang, Y. Dkhissi, Y. Zhu, J. Etheridge, A. Gray-Weale, U. Bach, Y. B. Cheng and L. Spiccia, A fast deposition-crystallization procedure for highly efficient lead iodide perovskite thin-film solar cells, *Angew. Chem., Int. Ed.*, 2014, **53**, 9898–9903.
15 N. J. Jeon, J. H. Noh, Y. C. Kim, W. S. Yang, S. Ryu and S. I. Seok, Solvent engineering for high-performance inorganic-organic hybrid perovskite solar cells, *Nat. Mater.*, 2014, **13**, 897–903.
16 M. R. Ahmadian-Yazdi, F. Zabihi, M. Habibi and M. Eslamian, Effects of process parameters on the characteristics of mixed-halide perovskite solar cells fabricated by one-step and two-step sequential coating, *Nanoscale Res. Lett.*, 2016, **11**, 408.
17 Z. Yang, S. Zhang, L. Li and W. Chen, Research progress on large-area perovskite thin films and solar modules, *J. of Materiomics*, 2017, **3**, 231–244.
18 A. Roy, A. Ghosh, S. Bhandari, S. Sundaram and T. K. Mallick, Perovskite Solar Cells for BIPV Application: A Review, *Buildings*, 2020, **10**, 129.
19 H. Sugimoto, Feasibility Study of Rechargeable Flexible Tandem Solar Cells for VIPV Applications Under Realistic Environments, *2023 Middle East and North Africa Solar Conference (MENA-SC)*, 2023, pp. 1–4.
20 M. Ayalasomayajula, M. R. Khurana, V. Balakrishnan, P. S. Chaudhary, S. B. Bal and R. K. Baranwal, Advancements in Wearable Solar Cell Technology: Integrating Perovskites and Dye-Sensitized Cells, *IEEE Journal on Flexible Electronics*, 2024, **3**, 205–213.
21 M. Pirc, Ž. Ajdič, D. Uršič, M. Jošt and M. Topič, Indoor Energy Harvesting With Perovskite Solar Cells for IoT Applications–A Full Year Monitoring Study, *ACS Appl. Energy Mater.*, 2024, **7**, 565–575.
22 A. Alberti, E. Smecca, S. Valastro, I. Deretzis, G. Mannino, C. Bongiorno, G. Fisicaro and A. La Magna, Perovskite solar cells from the viewpoint of innovation and sustainability, *Phys. Chem. Chem. Phys.*, 2022, **24**, 21549–21566.
23 S. Sidhik, I. Metcalf, W. Li, T. Kodalle, C. J. Dolan, M. Khalili, J. Hou, F. Mandani, A. Torma, H. Zhang, R. Garai, J. Persaud, A. Marciel, I. A. Muro Puente, G. N. M. Reddy, A. Balvanz, M. A. Alam, C. Katan, E. Tsai, D. Ginger, D. P. Fenning, M. G. Kanatzidis, C. M. Sutter-Fella, J. Even and A. D. Mohite, Two-dimensional perovskite templates for durable, efficient formamidinium perovskite solar cells, *Science*, 2024, **384**, 1227–1235.
24 M. H. Kumar, N. Yantara, S. Dharani, M. Graetzel, S. Mhaisalkar, P. P. Boix and N. Mathews, Flexible, low-temperature, solution processed ZnO-based perovskite solid state solar cells, *Chem. Commun.*, 2013, **49**, 11089–11091.
25 C. Roldán-Carmona, O. Malinkiewicz, A. Soriano, G. Mínguez Espallargas, A. Garcia, P. Reinecke, T. Kroyer, M. I. Dar, M. K. Nazeeruddin and H. J. Bolink, Flexible high efficiency perovskite solar cells, *Energy Environ. Sci.*, 2014, **7**, 994–997.
26 S. S. Shin, W. S. Yang, J. H. Noh, J. H. Suk, N. J. Jeon, J. H. Park, J. S. Kim, W. M. Seong and S. I. Seok, High-performance flexible perovskite solar cells exploiting Zn2SnO4 prepared in solution below 100 °C, *Nat. Commun.*, 2015, **6**, 7410.
27 J. Yoon, H. Sung, G. Lee, W. Cho, N. Ahn, H. S. Jung and M. Choi, Superflexible, high-efficiency perovskite solar cells utilizing graphene electrodes: towards future foldable power sources, *Energy Environ. Sci.*, 2017, **10**, 337–345.
28 C. Bi, B. Chen, H. Wei, S. DeLuca and J. Huang, Efficient Flexible Solar Cell based on Composition-Tailored Hybrid Perovskite, *Adv. Mater.*, 2017, **29**, 1605900.
29 J. Feng, X. Zhu, Z. Yang, X. Zhang, J. Niu, Z. Wang, S. Zuo, S. Priya, S. Liu and D. Yang, Record Efficiency Stable Flexible Perovskite Solar Cell Using Effective Additive Assistant Strategy, *Adv. Mater.*, 2018, **30**, 1801418.
30 K. Huang, Y. Peng, Y. Gao, J. Shi, H. Li, X. Mo, H. Huang, Y. Gao, L. Ding and J. Yang, High-Performance Flexible Perovskite Solar Cells via Precise Control of Electron Transport Layer, *Adv. Energy Mater.*, 2019, **9**, 1901419.
31 L. Yang, Q. Xiong, Y. Li, P. Gao, B. Xu, H. Lin, X. Li and T. Miyasaka, Artemisinin-passivated mixed-cation perovskite films for durable flexible perovskite solar cells with over 21% efficiency, *J. Mater. Chem. A*, 2021, **9**, 1574–1582.
32 S. Wu, Z. Li, J. Zhang, X. Wu, X. Deng, Y. Liu, J. Zhou, C. Zhi, X. Yu, W. C. H. Choy, Z. Zhu and A. K. Y. Jen, Low-Bandgap Organic Bulk-Heterojunction Enabled Efficient and Flexible Perovskite Solar Cells, *Adv. Mater.*, 2021, **33**, 2105539.
33 D. Gao, B. Li, Z. Li, X. Wu, S. Zhang, D. Zhao, X. Jiang, C. Zhang, Y. Wang, Z. Li, N. Li, S. Xiao, W. C. H. Choy, A. K. Y. Jen, S. Yang and Z. Zhu, Highly Efficient Flexible Perovskite Solar Cells through Pentylammonium Acetate Modification with Certified Efficiency of 23.35%, *Adv. Mater.*, 2023, **35**, 2206387.
34 R. Xu, F. Pan, J. Chen, J. Li, Y. Yang, Y. Sun, X. Zhu, P. Li, X. Cao, J. Xi, J. Xu, F. Yuan, J. Dai, C. Zuo, L. Ding, H. Dong, A. K. Y. Jen and Z. Wu, Optimizing the Buried Interface in Flexible Perovskite Solar Cells to Achieve Over 24% Efficiency and Long-Term Stability, *Adv. Mater.*, 2024, **36**, 2308039.
35 X. Tong, L. Xie, J. Li, Z. Pu, S. Du, M. Yang, Y. Gao, M. He, S. Wu, Y. Mai and Z. Ge, Large Orientation Angle Buried Substrate Enables Efficient Flexible Perovskite Solar Cells and Modules, *Adv. Mater.*, 2024, **36**, 2407032.
36 W. Zhang, J. Liu, W. Song, J. Shan, H. Guan, J. Zhou, Y. Meng, X. Tong, J. Zhu, M. Yang and Z. Ge, Chemical passivation and grain-boundary manipulation via in situ cross-linking strategy for scalable flexible perovskite solar cells, *Sci. Adv.*, 2025, **11**, eadr2290.

37 X. Huang, F. Zhang, Y. Liu and J. Leng, Active and Deformable Organic Electronic Devices based on Conductive Shape Memory Polyimide, *ACS Appl. Mater. Interfaces*, 2020, **12**, 23236–23243.
38 S. S. Siwal, A. K. Saini, S. Rarotra, Q. Zhang and V. K. Thakur, Recent advancements in transparent carbon nanotube films: chemistry and imminent challenges, *J. Nanostruct. Chem.*, 2021, **11**, 93–130.
39 S. Pisoni, F. Fu, T. Feurer, M. Makha, B. Bissig, S. Nishiwaki, A. N. Tiwari and S. Buecheler, Flexible NIR-transparent perovskite solar cells for all-thin-film tandem photovoltaic devices, *J. Mater. Chem. A*, 2017, **5**, 13639–13647.
40 S. Pisoni, R. Carron, T. Moser, T. Feurer, F. Fu, S. Nishiwaki, A. N. Tiwari and S. Buecheler, Tailored lead iodide growth for efficient flexible perovskite solar cells and thin-film tandem devices, *NPG Asia Mater.*, 2018, **10**, 1076–1085.
41 J. Luo, L. Tang, S. Wang, H. Yan, W. Wang, Z. Chi, J. Gong, J. Li and X. Xiao, Manipulating Ga growth profile enables all-flexible high-performance single-junction CIGS and 4 T perovskite/CIGS tandem solar cells, *Chem. Eng. J.*, 2023, **455**, 140960.
42 J. Zheng, C. Xue, G. Wang, M. A. Mahmud, Z. Sun, C. Liao, J. Yi, J. Qu, L. Yang, L. Wang, S. Bremner, J. M. Cairney, J. Zhang and A. W. Y. Ho-Baillie, Efficient Flexible Monolithic Perovskite–CIGS Tandem Solar Cell on Conductive Steel Substrate, *ACS Energy Lett.*, 2024, **9**, 1545–1547.
43 L. Tang, L. Zeng, J. Luo, W. Wang, Z. Xue, Z. Luo, H. Yan, J. Gong, S. Wang, J. Li and X. Xiao, All-Round Passivation Strategy Yield Flexible Perovskite/CuInGaSe2 Tandem Solar Cells with Efficiency Exceeding 26.5%, *Adv. Mater.*, 2024, **36**, 2402480.
44 W. Tian, L. Yao, E. Bi, S. Zhang, Y. Tian, J. Zhou, X. Wang, M. Haider, J. Xue and R. Wang, Inert Interlayer Secures Flexible Monolithic Perovskite/CIGS Tandem Solar Cells with Efficiency Beyond 21%, *ACS Energy Lett.*, 2025, **10**, 562–568.
45 I. Jeong, T. K. Lee, H. Van Tran, I. Hwang, J. Hwang, A. Lee, S. Ham, H. Tran, Y. Cho, D. Shin, S. Song, S. Lee, S. K. Ahn, Y.-J. Eo, A. Cho, J. H. Park, J.-S. Cho, J. Byeon, W. M. Kim, J. H. Yun, J. Gwak, S. Hong, S. Ahn, H.-J. Kim and K. Kim, Flexible and lightweight perovskite/Cu(In,Ga)Se_2 tandem solar cells, *Joule*, 2025, **9**, 101794.
46 L. Tang, H. Yan, L. Zeng, Z. Xue, Z. Luo, J. Luo, W. Wang, S. Wang, J. Gong, J. Li and X. Xiao, Record-Efficient Flexible Monolithic Perovskite–CIGS Tandem Solar Cell with VOC Exceeding 1.8 V on Polymer Substrate, *Adv. Energy Mater.*, 2025, 2403682.
47 Z. Ying, S. Su, X. Li, G. Chen, C. Lian, D. Lu, M. Zhang, X. Guo, H. Tian, Y. Sun, L. Liu, C. Xiao, Y. Zeng, C. Zhang, X. Yang and J. Ye, Antisolvent seeding of self-assembled monolayers for flexible monolithic perovskite/Cu(In,Ga)Se2 tandem solar cells, *Nat. Energy*, 2025, 737–749.
48 A. F. Palmstrom, G. E. Eperon, T. Leijtens, R. Prasanna, S. N. Habisreutinger, W. Nemeth, E. A. Gaulding, S. P. Dunfield, M. Reese, S. Nanayakkara, T. Moot, J. Werner, J. Liu, B. To, S. T. Christensen, M. D. McGehee, M. F. A. M. van Hest, J. M. Luther, J. J. Berry and D. T. Moore, Enabling Flexible All-Perovskite Tandem Solar Cells, *Joule*, 2019, **3**, 2193–2204.
49 H. Lai, J. Luo, Y. Zwirner, S. Olthof, A. Wieczorek, F. Ye, Q. Jeangros, X. Yin, F. Akhundova, T. Ma, R. He, R. K. Kothandaraman, X. Chin, E. Gilshtein, A. Müller, C. Wang, J. Thiesbrummel, S. Siol, J. M. Prieto, T. Unold, M. Stolterfoht, C. Chen, A. N. Tiwari, D. Zhao and F. Fu, High-Performance Flexible All-Perovskite Tandem Solar Cells with Reduced VOC-Deficit in Wide-Bandgap Subcell, *Adv. Energy Mater.*, 2022, **12**, 2202438.
50 L. Li, Y. Wang, X. Wang, R. Lin, X. Luo, Z. Liu, K. Zhou, S. Xiong, Q. Bao, G. Chen, Y. Tian, Y. Deng, K. Xiao, J. Wu, M. I. Saidaminov, H. Lin, C.-Q. Ma, Z. Zhao, Y. Wu, L. Zhang and H. Tan, Flexible all-perovskite tandem solar cells approaching 25% efficiency with molecule-bridged hole-selective contact, *Nat. Energy*, 2022, **7**, 708–717.
51 V. Babu, M. A. Mejia Escobar, R. Fuentes Pineda, M. Ścigaj, P. Spinelli and K. Wojciechowski, Toward up-scaling the four-terminal all-perovskite tandem solar modules on flexible substrates, *Mater. Today Energy*, 2022, **28**, 101073.
52 J. Kurisinkal Pious, Y. Zwirner, H. Lai, S. Olthof, Q. Jeangros, E. Gilshtein, R. K. Kothandaraman, K. Artuk, P. Wechsler, C. Chen, C. M. Wolff, D. Zhao, A. N. Tiwari and F. Fu, Revealing the Role of Tin Fluoride Additive in Narrow Bandgap Pb-Sn Perovskites for Highly Efficient Flexible All-Perovskite Tandem Cells, *ACS Appl. Mater. Interfaces*, 2023, **15**, 10150–10157.
53 L. Geng, Y. Ma, Y. Sun, Z. Cai, L. Lan, H. Ma, H. Zhang, L. Mao, F. Li and M. Liu, Bilateral Anchoring for Enhanced Mechanical Stability and Efficiency in Flexible all-Perovskite Tandem Solar Cells, *Adv. Mater.*, 2025, 2419018.
54 X. Wang, J. Zheng, Z. Ying, X. Li, M. Zhang, X. Guo, S. Su, J. Sun, X. Yang and J. Ye, Ultrathin (∼30 μm) flexible monolithic perovskite/silicon tandem solar cell, *Sci. Bull.*, 2024, **69**, 1887–1894.
55 H. Shishido, R. Sato, D. Ieki, G. Matsuo, K. Saito, M. Konagai and R. Ishikawa, High-Efficiency Perovskite/Silicon Tandem Solar Cells with Flexibility, *Sol. RRL*, 2025, **9**, 2400899.
56 Y. Sun, F. Li, H. Zhang, W. Liu, Z. Wang, L. Mao, Q. Li, Y. He, T. Yang, X. Sun, Y. Qian, Y. Ma, L. Zhang, J. Du, J. Shi, G. Wang, A. Han, N. Wang, F. Meng, Z. Liu and M. Liu, Flexible perovskite/silicon monolithic tandem solar cells approaching 30% efficiency, *Nat. Commun.*, 2025, **16**, 5733.
57 Z. Li, S. Wu, J. Zhang, K. C. Lee, H. Lei, F. Lin, Z. Wang, Z. Zhu and A. K. Y. Jen, Hybrid Perovskite-Organic Flexible Tandem Solar Cell Enabling Highly Efficient Electrocatalysis Overall Water Splitting, *Adv. Energy Mater.*, 2020, **10**, 2000361.
58 B. Gao and J. Meng, Flexible CH3NH3PbI3 perovskite solar cells with high stability based on all inkjet printing, *Sol. Energy*, 2021, **230**, 598–604.

59 D. Beynon, E. Parvazian, K. Hooper, J. McGettrick, R. Patidar, T. Dunlop, Z. Wei, P. Davies, R. Garcia-Rodriguez, M. Carnie, M. Davies and T. Watson, All-Printed Roll-to-Roll Perovskite Photovoltaics Enabled by Solution-Processed Carbon Electrode, *Adv. Mater.*, 2023, **35**, 2208561.

60 L. Dong, S. Qiu, J. García Cerrillo, M. Wagner, O. Kasian, S. Feroze, D. Jang, C. Li, V. M. Le Corre, K. Zhang, H. Peisert, F. U. Kosasih, C. Ducati, C. Arrive, T. Du, F. Yang, C. J. Brabec and H.-J. Egelhaaf, Fully printed flexible perovskite solar modules with improved energy alignment by tin oxide surface modification, *Energy Environ. Sci.*, 2024, **17**, 7097–7106.

61 M. Yang, Z. Li, M. O. Reese, O. G. Reid, D. H. Kim, S. Siol, T. R. Klein, Y. Yan, J. J. Berry and M. F. Van Hest, Perovskite ink with wide processing window for scalable high-efficiency solar cells, *Nat. Energy*, 2017, **2**, 1–9.

62 S. Tang, Y. Deng, X. Zheng, Y. Bai, Y. Fang, Q. Dong, H. Wei and J. Huang, Composition engineering in doctor-blading of perovskite solar cells, *Adv. Energy Mater.*, 2017, **7**, 1700302.

63 Z. Xu, L. Zeng, J. Hu, Z. Wang, P. Zhang, C. J. Brabec, K. Forberich, Y. Mai and F. Guo, Reducing energy barrier of δ-to-α phase transition for printed formamidinium lead iodide photovoltaic devices, *Nano Energy*, 2022, **91**, 106658.

64 W. S. Yang, J. H. Noh, N. J. Jeon, Y. C. Kim, S. Ryu, J. Seo and S. I. Seok, High-performance photovoltaic perovskite layers fabricated through intramolecular exchange, *Science*, 2015, **348**, 1234.

65 J. W. Lee, D. H. Kim, H. S. Kim, S. W. Seo, S. M. Cho and N. G. Park, Formamidinium and cesium hybridization for photo-and moisture-stable perovskite solar cell, *Adv. Energy Mater.*, 2015, **5**, 1501310.

66 M. Kim, G.-H. Kim, T. K. Lee, I. W. Choi, H. W. Choi, Y. Jo, Y. J. Yoon, J. W. Kim, J. Lee and D. Huh, Methylammonium chloride induces intermediate phase stabilization for efficient perovskite solar cells, *Joule*, 2019, **3**, 2179–2192.

67 Q. Jiang, Y. Zhao, X. Zhang, X. Yang, Y. Chen, Z. Chu, Q. Ye, X. Li, Z. Yin and J. You, Surface passivation of perovskite film for efficient solar cells, *Nat. Photonics*, 2019, **13**, 460–466.

68 W. Hui, L. Chao, H. Lu, F. Xia, Q. Wei, Z. Su, T. Niu, L. Tao, B. Du and D. Li, Stabilizing black-phase formamidinium perovskite formation at room temperature and high humidity, *Science*, 2021, **371**, 1359–1364.

69 H. Li, T. Bu, J. Li, Z. Lin, J. Pan, Q. Li, X.-L. Zhang, Z. Ku, Y.-B. Cheng and F. Huang, Ink engineering for blade coating FA-dominated perovskites in ambient air for efficient solar cells and modules, *ACS Appl. Mater. Interfaces*, 2021, **13**, 18724–18732.

70 W. Q. Wu, P. N. Rudd, Q. Wang, Z. Yang and J. Huang, Blading phase-pure formamidinium-alloyed perovskites for high-efficiency solar cells with low photovoltage deficit and improved stability, *Adv. Mater.*, 2020, **32**, 2000995.

71 C. Li, J. Yin, R. Chen, X. Lv, X. Feng, Y. Wu and J. Cao, Monoammonium Porphyrin for Blade-Coating Stable Large-Area Perovskite Solar Cells with >18% Efficiency, *J. Am. Chem. Soc.*, 2019, **141**, 6345–6351.

72 C. Huang, S. Tan, B. Yu, Y. Li, J. Shi, H. Wu, Y. Luo, D. Li and Q. Meng, Meniscus-modulated blade coating enables high-quality α-phase formamidinium lead triiodide crystals and efficient perovskite minimodules, *Joule*, 2024, **8**, 2539–2553.

73 Z. Wang, L. Zeng, C. Zhang, Y. Lu, S. Qiu, C. Wang, C. Liu, L. Pan, S. Wu, J. Hu, G. Liang, P. Fan, H.-J. Egelhaaf, C. J. Brabec, F. Guo and Y. Mai, Rational Interface Design and Morphology Control for Blade-Coating Efficient Flexible Perovskite Solar Cells with a Record Fill Factor of 81%, *Adv. Funct. Mater.*, 2020, **30**, 2001240.

74 X. Dai, Y. Deng, C. H. Van Brackle, S. Chen, P. N. Rudd, X. Xiao, Y. Lin, B. Chen and J. Huang, Scalable fabrication of efficient perovskite solar modules on flexible glass substrates, *Adv. Energy Mater.*, 2020, **10**, 1903108.

75 T. Xue, Z. Huang, P. Zhang, M. Su, X. Hu, T. Wu, B. Fan, G. Chen, G. Yu, W. Liu, X. Liu, Y. Zhang and Y. Song, A shape memory scaffold for body temperature self-repairing wearable perovskite solar cells with efficiency exceeding 21%, *InfoMat*, 2022, **4**, e12358.

76 F. Jafarzadeh, L. A. Castriotta, F. De Rossi, J. Ali, F. Di Giacomo, A. Di Carlo, F. Matteocci and F. Brunetti, All-blade-coated flexible perovskite solar cells & modules processed in air from a sustainable dimethyl sulfoxide (DMSO)-based solvent system, *Sustain. Energy Fuels*, 2023, **7**, 2219–2228.

77 C. Gong, C. Wang, X. Meng, B. Fan, Z. Xing, S. Shi, T. Hu, Z. Huang, X. Hu and Y. Chen, An Equalized Flow Velocity Strategy for Perovskite Colloidal Particles in Flexible Perovskite Solar Cells, *Adv. Mater.*, 2024, **36**, 2405572.

78 P. Liu, H. Wang, T. Niu, L. Yin, Y. Du, L. Lang, Z. Zhang, Y. Tu, X. Liu, X. Chen, S. Wang, N. Wu, R. Qin, L. Wang, S. Yang, C. Zhang, X. Pan, S. Liu and K. Zhao, Ambient scalable fabrication of high-performance flexible perovskite solar cells, *Energy Environ. Sci.*, 2024, **17**, 7069–7080.

79 D. Vak, K. Hwang, A. Faulks, Y.-S. Jung, N. Clark, D.-Y. Kim, G. J. Wilson and S. E. Watkins, 3D Printer Based Slot-Die Coater as a Lab-to-Fab Translation Tool for Solution-Processed Solar Cells, *Adv. Energy Mater.*, 2015, **5**, 1401539.

80 K. Hwang, Y. S. Jung, Y. J. Heo, F. H. Scholes, S. E. Watkins, J. Subbiah, D. J. Jones, D. Y. Kim and D. Vak, Toward large scale roll-to-roll production of fully printed perovskite solar cells, *Adv. Mater.*, 2015, **27**, 1241–1247.

81 Y. Tu, J. Ye, G. Yang, Y. Zang, L. Zhang, Y. Wang, G. Li, L. Chu and W. Yan, Slot-die coating fabrication of perovskite solar cells toward commercialization, *J. Alloys Compd.*, 2023, **942**, 169104.

82 H. Hu, M. Singh, X. Wan, J. Tang, C.-W. Chu and G. Li, Nucleation and crystal growth control for scalable solution-processed organic–inorganic hybrid perovskite solar cells, *J. Mater. Chem. A*, 2020, **8**, 1578–1603.

83 G. Cotella, J. Baker, D. Worsley, F. De Rossi, C. Pleydell-Pearce, M. Carnie and T. Watson, One-step deposition by slot-die coating of mixed lead halide perovskite for

photovoltaic applications, *Sol. Energy Mater. Sol. Cells*, 2017, **159**, 362–369.
84 Y. Galagan, F. Di Giacomo, H. Gorter, G. Kirchner, I. de Vries, R. Andriessen and P. Groen, Roll-to-roll slot die coated perovskite for efficient flexible solar cells, *Adv. Energy Mater.*, 2018, **8**, 1801935.
85 Y.-C. Huang, C.-F. Li, Z.-H. Huang, P.-H. Liu and C.-S. Tsao, Rapid and sheet-to-sheet slot-die coating manufacture of highly efficient perovskite solar cells processed under ambient air, *Sol. Energy*, 2019, **177**, 255–261.
86 S. H. Huang, C. K. Guan, P. H. Lee, H. C. Huang, C. F. Li, Y. C. Huang and W. F. Su, Toward All Slot-Die Fabricated High Efficiency Large Area Perovskite Solar Cell Using Rapid Near Infrared Heating in Ambient Air, *Adv. Energy Mater.*, 2020, **10**, 2001567.
87 M. Du, X. Zhu, L. Wang, H. Wang, J. Feng, X. Jiang, Y. Cao, Y. Sun, L. Duan and Y. Jiao, High-pressure nitrogen-extraction and effective passivation to attain highest large-area perovskite solar module efficiency, *Adv. Mater.*, 2020, **32**, 2004979.
88 I. Zimmermann, M. Al Atem, O. Fournier, S. Bernard, S. Jutteau, L. Lombez and J. Rousset, Sequentially slot-die-coated perovskite for efficient and scalable solar cells, *Adv. Mater. Interfaces*, 2021, **8**, 2100743.
89 Y.-J. Heo, J.-E. Kim, H. Weerasinghe, D. Angmo, T. Qin, K. Sears, K. Hwang, Y.-S. Jung, J. Subbiah and D. J. Jones, Printing-friendly sequential deposition via intra-additive approach for roll-to-roll process of perovskite solar cells, *Nano Energy*, 2017, **41**, 443–451.
90 H. Li, C. Zuo, D. Angmo, H. Weerasinghe, M. Gao and J. Yang, Fully roll-to-roll processed efficient perovskite solar cells via precise control on the morphology of PbI2: CsI layer, *Nano-Micro Lett.*, 2022, **14**, 79.
91 Y. Y. Kim, E. Y. Park, T.-Y. Yang, J. H. Noh, T. J. Shin, N. J. Jeon and J. Seo, Fast two-step deposition of perovskite via mediator extraction treatment for large-area, high-performance perovskite solar cells, *J. Mater. Chem. A*, 2018, **6**, 12447–12454.
92 T. Bu, J. Li, F. Zheng, W. Chen, X. Wen, Z. Ku, Y. Peng, J. Zhong, Y.-B. Cheng and F. Huang, Universal passivation strategy to slot-die printed SnO2 for hysteresis-free efficient flexible perovskite solar module, *Nat. Commun.*, 2018, **9**, 4609.
93 Z. Yang, W. Zhang, S. Wu, H. Zhu, Z. Liu, Z. Liu, Z. Jiang, R. Chen, J. Zhou, Q. Lu, Z. Xiao, L. Shi, H. Chen, L. K. Ono, S. Zhang, Y. Zhang, Y. Qi, L. Han and W. Chen, Slot-die coating large-area formamidinium-cesium perovskite film for efficient and stable parallel solar module, *Sci. Adv.*, 2021, **7**, eabg3749.
94 P. J. S. Rana, B. Febriansyah, T. M. Koh, A. Kanwat, J. Xia, T. Salim, T. J. N. Hooper, M. Kovalev, D. Giovanni, Y. C. Aw, B. Chaudhary, Y. Cai, G. Xing, T. C. Sum, J. W. Ager, S. G. Mhaisalkar and N. Mathews, Molecular Locking with All-Organic Surface Modifiers Enables Stable and Efficient Slot-Die-Coated Methyl-Ammonium-Free Perovskite Solar Modules, *Adv. Mater.*, 2023, **35**, 2210176.
95 S. Y. Abate, Z. Yang, S. Jha, J. Emodogo, G. Ma, Z. Ouyang, S. Muhammad, N. Pradhan, X. Gu, D. Patton, D. Li, J. Cai and Q. Dai, Promoting Large-Area Slot-Die-Coated Perovskite Solar Cell Performance and Reproducibility by Acid-Based Sulfono-γ-AApeptide, *ACS Appl. Mater. Interfaces*, 2023, **15**, 25495–25505.
96 T. R. Rana, M. Abbas, E. Schwartz, F. Jiang, M. Y. Yaman, Z. Xu, D. S. Ginger and D. MacKenzie, Scalable Passivation Strategies to Improve Efficiency of Slot Die-Coated Perovskite Solar Cells, *ACS Energy Lett.*, 2024, **9**, 1888–1894.
97 J. Li, J. Dagar, O. Shargaieva, O. Maus, M. Remec, Q. Emery, M. Khenkin, C. Ulbrich, F. Akhundova and J. A. Márquez, Ink Design Enabling Slot-Die Coated Perovskite Solar Cells with> 22% Power Conversion Efficiency, Micro-Modules, and 1 Year of Outdoor Performance Evaluation, *Adv. Energy Mater.*, 2023, **13**, 2203898.
98 **https://www.businesswire.com/news/home/20230214005803/en/qd-solar-report-cells-developed-for-large-scale-manufacturing**, 2023.
99 F. Bisconti, A. Giuri, G. Marra, A. Savoini, P. Fumo, R. Marrazzo, S. Zanardi, G. Corso, R. Po, P. Biagini, E. Quadrivi, R. Suhonen, T. M. Kraft, M. Ylikunnari, A. Listorti, C. E. Corcione, S. Colella and A. Rizzo, Polymer-Assisted Single-Step Slot-Die Coating of Flexible Perovskite Solar Cells at Mild Temperature from Dimethyl Sulfoxide, *ChemPlusChem*, 2021, **86**, 1442–1450.
100 E. Rezaee, D. I. Kutsarov, J. Zhang, G. Koutsourakis, B. Li, F. A. Castro and S. R. P. Silva, Green Solvent Ethanol-Based Inks for Industrially Applicable Deposition of High-Quality Perovskite Films for Optoelectronic Device Applications, *Small Methods*, 2024, **8**, 2300564.
101 M. S. Kiani, Z. T. Sadirkhanov, A. G. Kakimov, H. P. Parkhomenko, A. Ng and A. N. Jumabekov, Solution-Processed SnO2 Quantum Dots for the Electron Transport Layer of Flexible and Printed Perovskite Solar Cells, *Nanomaterials*, 2022, **12**, 2615.
102 M. R. Kokaba, Y. Ahmed, V. Yeddu, D. Zhang, P. Moazzezi, V. Kamraninejad, S. Dayneko, S. B. Reinecke, A. Amaro, B. Villarejo, A. Shyla, S. Malek and M. I. Saidaminov, Enhanced Particle-to-Particle Interaction of Tin Oxide Electron Transporter Layer for Scalable Flexible Perovskite Solar Cells, *Sol. RRL*, 2024, **8**, 2301013.
103 Z. Wu, X. Liu, H. Zhong, Z. Wu, H. Chen, J. Su, Y. Xu, X. Wang, X. Li and H. Lin, Natural Amino Acid Enables Scalable Fabrication of High-Performance Flexible Perovskite Solar Cells and Modules with Areas over 300 cm2, *Small Methods*, 2022, **6**, 2200669.
104 H. C. Weerasinghe, N. Macadam, J.-E. Kim, L. J. Sutherland, D. Angmo, L. W. T. Ng, A. D. Scully, F. Glenn, R. Chantler, N. L. Chang, M. Dehghanimadvar, L. Shi, A. W. Y. Ho-Baillie, R. Egan, A. S. R. Chesman, M. Gao, J. J. Jasieniak, T. Hasan and D. Vak, The first demonstration of entirely roll-to-roll fabricated perovskite solar cell modules under ambient room conditions, *Nat. Commun.*, 2024, **15**, 1656.

105 Y. Zhao, F. Ma, F. Gao, Z. Yin, X. Zhang and J. You, Research progress in large-area perovskite solar cells, *Photon. Res.*, 2020, **8**, A1–A15.
106 S. Das, B. Yang, G. Gu, P. C. Joshi, I. N. Ivanov, C. M. Rouleau, T. Aytug, D. B. Geohegan and K. Xiao, High-performance flexible perovskite solar cells by using a combination of ultrasonic spray-coating and low thermal budget photonic curing, *ACS Photonics*, 2015, **2**, 680–686.
107 F. Li, C. Bao, H. Gao, W. Zhu, T. Yu, J. Yang, G. Fu, X. Zhou and Z. Zou, A facile spray-assisted fabrication of homogenous flat CH3NH3PbI3 films for high performance mesostructure perovskite solar cells, *Mater. Lett.*, 2015, **157**, 38–41.
108 A. T. Barrows, A. J. Pearson, C. K. Kwak, A. D. Dunbar, A. R. Buckley and D. G. Lidzey, Efficient planar heterojunction mixed-halide perovskite solar cells deposited via spray-deposition, *Energy Environ. Sci.*, 2014, **7**, 2944–2950.
109 W. C. Chang, D. H. Lan, K. M. Lee, X. F. Wang and C. L. Liu, Controlled deposition and performance optimization of perovskite solar cells using ultrasonic spray-coating of photoactive layers, *ChemSusChem*, 2017, **10**, 1405–1412.
110 L.-H. Chou, X.-F. Wang, I. Osaka, C.-G. Wu and C.-L. Liu, Scalable ultrasonic spray-processing technique for manufacturing large-area CH3NH3PbI3 perovskite solar cells, *ACS Appl. Mater. Interfaces*, 2018, **10**, 38042–38050.
111 J. Silvano, J. Sala, T. Merckx, Y. Kuang, P. Verding, J. D'Haen, T. Aernouts, B. Vermang and W. Deferme, A study of quenching approaches to optimize ultrasonic spray coated perovskite layers scalable for PV, *EPJ Photovoltaics*, 2022, **13**, 12.
112 S. a. Uličná, B. Dou, D. H. Kim, K. Zhu, J. M. Walls, J. W. Bowers and M. F. Van Hest, Scalable deposition of high-efficiency perovskite solar cells by spray-coating, *ACS Appl. Energy Mater.*, 2018, **1**, 1853–1857.
113 H. Huang, J. Shi, L. Zhu, D. Li, Y. Luo and Q. Meng, Two-step ultrasonic spray deposition of CH3NH3PbI3 for efficient and large-area perovskite solar cell, *Nano Energy*, 2016, **27**, 352–358.
114 L.-H. Chou, J. M. Chan and C.-L. Liu, Progress in spray coated perovskite films for solar cell applications, *Sol. RRL*, 2022, **6**, 2101035.
115 Z. Liu, G. Liu, C. Xu and X. Xie, Scalable fabrication for efficient quasi two-dimensional perovskite solar cells via ultrasonic spray-coating method, *Org. Electron.*, 2022, **102**, 106440.
116 S. Sansoni, M. De Bastiani, E. Aydin, E. Ugur, F. H. Isikgor, A. Al-Zahrani, F. Lamberti, F. Laquai, M. Meneghetti and S. De Wolf, Eco-Friendly Spray Deposition of Perovskite Films on Macroscale Textured Surfaces, *Adv. Mater. Technol.*, 2020, **5**, 1901009.
117 C. Gao, P. Wang, H. Wang, C. Yu, B. Du, H. Zhang, T. Li, D. Liu and T. Wang, Binary Additive Engineering Enables Efficient Perovskite Solar Cells via Spray-Coating in Air, *ACS Appl. Energy Mater.*, 2021, **4**, 11496–11504.
118 H. Cai, X. Liang, X. Ye, J. Su, J. Guan, J. Yang, Y. Liu, X. Zhou, R. Han, J. Ni, J. Li and J. Zhang, High Efficiency over 20% of Perovskite Solar Cells by Spray Coating via a Simple Process, *ACS Appl. Energy Mater.*, 2020, **3**, 9696–9702.
119 T.-W. Chen, S. N. Afraj, S.-H. Hong, L.-H. Chou, A. Velusamy, C.-Y. Chen, Y. Ezhumalai, S.-H. Yang, I. Osaka, X.-F. Wang, M.-C. Chen and C.-L. Liu, Synergetic Effect on Enhanced Photovoltaic Performance of Spray-Coated Perovskite Solar Cells Enabled by Additive Doping and Antisolvent Additive Spraying Treatment, *ACS Appl. Energy Mater.*, 2022, **5**, 4149–4158.
120 Y.-T. Yu, S.-H. Yang, L.-H. Chou, I. Osaka, X.-F. Wang and C.-L. Liu, One-Step Spray-Coated All-Inorganic CsPbI2Br Perovskite Solar Cells, *ACS Appl. Energy Mater.*, 2021, **4**, 5466–5474.
121 T. Xu, Y. Li, H. Cai, Y. Zhu, C. Liu, B. Han, Z. Hu, F. Zhang, J. Ni, J. Li and J. Zhang, Co-solvent strategy for highly efficient perovskite solar cells by spray coating, *Sol. Energy*, 2024, **272**, 112461.
122 C. Liu, Y.-B. Cheng and Z. Ge, Understanding of perovskite crystal growth and film formation in scalable deposition processes, *Chem. Soc. Rev.*, 2020, **49**, 1653–1687.
123 R. Wang, J. Xue, L. Meng, J.-W. Lee, Z. Zhao, P. Sun, L. Cai, T. Huang, Z. Wang and Z.-K. Wang, Caffeine improves the performance and thermal stability of perovskite solar cells, *Joule*, 2019, **3**, 1464–1477.
124 P. Zhou, W. Li, T. Li, T. Bu, X. Liu, J. Li, J. He, R. Chen, K. Li, J. Zhao and F. Huang, Ultrasonic Spray-Coating of Large-Scale TiO2 Compact Layer for Efficient Flexible Perovskite Solar Cells, *Micromachines*, 2017, **8**, 55.
125 M. Park, S. C. Hong, Y.-W. Jang, J. Byeon, J. Jang, M. Han, U. Kim, K. Jeong, M. Choi and G. Lee, Scalable Production of High Performance Flexible Perovskite Solar Cells via Film-Growth-Megasonic-Spray-Coating System, *Int. J. Precis. Eng. Manuf.–Green Technol.*, 2023, **10**, 1223–1234.
126 A. Huang, J. Zhu, Y. Zhou, Y. Yu, Y. Liu, S. Yang, S. Ji, L. Lei and P. Jin, One step spray-coated TiO2 electron-transport layers for decent perovskite solar cells on large and flexible substrates, *Nanotechnology*, 2017, **28**, 01LT02.
127 B. Taheri, F. De Rossi, G. Lucarelli, L. A. Castriotta, A. Di Carlo, T. M. Brown and F. Brunetti, Laser-Scribing Optimization for Sprayed SnO2-Based Perovskite Solar Modules on Flexible Plastic Substrates, *ACS Appl. Energy Mater.*, 2021, **4**, 4507–4518.
128 S. Jon, G. Sin, G. Kim, G. Jong and J. Ri, Flexible perovskite solar cells based on AgNW/ATO composite transparent electrodes, *Synth. Met.*, 2020, **262**, 116286.
129 K. Poorkazem, D. Liu and T. L. Kelly, Fatigue resistance of a flexible, efficient, and metal oxide-free perovskite solar cell, *J. Mater. Chem. A*, 2015, **3**, 9241–9248.
130 S. Kim, H. Oh, I. Jeong, G. Kang and M. Park, Influence of a solvent trap in ITO/PEN substrates on the performance of flexible perovskite solar cells and light-emitting diodes, *ACS Appl. Electron. Mater.*, 2021, **3**, 3207–3217.

131 M. Soldera, Q. Wang, F. Soldera, V. Lang, A. Abate and A. F. Lasagni, Toward high-throughput texturing of polymer foils for enhanced light trapping in flexible perovskite solar cells using roll-to-roll hot embossing, *Adv. Eng. Mater.*, 2020, **22**, 1901217.

132 C. Sílvia Manuela Ferreira, A. R. Luís and C. V. Júlio, Printing Technologies on Flexible Substrates for Printed Electronics, in *Flexible Electronics*, ed. R. Simas, IntechOpen, Rijeka, 2018, ch. 3.

133 Z. Skafi, J. Xu, V. Mottaghitalab, L. Mivehi, B. Taheri, F. Jafarzadeh, S. K. Podapangi, D. Altamura, M. R. Guascito, L. Barba, C. Giannini, A. Rizzo, F. De Rossi, H. Javanbakht Lomeri, L. Sorbello, F. Matteocci, F. Brunetti and T. M. Brown, Highly Efficient Flexible Perovskite Solar Cells on Polyethylene Terephthalate Films via Dual Halide and Low-Dimensional Interface Engineering for Indoor Photovoltaics, *Sol. RRL*, 2023, **7**, 2300324.

134 C. H. Chen, F. Hu, Z. H. Su, Y. J. Yu, K. L. Wang, Y. R. Shi, J. Chen, Y. Xia, X. Y. Gao and Z. K. Wang, Spring-Like Ammonium Salt Assisting Stress Release for Low-Temperature Deposited FAPbI3 Films Toward Flexible Photovoltaic Application, *Adv. Funct. Mater.*, 2023, **33**, 2213661.

135 J.-I. Park, J. H. Heo, S.-H. Park, K. I. Hong, H. G. Jeong, S. H. Im and H.-K. Kim, Highly flexible InSnO electrodes on thin colourless polyimide substrate for high-performance flexible CH3NH3PbI3 perovskite solar cells, *J. Power Sources*, 2017, **341**, 340–347.

136 Y. Gao, K. Huang, C. Long, Y. Ding, J. Chang, D. Zhang, L. Etgar, M. Liu, J. Zhang and J. Yang, Flexible perovskite solar cells: From materials and device architectures to applications, *ACS Energy Lett.*, 2022, **7**, 1412–1445.

137 Z. Skafi, L. A. Castriotta, B. Taheri, F. Matteocci, M. Fahland, F. Jafarzadeh, E. Joseph, A. Chakraborty, V. Singh, V. Mottaghitalab, L. Mivehi, F. Brunetti, L. Sorbello, A. Di Carlo and T. M. Brown, Flexible Perovskite Solar Cells on Polycarbonate Film Substrates, *Adv. Energy Mater.*, 2024, **14**, 2400912.

138 G. Zhang, Q. Chen, C. Xie, Y. Wang, C. Zhao, C. Xiao, Y. Wei and W. Li, Mechanical-robust and recyclable polyimide substrates coordinated with cyclic Ti-oxo cluster for flexible organic solar cells, *npj Flexible Electron.*, 2022, **6**, 37.

139 H. Zhang, J. Cheng, D. Li, F. Lin, J. Mao, C. Liang, A. K.-Y. Jen, M. Grätzel and W. C. Choy, Toward all room-temperature, solution-processed, high-performance planar perovskite solar cells: a new scheme of pyridine-promoted perovskite formation, *Adv. Mater.*, 2017, **29**, 1604695.

140 X. Zhang, Y. Gang, S. Jiang, M. Li, H. Xue and X. Li, One-Stone-for-Two-Birds Method to Improve the SnO2 Layers for High Power-per-Weight Flexible Perovskite Solar Cell Mini-modules, *ACS Appl. Mater. Interfaces*, 2024, **16**, 27368–27380.

141 G. S. Han, S. Lee, M. L. Duff, F. Qin and J.-K. Lee, Highly Bendable Flexible Perovskite Solar Cells on a Nanoscale Surface Oxide Layer of Titanium Metal Plates, *ACS Appl. Mater. Interfaces*, 2018, **10**, 4697–4704.

142 M. Lee, Y. Jo, D. S. Kim and Y. Jun, Flexible organo-metal halide perovskite solar cells on a Ti metal substrate, *J. Mater. Chem. A*, 2015, **3**, 4129–4133.

143 J. H. Heo, D. H. Shin, M. L. Lee, M. G. Kang and S. H. Im, Efficient organic–inorganic hybrid flexible perovskite solar cells prepared by lamination of polytriarylamine/CH3NH3PbI3/anodized Ti metal substrate and graphene/PDMS transparent electrode substrate, *ACS Appl. Mater. Interfaces*, 2018, **10**, 31413–31421.

144 B. T. Feleki, R. K. Bouwer, M. M. Wienk and R. A. Janssen, Perovskite solar cells on polymer-coated smooth and rough steel substrates, *Sol. RRL*, 2022, **6**, 2100898.

145 B. Dou, E. M. Miller, J. A. Christians, E. M. Sanehira, T. R. Klein, F. S. Barnes, S. E. Shaheen, S. M. Garner, S. Ghosh and A. Mallick, High-performance flexible perovskite solar cells on ultrathin glass: implications of the TCO, *J. Phys. Chem. Lett.*, 2017, **8**, 4960–4966.

146 M. M. Tavakoli, K.-H. Tsui, Q. Zhang, J. He, Y. Yao, D. Li and Z. Fan, Highly efficient flexible perovskite solar cells with antireflection and self-cleaning nanostructures, *ACS Nano*, 2015, **9**, 10287–10295.

147 S. Castro-Hermosa, G. Lucarelli, M. Top, M. Fahland, J. Fahlteich and T. M. Brown, Perovskite Photovoltaics on Roll-To-Roll Coated Ultra-thin Glass as Flexible High-Efficiency Indoor Power Generators, *Cell Rep. Phys. Sci.*, 2020, **1**, 100045.

148 P. Subudhi and D. Punetha, Progress, challenges, and perspectives on polymer substrates for emerging flexible solar cells: A holistic panoramic review, *Prog. Photovoltaics Res. Appl.*, 2023, **31**, 753–789.

149 Z. a. Tan, S. Li, F. Wang, D. Qian, J. Lin, J. Hou and Y. Li, High performance polymer solar cells with as-prepared zirconium acetylacetonate film as cathode buffer layer, *Sci. Rep.*, 2014, **4**, 4691.

150 F. Yang, J. Liu, H. E. Lim, Y. Ishikura, K. Shinokita, Y. Miyauchi, A. Wakamiya, Y. Murata and K. Matsuda, High Bending Durability of Efficient Flexible Perovskite Solar Cells Using Metal Oxide Electron Transport Layer, *J. Phys. Chem. C*, 2018, **122**, 17088–17095.

151 Y. Hu, T. Niu, Y. Liu, Y. Zhou, Y. Xia, C. Ran, Z. Wu, L. Song, P. Müller-Buschbaum and Y. Chen, Flexible perovskite solar cells with high power-per-weight: progress, application, and perspectives, *ACS Energy Lett.*, 2021, **6**, 2917–2943.

152 S. Suragtkhuu, S. Sunderiya, P. Myagmarsereejid, S. Purevdorj, A. S. Bati, B. Bold, Y. L. Zhong, S. Davaasambuu and M. Batmunkh, Graphene-like monoelemental 2D materials for perovskite solar cells, *Adv. Energy Mater.*, 2023, **13**, 2204074.

153 P. Ma, Y. Lou, S. Cong, Z. Lu, K. Zhu, J. Zhao and G. Zou, Malleability and Pliability of Silk-Derived Electrodes for Efficient Deformable Perovskite Solar Cells, *Adv. Energy Mater.*, 2020, **10**, 1903357.

154 M. Pandey, Z. Wang, G. Kapil, A. K. Baranwal, D. Hirotani, K. Hamada and S. Hayase, Dependence of ITO-Coated

Flexible Substrates in the Performance and Bending Durability of Perovskite Solar Cells, *Adv. Eng. Mater.*, 2019, **21**, 1900288.

155 J.-H. Kim, H.-J. Seok, H.-J. Seo, T.-Y. Seong, J. H. Heo, S.-H. Lim, K.-J. Ahn and H.-K. Kim, Flexible ITO films with atomically flat surfaces for high performance flexible perovskite solar cells, *Nanoscale*, 2018, **10**, 20587–20598.

156 B. J. Kim, D. H. Kim, Y.-Y. Lee, H.-W. Shin, G. S. Han, J. S. Hong, K. Mahmood, T. K. Ahn, Y.-C. Joo and K. S. Hong, Highly efficient and bending durable perovskite solar cells: toward a wearable power source, *Energy Environ. Sci.*, 2015, **8**, 916–921.

157 M. Li, W. W. Zuo, A. G. Ricciardulli, Y. G. Yang, Y. H. Liu, Q. Wang, K. L. Wang, G. X. Li, M. Saliba and D. Di Girolamo, Embedded nickel-mesh transparent electrodes for highly efficient and mechanically stable flexible perovskite photovoltaics: toward a portable mobile energy source, *Adv. Mater.*, 2020, **32**, 2003422.

158 T. Y. Jin, W. Li, Y. Q. Li, Y. X. Luo, Y. Shen, L. P. Cheng and J. X. Tang, High-Performance Flexible Perovskite Solar Cells Enabled by Low-Temperature ALD-Assisted Surface Passivation, *Adv. Opt. Mater.*, 2018, **6**, 10.

159 G. Jeong, D. Koo, J. Seo, S. Jung, Y. Choi, J. Lee and H. Park, Suppressed Interdiffusion and Degradation in Flexible and Transparent Metal Electrode-Based Perovskite Solar Cells with a Graphene Interlayer, *Nano Lett.*, 2020, **20**, 3718–3727.

160 Y. Li, L. Meng, Y. Yang, G. Xu, Z. Hong, Q. Chen, J. You, G. Li, Y. Yang and Y. Li, High-efficiency robust perovskite solar cells on ultrathin flexible substrates, *Nat. Commun.*, 2016, **7**, 10214.

161 Q. Sun, J. D. Chen, J. W. Zheng, T. Y. Qu, T. Y. Jin, Y. Q. Li and J. X. Tang, Surface Plasmon-Assisted Transparent Conductive Electrode for Flexible Perovskite Solar Cells, *Adv. Opt. Mater.*, 2019, **7**, 1900847.

162 J. Jin, J. Li, Q. Tai, Y. Chen, D. D. Mishra, W. Deng, J. Xin, S. Guo, B. Xiao and X. Wang, Efficient and stable flexible perovskite solar cells based on graphene-AgNWs substrate and carbon electrode without hole transport materials, *J. Power Sources*, 2021, **482**, 228953.

163 J. Kang, K. Han, X. Sun, L. Zhang, R. Huang, I. Ismail, Z. Wang, C. Ding, W. Zha and F. Li, Suppression of Ag migration by low-temperature sol-gel zinc oxide in the Ag nanowires transparent electrode-based flexible perovskite solar cells, *Org. Electron.*, 2020, **82**, 105714.

164 E. Lee, J. Ahn, H. C. Kwon, S. Ma, K. Kim, S. Yun and J. Moon, All-solution-processed silver nanowire window electrode-based flexible perovskite solar cells enabled with amorphous metal oxide protection, *Adv. Energy Mater.*, 2018, **8**, 1702182.

165 F. Deng, X. Sun, X. Lv, Y. Li, S. Li, Y.-Z. Zheng and X. Tao, All room-temperature processing efficient planar carbon-based perovskite solar cells, *J. Power Sources*, 2021, **489**, 229345.

166 V. Babu, R. Fuentes Pineda, T. Ahmad, A. O. Alvarez, L. A. Castriotta, A. Di Carlo, F. Fabregat-Santiago and K. Wojciechowski, Improved stability of inverted and flexible perovskite solar cells with carbon electrode, *ACS Appl. Energy Mater.*, 2020, **3**, 5126–5134.

167 J. Zhang, X. Hu, H. Li, K. Ji, B. Li, X. Liu, Y. Xiang, P. Hou, C. Liu and Z. Wu, High-performance ITO-free perovskite solar cells enabled by single-walled carbon nanotube films, *Adv. Funct. Mater.*, 2021, **31**, 2104396.

168 D. H. Jung, Y. J. Oh, Y. S. Nam and H. Lee, Effect of layer number on the properties of stable and flexible perovskite solar cells using two dimensional material, *J. Alloys Compd.*, 2021, **850**, 156752.

169 X. Xu, H. Wang, J. Wang, M. Muhammad, Z. Wang, P. Chen, W. Zhao, B. Kang, J. Zhang and C. Li, Surface functionalization of a graphene cathode to facilitate ALD growth of an electron transport layer and realize high-performance flexible perovskite solar cells, *ACS Appl. Energy Mater.*, 2020, **3**, 4208–4216.

170 C. Peng, H. Su, J. Li, Q. Duan, Q. Li, J. Xiao, Z. Ku, J. Zhong, W. Li and Y. Peng, Scalable, efficient and flexible perovskite solar cells with carbon film based electrode, *Sol. Energy Mater. Sol. Cells*, 2021, **230**, 111226.

171 Q. Luo, H. Ma, Q. Hou, Y. Li, J. Ren, X. Dai, Z. Yao, Y. Zhou, L. Xiang and H. Du, All-carbon-electrode-based endurable flexible perovskite solar cells, *Adv. Funct. Mater.*, 2018, **28**, 1706777.

172 V.-D. Tran, S. Pammi, B.-J. Park, Y. Han, C. Jeon and S.-G. Yoon, Transfer-free graphene electrodes for super-flexible and semi-transparent perovskite solar cells fabricated under ambient air, *Nano Energy*, 2019, **65**, 104018.

173 S.-H. Huang, Y.-H. Chen, H.-C. Cha, D. Glowienka, M.-C. Wu and Y.-C. Huang, Polymer-Enhanced Active Layer Crystallization in Low-Temperature Carbon-Based Perovskite Solar Cells, *Energy Fuels*, 2025, **39**, 1401–1408.

174 J. You, Z. Hong, Y. Yang, Q. Chen, M. Cai, T.-B. Song, C.-C. Chen, S. Lu, Y. Liu and H. Zhou, Low-temperature solution-processed perovskite solar cells with high efficiency and flexibility, *ACS Nano*, 2014, **8**, 1674–1680.

175 Z. Xing, S. Lin, X. Meng, T. Hu, D. Li, B. Fan, Y. Cui, F. Li, X. Hu and Y. Chen, A highly tolerant printing for scalable and flexible perovskite solar cells, *Adv. Funct. Mater.*, 2021, **31**, 2107726.

176 X. Meng, Z. Cai, Y. Zhang, X. Hu, Z. Xing, Z. Huang, Z. Huang, Y. Cui, T. Hu, M. Su, X. Liao, L. Zhang, F. Wang, Y. Song and Y. Chen, Bio-inspired vertebral design for scalable and flexible perovskite solar cells, *Nat. Commun.*, 2020, **11**, 3016.

177 Y. Wang, L. Duan, M. Zhang, Z. Hameiri, X. Liu, Y. Bai and X. Hao, PTAA as efficient hole transport materials in perovskite solar cells: a review, *Sol. RRL*, 2022, **6**, 2200234.

178 M. M. Tavakoli and R. Tavakoli, All-Vacuum-Processing for Fabrication of Efficient, Large-Scale, and Flexible Inverted Perovskite Solar Cells, *Phys. Status Solidi RRL*, 2021, **15**, 2000449.

179 C. Ge, X. Liu, Z. Yang, H. Li, W. Niu, X. Liu and Q. Dong, Thermal dynamic self-healing supramolecular dopant towards efficient and stable flexible perovskite solar cells, *Angew. Chem.*, 2022, **134**, e202116602.

180 M. Najafi, F. Di Giacomo, D. Zhang, S. Shanmugam, A. Senes, W. Verhees, A. Hadipour, Y. Galagan, T. Aernouts and S. Veenstra, Highly efficient and stable flexible perovskite solar cells with metal oxides nanoparticle charge extraction layers, *Small*, 2018, **14**, 1702775.

181 H. Wang, Z. Huang, S. Xiao, X. Meng, Z. Xing, L. Rao, C. Gong, R. Wu, T. Hu, L. Tan, X. Hu, S. Zhang and Y. Chen, An in situ bifacial passivation strategy for flexible perovskite solar module with mechanical robustness by roll-to-roll fabrication, *J. Mater. Chem. A*, 2021, **9**, 5759–5768.

182 B. Fan, J. Xiong, Y. Zhang, C. Gong, F. Li, X. Meng, X. Hu, Z. Yuan, F. Wang and Y. Chen, A Bionic Interface to Suppress the Coffee-Ring Effect for Reliable and Flexible Perovskite Modules with a Near-90% Yield Rate, *Adv. Mater.*, 2022, **34**, 2201840.

183 J. Dagar, S. Castro-Hermosa, M. Gasbarri, A. L. Palma, L. Cina, F. Matteocci, E. Calabrò, A. Di Carlo and T. M. Brown, Efficient fully laser-patterned flexible perovskite modules and solar cells based on low-temperature solution-processed SnO 2/mesoporous-TiO 2 electron transport layers, *Nano Res.*, 2018, **11**, 2669–2681.

184 J. Hu, X. Xu, Y. Chen, S. Wu, Z. Wang, Y. Wang, X. Jiang, B. Cai, T. Shi and C. J. Brabec, Overcoming photovoltage deficit via natural amino acid passivation for efficient perovskite solar cells and modules, *J. Mater. Chem. A*, 2021, **9**, 5857–5865.

185 C. Li, J. Yin, R. Chen, X. Lv, X. Feng, Y. Wu and J. Cao, Monoammonium porphyrin for blade-coating stable large-area perovskite solar cells with> 18% efficiency, *J. Am. Chem. Soc.*, 2019, **141**, 6345–6351.

186 S. Chen, X. Dai, S. Xu, H. Jiao, L. Zhao and J. Huang, Stabilizing perovskite-substrate interfaces for high-performance perovskite modules, *Science*, 2021, **373**, 902–907.

187 Y. Deng, X. Zheng, Y. Bai, Q. Wang, J. Zhao and J. Huang, Surfactant-controlled ink drying enables high-speed deposition of perovskite films for efficient photovoltaic modules, *Nat. Energy*, 2018, **3**, 560–566.

188 R. He, S. Nie, X. Huang, Y. Wu, R. Chen, J. Yin, B. Wu, J. Li and N. Zheng, Scalable Preparation of High-Performance ZnO–SnO2 Cascaded Electron Transport Layer for Efficient Perovskite Solar Modules, *Sol. RRL*, 2022, **6**, 2100639.

189 C. Fei, N. Li, M. Wang, X. Wang, H. Gu, B. Chen, Z. Zhang, Z. Ni, H. Jiao, W. Xu, Z. Shi, Y. Yan and J. Huang, Lead-chelating hole-transport layers for efficient and stable perovskite minimodules, *Science*, 2023, **380**, 823–829.

190 W. Liu, R. Chen, Z. Tan, J. Wang, S. Liu, C. Shi, X. Liu, Y. Cai, F. Ren, Z. Zhou, Q. Zhou, W. Li, T. Miao, H. Zhu, T. Imran, Z. Liu and W. Chen, Buried Interface Engineering for Scalable Processing of High-Performance Inverted Perovskite Solar Modules, *Adv. Energy Mater.*, 2024, 2404374.

191 J. Zhang, T. Bu, J. Li, H. Li, Y. Mo, Z. Wu, Y. Liu, X.-L. Zhang, Y.-B. Cheng and F. Huang, Two-step sequential blade-coating of high quality perovskite layers for efficient solar cells and modules, *J. Mater. Chem. A*, 2020, **8**, 8447–8454.

192 Y. Wen, J. Li, X. Gao, C. Tian, H. Zhu, G. Yu, X. Zhang, H. Park and F. Huang, Two-Step sequential blade-coating large-area FA-based perovskite thin film via a controlled PbI2 microstructure, *Acta Phys.–Chim. Sin.*, 2023, **39**, 2203048.

193 Y. Li, Y. Zhang, J. Chung, M. Rajakaruna, M. M. Saeed, A. Abudulimu, P. N. Kaluarachchi, D.-B. Li, T. Mariam, L. Chen, S. Fu, N. Sun, R. J. Ellingson, M. J. Heben, Z. Song and Y. Yan, Seed-Assisted Growth for Scalable and Efficient Perovskite Solar Modules, *Sol. RRL*, 2023, **7**, 2300541.

194 J. Chang, E. Feng, X. Feng, H. Li, Y. Ding, C. Long, S. Lu, H. Zhu, W. Deng, J. Shi, Y. Yang, S. Xiao, Y. Yuan and J. Yang, Bridging buried interface enable 24.67%-efficiency doctor-bladed perovskite solar cells in ambient condition, *Nano Res.*, 2024, **17**, 8068–8076.

195 K.-S. Lim, D.-K. Lee, J.-W. Lee and N.-G. Park, 17% efficient perovskite solar mini-module via hexamethylphosphoramide (HMPA)-adduct-based large-area D-bar coating, *J. Mater. Chem. A*, 2020, **8**, 9345–9354.

196 Z. Zhang, J. Shang, H. Ge, Y. Zhang, L. Zhou, W. Zhu, D. Chen, J. Zhang, C. Zhang and Y. Hao, Fabrication of high-efficiency perovskite solar cells and mini-modules by expanding the processing window with KSCN additive, Mater, *Today Energy*, 2023, **36**, 101343.

197 L. Yuan, X. Chen, X. Guo, S. Huang, X. Wu, Y. Shen, H. Gu, Y. Chen, G. Zeng, H.-J. Egelhaaf, C. J. Brabec, F. Yang, Y. Li and Y. Li, Volatile Perovskite Precursor Ink Enables Window Printing of Phase-Pure FAPbI3 Perovskite Solar Cells and Modules in Ambient Atmosphere, *Angew Chem. Int. Ed. Engl.*, 2024, **63**, e202316954.

198 X. Chen, F. Yang, L. Yuan, S. Huang, H. Gu, X. Wu, Y. Shen, Y. Chen, N. Li, H.-J. Egelhaaf, C. J. Brabec, R. Zhang, F. Gao, Y. Li and Y. Li, Perfluoroalkylsulfonyl ammonium for humidity- resistant printing high-performance phase-pure FAPbI3 perovskite solar cells and modules, *Joule*, 2024, **8**, 2265–2282.

199 K. Xiao, Y.-H. Lin, M. Zhang, R. D. J. Oliver, X. Wang, Z. Liu, X. Luo, J. Li, D. Lai, H. Luo, R. Lin, J. Xu, Y. Hou, H. J. Snaith and H. Tan, Scalable processing for realizing 21.7%-efficient all-perovskite tandem solar modules, *Science*, 2022, **376**, 762–767.

200 F. Jafarzadeh, L. A. Castriotta, E. Calabrò, P. Spinelli, A. Generosi, B. Paci, D. Becerril Rodriguez, M. Luce, A. Cricenti, F. Di Giacomo, F. Matteocci, F. Brunetti and A. Di Carlo, Stable and sustainable perovskite solar modules by optimizing blade coating nickel oxide deposition over 15 × 15 cm2 area, *Commun. Mater.*, 2024, **5**, 186.

201 M. Du, S. Zhao, L. Duan, Y. Cao, H. Wang, Y. Sun, L. Wang, X. Zhu, J. Feng, L. Liu, X. Jiang, Q. Dong, Y. Shi, K. Wang and S. Liu, Surface redox engineering of vacuum-deposited NiO_x for top-performance perovskite solar cells and modules, *Joule*, 2022, **6**, 1931–1943.

202 I. Zimmermann, N. Harada, T. Guillemot, C. Aider, K. M. Muhammed Salim, V. S. Nguyen, J. Castillon, M. Provost, K. Medjoubi, S. Cacovich, D. Ory and J. Rousset, Slot-Die Deposition of CuSCN Using Asymmetric Alkyl Sulfides as Cosolvent for Low-Cost and Fully Scalable Perovskite Solar Cell Fabrication, *Sol. RRL*, 2024, **8**, 2400064.

203 H. Liu, K. Yan, J. Rao, Z. Chen, B. Niu, Y. Huang, H. Ju, B. Yan, J. Yao, H. Zhu, H. Chen and C.-Z. Li, Self-Assembled Donor–Acceptor Dyad Molecules Stabilize the Heterojunction of Inverted Perovskite Solar Cells and Modules, *ACS Appl. Mater. Interfaces*, 2022, **14**, 6794–6800.

204 F. Di Giacomo, S. Shanmugam, H. Fledderus, B. J. Bruijnaers, W. J. H. Verhees, M. S. Dorenkamper, S. C. Veenstra, W. Qiu, R. Gehlhaar, T. Merckx, T. Aernouts, R. Andriessen and Y. Galagan, Up-scalable sheet-to-sheet production of high efficiency perovskite module and solar cells on 6-in. substrate using slot die coating, *Sol. Energy Mater. Sol. Cells*, 2018, **181**, 53–59.

205 P. J. S. Rana, B. Febriansyah, T. M. Koh, B. T. Muhammad, T. Salim, T. J. N. Hooper, A. Kanwat, B. Ghosh, P. Kajal, J. H. Lew, Y. C. Aw, N. Yantara, A. Bruno, S. A. Pullarkat, J. W. Ager, W. L. Leong, S. G. Mhaisalkar and N. Mathews, Alkali Additives Enable Efficient Large Area (>55 cm2) Slot-Die Coated Perovskite Solar Modules, *Adv. Funct. Mater.*, 2022, **32**, 2113026.

206 L. Vesce, M. Stefanelli, F. Rossi, L. A. Castriotta, R. Basosi, M. L. Parisi, A. Sinicropi and A. Di Carlo, Perovskite solar cell technology scaling-up: Eco-efficient and industrially compatible sub-module manufacturing by fully ambient air slot-die/blade meniscus coating, *Prog. Photovolt.: Res. Appl.*, 2024, **32**, 115–129.

207 R. Xu, Y. Sun, J. Dai, X. Zhu, P. Li, X. Cao, J. Xi, F. Yuan, C. Zuo, L. Ding, Y. Yang, J. Li, J. Xu, A. K. Y. Jen, Z. Wu and H. Dong, Buried interface regulation for efficient and stable perovskite minimodules, *Nano Energy*, 2025, **133**, 110406.

208 C. Li, Y. Zhang, X. Zhang, P. Zhang, X. Yang and H. Chen, Efficient Inverted Perovskite Solar Cells with a Fill Factor Over 86% via Surface Modification of the Nickel Oxide Hole Contact, *Adv. Funct. Mater.*, 2023, **33**, 2214774.

209 L. Wang, D. Zheng, Z. Li, B. Farhadi, L. Peng, S. Zhao, Z. Chang, L. Duan, Y. Cao, H. Wang, Y. Tong, M. Du, K. Wang and S. Liu, Surfactant engineering for perovskite solar cells and submodules, *Matter*, 2023, **6**, 2987–3005.

210 M. Yang, D. H. Kim, T. R. Klein, Z. Li, M. O. Reese, B. J. Tremolet de Villers, J. J. Berry, M. F. Van Hest and K. Zhu, Highly efficient perovskite solar modules by scalable fabrication and interconnection optimization, *ACS Energy Lett.*, 2018, **3**, 322–328.

211 L.-H. Chou, Y.-T. Yu, X.-F. Wang, I. Osaka, C.-G. Wu and C.-L. Liu, Sequential Ultrasonic Spray-Coating Planar Three Layers for 1 cm2 Active Area Inverted Perovskite Solar Cells, *Energy Technol.*, 2020, **8**, 2000216.

212 C. Gong, S. Tong, K. Huang, H. Li, H. Huang, J. Zhang and J. Yang, Flexible Planar Heterojunction Perovskite Solar Cells Fabricated via Sequential Roll-to-Roll Microgravure Printing and Slot-Die Coating Deposition, *Sol. RRL*, 2020, **4**, 1900204.

213 H. C. Weerasinghe, Y. Dkhissi, A. D. Scully, R. A. Caruso and Y.-B. Cheng, Encapsulation for improving the lifetime of flexible perovskite solar cells, *Nano Energy*, 2015, **18**, 118–125.

214 F. Matteocci, L. Cinà, E. Lamanna, S. Cacovich, G. Divitini, P. A. Midgley, C. Ducati and A. Di Carlo, Encapsulation for long-term stability enhancement of perovskite solar cells, *Nano Energy*, 2016, **30**, 162–172.

215 K. Qi, M. Chhowalla and D. Voiry, Single atom is not alone: Metal–support interactions in single-atom catalysis, *Mater. Today*, 2020, **40**, 173–192.

216 M. Wong-Stringer, O. S. Game, J. A. Smith, T. J. Routledge, B. A. Alqurashy, B. G. Freestone, A. J. Parnell, N. Vaenas, V. Kumar and M. O. Alawad, High-performance multilayer encapsulation for perovskite photovoltaics, *Adv. Energy Mater.*, 2018, **8**, 1801234.

217 P. F. Carcia, R. S. McLean, M. H. Reilly, M. D. Groner and S. M. George, Ca test of Al2O3 gas diffusion barriers grown by atomic layer deposition on polymers, *Appl. Phys. Lett.*, 2006, **89**, 031915.

218 S. Ma, Y. Bai, H. Wang, H. Zai, J. Wu, L. Li, S. Xiang, N. Liu, L. Liu and C. Zhu, 1000 h operational lifetime perovskite solar cells by ambient melting encapsulation, *Adv. Energy Mater.*, 2020, **10**, 1902472.

219 Y. I. Lee, N. J. Jeon, B. J. Kim, H. Shim, T. Y. Yang, S. I. Seok, J. Seo and S. G. Im, A low-temperature thin-film encapsulation for enhanced stability of a highly efficient perovskite solar cell, *Adv. Energy Mater.*, 2018, **8**, 1701928.

220 J. Anguita, C. Smith, T. Stute, M. Funke, M. Delkowski and S. Silva, Dimensionally and environmentally ultra-stable polymer composites reinforced with carbon fibres, *Nat. Mater.*, 2020, **19**, 317–322.

221 W. Luo, C. E. Clement, Y. S. Khoo, Y. Wang, A. M. Khaing, T. Reindl, A. Kumar and M. Pravettoni, Photovoltaic module failures after 10 years of operation in the tropics, *Renewable energy*, 2021, **177**, 327–335.

222 A. Mei, Y. Sheng, Y. Ming, Y. Hu, Y. Rong, W. Zhang, S. Luo, G. Na, C. Tian, X. Hou, Y. Xiong, Z. Zhang, S. Liu, S. Uchida, T.-W. Kim, Y. Yuan, L. Zhang, Y. Zhou and H. Han, Stabilizing Perovskite Solar Cells to IEC61215:2016 Standards with over 9,000-h Operational Tracking, *Joule*, 2020, **4**, 2646–2660.

223 M. V. Khenkin, E. A. Katz, A. Abate, G. Bardizza, J. J. Berry, C. Brabec, F. Brunetti, V. Bulović, Q. Burlingame, A. Di Carlo, R. Cheacharoen, Y.-B. Cheng, A. Colsmann, S. Cros, K. Domanski, M. Dusza, C. J. Fell, S. R. Forrest, Y. Galagan, D. Di Girolamo, M. Grätzel, A. Hagfeldt, E. von Hauff, H. Hoppe, J. Kettle, H. Köbler, M. S. Leite, S. Liu, Y.-L. Loo, J. M. Luther, C.-Q. Ma, M. Madsen, M. Manceau, M. Matheron, M. McGehee, R. Meitzner, M. K. Nazeeruddin, A. F. Nogueira, Ç. Odabaşı, A. Osherov, N.-G. Park, M. O. Reese, F. De Rossi, M. Saliba, U. S. Schubert, H. J. Snaith, S. D. Stranks, W. Tress, P. A. Troshin, V. Turkovic, S. Veenstra, I. Visoly-Fisher, A. Walsh, T. Watson, H. Xie, R. Yıldırım,

S. M. Zakeeruddin, K. Zhu and M. Lira-Cantu, Consensus statement for stability assessment and reporting for perovskite photovoltaics based on ISOS procedures, *Nat. Energy*, 2020, **5**, 35–49.

224 P. Zhu, C. Chen, J. Dai, Y. Zhang, R. Mao, S. Chen, J. Huang and J. Zhu, Toward the Commercialization of Perovskite Solar Modules, *Adv. Mater.*, 2024, **36**, 2307357.

225 O.o.S. company, **https://www.diva-portal.org/smash/get/diva2:1305998/FULLTEXT01.pdf**, 2023.

226 O.o.M. company, **http://www.microquanta.com**, 2023.

227 O.o.U. company, **http://www.utmolight.com**, 2023.

228 L. Pei, H. Yu, Q. Zhang, J. Li, K. Wang and B. Hu, Concave and Convex Bending Influenced Mechanical Stability in Flexible Perovskite Solar Cells, *J. Phys. Chem. C*, 2020, **124**, 2340–2345.

229 K. Fukuda, L. Sun, B. Du, M. Takakuwa, J. Wang, T. Someya, L. F. Marsal, Y. Zhou, Y. Chen, H. Chen, S. R. P. Silva, D. Baran, L. A. Castriotta, T. M. Brown, C. Yang, W. Li, A. W. Y. Ho-Baillie, T. Österberg, N. P. Padture, K. Forberich, C. J. Brabec and O. Almora, A bending test protocol for characterizing the mechanical performance of flexible photovoltaics, *Nat. Energy*, 2024, **9**, 1335–1343.

230 T. H. Han, Y. Zhao, J. Yoon, J. Y. Woo, E. H. Cho, W. D. Kim, C. Lee, J. W. Lee, J. M. Choi and J. Han, Spontaneous Hybrid Cross-Linked Network Induced by Multifunctional Copolymer toward Mechanically Resilient Perovskite Solar Cells, *Adv. Funct. Mater.*, 2022, **32**, 2207142.

231 X. Li, H. Yu, Z. Liu, J. Huang, X. Ma, Y. Liu, Q. Sun, L. Dai, S. Ahmad and Y. Shen, Progress and challenges toward effective flexible perovskite solar cells, *Nano-Micro Lett.*, 2023, **15**, 206.

232 W. Fu, A. G. Ricciardulli, Q. A. Akkerman, R. A. John, M. M. Tavakoli, S. Essig, M. V. Kovalenko and M. Saliba, Stability of perovskite materials and devices, *Mater. Today*, 2022, **58**, 275–296.

233 X. Dong, L. Chao, T. Niu, Y. Li, P. Guo, W. Hui, L. Song, Z. Wu and Y. Chen, Phase-Pure Engineering for Efficient and Stable Formamidinium-Based Perovskite Solar Cells, *Sol. RRL*, 2022, **6**, 2200060.

234 M. Li, H. Li, Q. Zhuang, D. He, B. Liu, C. Chen, B. Zhang, T. Pauporté, Z. Zang and J. Chen, Stabilizing perovskite precursor by synergy of functional groups for NiOx-based inverted solar cells with 23.5% efficiency, *Angew. Chem.*, 2022, **134**, e202206914.

235 Z. Yang, Y. Jiang, D. Xu, Z. Wang, X. Gao, X. Lu, G. Zhou, J.-M. Liu and J. Gao, Self-healing and efficient flexible perovskite solar cells enabled by host–guest interaction and a 2D/3D heterostructure, *J. Mater. Chem. A*, 2022, **10**, 22445–22452.

236 Y. Xu, X. Guo, Z. Lin, Q. Wang, J. Su, J. Zhang, Y. Hao, K. Yang and J. Chang, Perovskite Films Regulation via Hydrogen-Bonded Polymer Network for Efficient and Stable Perovskite Solar Cells, *Angew. Chem.*, 2023, **135**, e202306229.

237 Z. Chen, Q. Cheng, H. Chen, Y. Wu, J. Ding, X. Wu, H. Yang, H. Liu, W. Chen and X. Tang, Perovskite grain-boundary manipulation using room-temperature dynamic self-healing "ligaments" for developing highly stable flexible perovskite solar cells with 23.8% efficiency, *Adv. Mater.*, 2023, **35**, 2300513.

238 C. Ge, Z. Yang, X. Liu, Y. Song, A. Wang and Q. Dong, Stable and highly flexible perovskite solar cells with power conversion efficiency approaching 20% by elastic grain boundary encapsulation, *CCS Chem.*, 2021, **3**, 2035–2044.

239 S. Ahn, W.-H. Chiu, W.-C. Chu, P.-Y. Chen, T.-H. Lin and K.-M. Lee, A systematic investigation of PVDF-HFP in perovskite solar cells for improved space mission reliability, *Chem. Eng. J.*, 2024, **496**, 153974.

